Republic of Iraq
Ministry of Higher Education and Scientific Research
University of Babylon
College of Materials Engineering
Department of Metallurgical Engineering

Modification of CoCrMo Alloy (F75) by ZrO_2 Additions Used in Biomedical Applications.

A Thesis

Submitted to Council of the College of Materials Engineering / University of Babylon in Partial Fulfillment of the Requirements for the Master Degree in Materials Engineering / Metallurgical

By

Zain Alabdeen Ali Kareem Mohammed

Supervised by

Prof. **Haydar Hassan Jaber** (Ph.D.)

2022A.D 1443A.H

بسم الله الرحمن الرحيم

((وَعَلَّمَكَ مَا لَمْ تَكُنْ تَعْلَمُ ۚ وَكَانَ فَضْلُ اللَّهِ عَلَيْكَ عَظِيمًا))

سورة النساء

الآية (113)

Supervisor Certificate

I certify that the thesis entitled **(Modification of CoCrMo (F75) alloys used in surgical applications)** was prepared by **(Zain ALabdeen Ali Kareem)** had been carried out under my supervision at the University of Babylon/ College of Material's Engineering/ Department of Metallurgical Engineering in partial fulfillment of the requirements for the degree of Master of Science in Material's Engineering/ Metallurgical.

Signature

Name: **Prof. Haydar Hassan Jaber (Ph.D.)**

(Supervisor)

Date: / / 202

Examining Committee Certification

We certify that we have read this thesis entitled (**Modification of CoCrMo Alloy (F75) by ZrO_2 additions Used in Biomedical Applications**) and as an examining committee, we have examined the student **(Zain ALabdeen Ali Kareem)** in contents and that is related to it, and that in our opinion it meets the standard of a thesis for the Master degree in Materials Engineering.

Signature

Prof. Dr. Nawal Mohmmed Dawood

Committee Chair

Date: / / 2022

Signature

Prof. Dr.Zuheir Talib Khulief

Committee Member

Date: / / 2022

Signature

Assist. Prof. Dr. Ali Mezher Resen

Committee Member

Date: / / 2022

Signature

Prof. Dr. Haydar Hassan Jaber

Supervisor

Date: / / 2022

Approval of the Department Metallurgical Engineering

Head of Metallurgy Engineering Department

Signature

Prof.Dr.Saad Hameed Al-Shafaie

Date: / / 2022

Approval of the College of Materials Engineering

Dean of the College of Materials Engineering

Signature

Prof. Dr.Imad A. Disher Al-Hydary

Date: / / 202

Acknowledgments

Great thanks to Allah Almighty my Creator and inspirational for being merciful to me and gave me health, strength and protection.
I cannot express enough thanks and gratitude to my supervisor, **prof. Dr. Haydar H.Jamal Al Deen** support, helped, encouraged, and gave me the entire acknowledgement to finish my research. It was a great privilege and honor to work and study under him guidance.
My thank to everyone work in metallic and non-metallic laboratories in Materials Engineering college/ University of Babylon.
Iam extremely grateful to my family and my wife for their love, prayers, caring and continuing support made this work possible. I am also extremely thankful to my friends for their kind support.

Zain Alabdeen Ali Kareem

2022

Dedication

The One whose throne is in the sky…To the One whom we praise and

Thank… *Allah.*

To *my dears* Dad and Mum;
The reason of what I have become today. Thanks for your great support and conditions care through my life.

To *my dear Wife*, you were my support and did not abandon me, you were with me step by step, I thank you for enduring my very difficult circumstances and without getting bored, you are a blessing and I thank God for that;

Ataa Abdulwahid

To everyone who stood by me and helped me and supported me.

To *my colleagues*, thank you for everything.

With Respect

Zain Alabdeen Ali Kareem

2022

Abstract

Cobalt-chromium-molybdenum alloy (F75) is considered one of the important alloys that are widely used in orthopedic applications and dental implants. The aim of study is to investigate effect addition of zirconium oxide to CoCrMo ASTM (F75) on physical, mechanical, electrochemical and biological properties. (0.5, 1, 1.5, 2, 2.5, 3, 3.5,4, 4.5, 5 wt. %) adding of zirconium oxide by powder metallurgy.

The powders are mixed for 5 hours, compacted at a constant pressure of 800 Mpa. The dimensions of the samples after the pressing process were d=12 mm and t = 4.5 mm. The sintering process was accomplished at temperature 1100°C for 4 hours for all samples are sufficient to satisfy completely and to transform all element into alloy structure.

The results indicate to decrease the density and porosity values with increase additive ratio of zirconium oxide.

The hardness values of prepared alloy were increased as zirconia addition increase from (109HB) of base alloy to (151HB) at (5%) adding of ZrO_2.

The wear resistance an increase significantly with zirconia additive compared with base CoCrMo alloy where the volume loss decrease from (0.002 cm^3 of the base) to (0.000671 cm^3) at (2.5% ZrO_2) as minimum of volume loss which consider the best improvement percentage of wear resistance.

The compressive strength increases with the addition of zirconia from 388.41 of the base alloy to 841.99, 835.10, 937.75, 942.97, 902.31, 949.6, 893.8, 877.09, 880.6 and 871, respectively.

The electrochemical properties, the results of corrosion of CoCrMo alloy illustrated significant improvement after the addition of ZrO_2 in synthetic saliva and hank's solution, where the corrosion rate decrease from (1.582 mpy) and (1.158 mpy) of base alloy in synthetic saliva and hank’s solution respectively to (0.144mpy) (0.169mpy) at 5% of ZrO_2. The best corrosion resistance of base alloy with (0.5%) adding of zirconium oxide where the improvement percentage reached to (87.83%) in hank’s solution, while the improvement percentage was (96.7%) at addition (0.5%) in synthetic saliva.

The ion release is tested for base alloy and with (2.5 and 5%) zirconia addition for 21 days in artificial saliva and Hank's, where the test result confirmed that of Co element in the hank’s and saliva solution decreased significantly after adding zirconium oxide particles.

Table of content

List of symbols

symbol	Meaning	Unit
D°	Density of oil	Kg/m^3
Dw	Density of water	Kg/m^3
Ew	Equilibrium weight	-----

List of Greek Symbols

symbol	Meaning	Unit
γ	Gama phase	----
ε	Abelson phase	----
p	Density	Kg/m^3
σ	Sigma phase	-----

List of Subscripts &Superscripts

symbol	Meaning	Unit
i_{Corr}	Corrosion current density	$\mu A/cm^2$
E_{corr}	Corrosion potential	mV
wt.	Weight percentage	%

List of Abbreviations

Abbreviation	Description
ASTM	American Society for Testing and Materials
BCC	Body Center Cubic
CoCrMo	Cobalt-Chrome-Molybdenum Alloy
EDS	Energy dispersive spectroscopy analysis
FCC	Face Center Cubic
HCP	Hexagonal Closed Packed
LOM	Light Optical Microscope
OCP	Open Circuit Potential
PM	Powder Metallurgy
SEM	Scanning Electron Microscope
Tm	Melting Temperature
XRD	X-Ray Diffraction
XRF	X-Ray Fluorescence Spectrometer

CHAPTER ONE
INTODUCTION

Chapter one

Introduction

1.1 Introduction

Biomaterials are any substance that may be utilized to fabricate devices that can be employed to restore a piece or function of the living body in a healthy, believable, conversing and physiologically appropriate way. It is including metals, ceramics, polymers and composite materials[1]. Since the 1960s, the use of biomaterials to reform, exchange or augment diseased, damaged body parts has increased enormously. Millions of patients have enjoyed mitigation of pain, increased function and a progress quality of live due to biomaterials and the implants and appliance made from them[2].

Most prosthetic implants are exposed to static or repeated loads, necessitating a mix of strength and ductility. Metals have this advantage over plastics and ceramics. The majority of metals used in implants are nonmagnetic and have a high intensity, which is required for the implants to be visible under X-ray imaging and compatible with magnetic resonance imaging (MRI) procedures. Table (1.1) lists of metals used in different implants, broken down into categories[3]. Metals and their alloys are often employed in biomaterials because of their mechanical qualities. Orthopedic and cardiovascular implants together make about 70% of all implants[4].

Stainless steel, titanium, and cobalt alloys are commonly utilized in orthopedic implants because of their mechanical characteristics, wear resistance, and corrosion resistance. When the prosthesis needs to high wear resistance, such as the artificial joint, cobalt base alloys are best. This justifies their widespread usage in artificial hip joints, since immediate connection between the bone and plate and the femoral head may deteriorate the joint over time. Because of its superior mix of high ductility and strength, CoCrMo alloys are one of the most frequently utilized alloys in clinical applications [3].

Using implanted metals poses many significant obstacles. Controlling the kinetics of biodegradation is important for biodegradable minerals like magnesium because early breakdown may result in a loss in mechanical strength before function or tissue is completely recovered. The prolonged existence of minerals like Ti, steel or CoCrMo alloys in vivo raises the risk of cutaneous and systemic harm. Because these metals have a high

modulus relative to typical bone tissue, they cause osteopenia and stress shielding [5].

Table (1.1): implant classification and type of metal alloys used[3].

Type of metal alloy	Example of implant	Classification
CoCrMo;316LSS; Ti6Al4V;Ti	Stent artificial valve	Cardiovascular
Ti6Al4V; Ti; Ti6AL7Nb; CoCrMo; 316L SS	Bone fixation artificial joints	Orthopedic
CoCrMo;316LSS; Ti6Al4V; Ti; TiNi; TiMO; AgSn(Cu); Au	Orthopedic wire filler	Dentistry
316L SS; Co Cr Mo; Ti6Al4V;Ti;	Screw and plate	Craniofacial
316L SS	Artificial eardrum	Otorhinology

1.3 Metals and alloys used as biomaterials

1.3.1 Titanium alloys

Titanium as well as its alloys are primarily designed for airplanes structural uses, but recent study is also focusing on biomaterial applications, with the goal of decreasing the elastic modulus and enhancing biological characteristics[4].

When comparison to CoCrMo and stainless steels alloys, titanium is noted for its light weight, good corrosion resistance, better biocompatibility, and low density ($4.5 g/cm^3$). When it comes to biomedical dentistry, two kinds of titanium alloys are often used: Ti-6Al-4V and pure Ti (cp-Ti)[6]. Despite this, titanium alloys are weak shear strength, and low wear resistance have restricted their usage in biomedicine [7,8].

1.3.2 Steel alloys

Sherman of Pittsburg developed the first metal alloy for human usage, "vanadium steel," which has been used to screws and make bone

fracture plates. It was utilized for a while, but in vivo corrosion caused its demise[8,1].

Following that, 18-8sMo st.st was developed. Mo is used for resistance against seawater corrosion. 316 stainless steel is the alloy designation. To improve resistance to chloride solution corrosion. In the 1950s, the carbon content was lowered from 0.08 to 0.03 percent, and the alloy was called 316L[1].

Until, medical grade stainless steels utilized a lot of nickel to maintain their austenitic microstructure. Nickel is responsible for up to 90% of clinically observed metal sensitivity and may cause additional issues when liberated from stainless steel implants. Fretting and wear, as well as other types of corrosion, can cause metallic ions to get into the tissues around stainless steel implants [9].

1.3.3 Other metals

1. Tantalum

It is a thermally metal used in arterial stents, vascular ligation clips, sutures and wire mesh. Notably, the porosity and stiffness in material are similar to those of cancellous bone. It integrates well with bone and soft tissue[10].

2. Magnesium

Biodegrades in vivo by pitting corrosion on its surface. Mg is designed to provide temporary support in the form of degradable metal bone fixes or bone scaffolds. Magnesium was first used to fix a lower leg fracture in 1907 by French surgeon LaMotte. In cardiac stents and fracture-fixing devices, magnesium (Mg) is used[10].

3. Platinum and other platinum group noble metals (Pd, Rh and Ir)

They are exceptionally corrosion resistant yet mechanically weak. Because of their strong corrosion resistance and low threshold potential, they are usually employed as electrode alloys such as pacemaker tips. Gold and silver alloys that exhibit high corrosion and oxidation resistance are used in dentistry[1].

1.3.1 Cobalt base alloy

The cobalt–chromium–molybdenum alloy is one of the most widely used metal-bearing materials in artificial joint systems. The Co–Cr–Mo alloy has good mechanical properties, castability, corrosion resistance, and wear resistance, whereas stainless steel and titanium alloys have a disadvantage with regard to corrosion resistance and wear resistance, respectively[11].

Cobalt chrome alloy has some issues. The mechanical properties, biocompatibility and corrosion resistance are affected by the microstructure which depends on the heat treatment applied to the material. The second issue is that the cobalt ions are mainly accumulated in the spleen when tissues are in direct contact with the implant[12].

The main and more serious issue is the life expectancy of the implanted alloys. There was a need to increase the expected life of the synthetic joints as they are being implanted in younger and more active patients. The cobalt chrome alloys satisfies because the mechanical properties of the alloy are highly affected by chemical composition[12].

There are two kinds: wrought CoNiCrMo alloy, and cast CoCrMo alloy. For many decades, castable alloys have been utilized in dentistry and in the construction of prosthetic joints. While the wrought CoNiCrMo alloy was used to create prosthetic stems for heavily loaded joints[1].

1.4 objective of this study

The aim of this study is investigate the influence of ZrO_2 addition with different percentages (0.5, 1, 1.5, 2, 2.5, 3, 3.5, 4, 4.5 and 5%).on the CoCrMo (75) alloy that prepare by powder metallurgy.

Many tests were done to evaluate the performance of preparing alloys, these tests include:

1. Microstructure characterization (OM, XRD, SEM and EDS).

2. Mechanical properties (hardness, compressive and wear resistance).

3. Electrochemical properties (Open circuit, Polarization and ion release).

CHAPTER TWO
Theoretical part and Literature Review

Chapter Two

Theoretical Part and Literature Review

1.2 Introduction

This chapter covers an overview of the cobalt alloys used for implants. There was be a focus on the types of biomaterials according to the biocompatibility and criteria for choosing crops, which include biological properties (biocompatibility and Osseointegration), chemical properties (corrosion behavior, types and characteristics of corrosion) and mechanical properties (wear resistance and types, compressive strength and hardness). The schemes of thermal balance, chemical composition and the effect of casting elements for cobalt chrome alloys and types of these alloys were discussed. ASTM (F75) manufacturing methods include casting and powder metallurgy (powder blending, pressing and sintering). Finally, the end of this chapter will cover some recent research and studies on CoCr alloys in general.

2.2 Corrosive Environment of the Human Body

For biomaterials applications, the living body presents a very complex and hostile electrolytic environment[13]. Proteins, Water, bacteria, dissolved oxygen, plasma, amino acids, and lymph, as well as different ions such as sodium (Na^+), hydroxide (OH^-), chloride (Cl^-), and trace quantities of calcium, potassium, sulphate, phosphate, bicarbonate, and magnesium, make up the biological fluid of the human body. These ions serve to complete the electrical circuit. Furthermore, the electrochemical processes are increased by the 37°C body temperature. The pH of the human body changes as a consequence of accidents, illnesses, infections, and other causes, all of which contribute significantly to biomaterial corrosion. Various biological molecules consume the products through anodic or cathodic processes. Preferential corrosion occurs as a consequence of reduced oxygen transport induced by proteins adsorbed on the surface in certain locations. The ion content of artificial body fluid (SBF) is analogues to blood plasma of the human body. Thus, immersing biomaterials in SBF to examine biological corrosion behavior is a more efficient in vitro approach[14].

2.5 Classification of biomaterials accordding to their biocompatibility

2.5.1 Bioinert Materials.

When the implant is enclosed inside fibrous layers, it becomes physiologically inert (material that does not begin a response or induce interaction with biological tissue), ensuring that it is neither poisonous nor inflammatory. where most often used in orthopedic devices and applications. Certain ones, on the other hand, may raise concerns regarding their long-term implantation and toxic reaction. Bimetallic materials include bioinert materials such as Co-based alloys[15].

2.5.2 Bioactive materials

The implant materials and the surrounding bone tissues form a strong bond as a result of specific biological responses at the contact between them. A common feature of bioactive implants is a time-dependent kinetic modification of the implant's surface upon implantation. Because none of the metallic materials utilized in orthopedics are bioactive, the surface of metallic implants may be covered with a bioactive ceramic substance[15].

2.5.3 Bioresorbable Materials

a class of biomaterials that disintegrate spontaneously in the body, including stents, screws, and wires [15].

2.6 The Criteria of Selection Implantable Metals

2.6.1 Biocompatibilty

Implant materials should be very nontoxic and should not induce inflammatory or allergic responses in the human body. The success of biomaterials is largely determined by the human body's response to the implant, which is a measure of the material's biocompatibility. The two most important aspects affecting a material's biocompatibility are the host response elicited by the substance and the material's deterioration in vivo environment[16].

2.6.2 Osseointegration

Osseointegrated implants are commonly employed in dental, orthopedic, and surgery maxillofacial, also in ear nose throat fields. Osseointegration, the direct structure-function adhesion between the implant surface and bone, is a necessary condition for dental implants to be successful over the long term [17].

The osseointegration process is a series of complex events that begin with proteins adsorabtion and blood coagulation on the implant's surface, progress to

infiltration and biological acceptance surface by osteoblasts and mesenchymal stem cells, and ultimately result in bone formation at the interface by these cells, resulting in an intimate bond between implant and the bone. These events are regulated directly or indirectly by the implant's surface characteristics, making them critical to the implant's success in vivo, in vitro, and clinically, as indicated in Fig (2.1)[18].

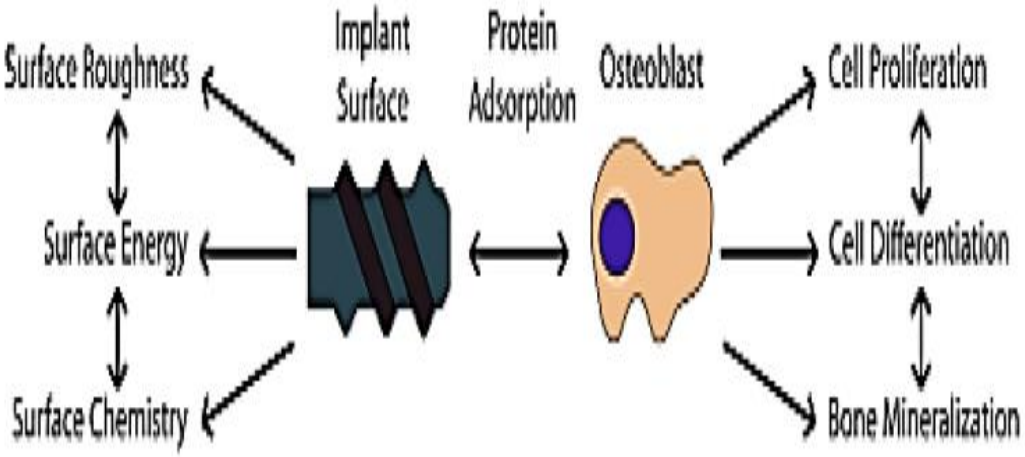

Figure (2.1) depicts the indirect and direct interactions between biological events and properties of surface such osteoblast response and protein adsorption[18].

2.6.3 Corrosion behavior

Corrosion is an attack on metallic materials that occurs when they come into contact with a chemical environment. The pH of living body fluids varies between one and nine, which may be considered an extremely corrosive environment for metallic materials due to the presence of a specific amount of sodium chloride and a series of acids. A high chloride concentration is also thought to accelerate the metallic implants corrosion, which utilize result in ion release of metal. Additionally, static or low frequency cyclic loading is applied to the majority of metallic implants. While corrosion damages to metallic biomaterials can manifest themselves in a variety of ways, including crevice, pitting, fretting, galvanic, wear, intergranular, and fatigue corrosion. the attack rate of generalcorrosion is very low because of the existence of spontaneous formation of passive surface layers on most metallic implants that are employed

at the present time [19]. The type of corrosion in Conventional Materials Utilized Biomaterial Implants are shown in table (2.1).

2.6.3.1 Types of corrosion

1. Corrosion Fatigue

It is a fracture in the metal caused by the interplay of cyclic stress and electrochemical processes. Resistance to Corrosion fatigue is an essential consideration of metals used in cyclic motion applications or load-bearing implant metals. Typically, no failure occurs, but fractures may form as a result of concealed faults, minute flaws, surface damage, chemical assault, and other factors[20].

2. Crevice Corrosion

The shape of the implant/prosthesis assembly causes this. Corrosion of an alloy is accelerated in the tiny protected volume generated by contact with another material. The other metal might be a fastener made of the same or a various alloy, a cement packing,, protected crown or an implant prosthesis joint[21].

3. Galvanic Corrosion

When two dissimilar metals come into physical contact with a medium that conducts ions such as interstitial fluid or serum, this is known as galvanic corrosion. Contact between incompatible materials is inevitable in many practical applications. When a bone screw and a bone plate are composed of various metals or alloys,in surgical implant galvanic corrosion occurs[22].

4. Intergranular Corrosion

This type of corrosion happens because of the technical errors and inhomogeneity that result in more reactive nature of boundaries of the grain(occurs at the grain boundaries due to the precipitation of secondary phases), that the corrosion of intergranular happens adjacent to boundaries of grain with comparatively very little corrosion of grains[23].

5. Pitting Corrosion

Localized Pitting corrosion occurs when an assault is made on a resistant surface. It often happens on base metals that are shielded by a naturally developing thin film of an oxide (for example, when the film's potential exceeds the oxide's breakdown potential in a hostile environment. When certain ions, such as chlorides and sulphides, are present, the film breaks down locally, resulting in fast dissolving of the underlying metal in the form of pits[24].

6. Fretting Corrosion

This is a type of erosion corrosion and is regarded as the more important type of corrosion in implantology. Fretting corrosion is a type of deterioration caused by the interaction of tiny movements between contacting parts and the corrosivity of the environment. This can trigger tissue irritation caused by the breakdown of metallic components used in prosthetic implants,resulting in the failure of orthopedic surgical procedures[23].

Table (2.1) shows Corrosion Types in Conventional Materials Utilized Biomaterial Implants[25].

Type of corrosion	Materials	Location of Implant	implant shape
Crevice	316 L stainless steel	Bone plates and screws	
Ferrting	Ti5Al2.5Fe, CoCr,SS	Ball Joints	
Pitting	304 SS, Co based alloy	Orthopedic/ Dental alloy	
Corrosion Fatigue	316 stainless steel, CoCrNiFe	Bone cement	
Selective Leaching	Mercury from gold	Oral implants	
Galvanic	304 SS/316SS, CoCr+Ti5Al2.5Fe., 316SS/Ti5Al2.5Fe or CoCrMo	Oral Implants Skrews and nuts	

2.6.4 Mechanical Prpoerties

Mechanical properties such as hardness, tensile strength, fracture resistance, eleasic of modulus, elongation (strain), and fatigue strength or life all play a large role in material selection for use in the living body.

The elasticity modulus of biomaterials may be matched to that of bone, which ranges from four to thirty GPa, to decrease stress shielding. Furthermore, the material should have a low modulus mixed with a high strength to extend the service life of the implant and prevent loosening, avoiding the need for revision surgery[26].

2.6.4.1 Wear Resistance

The term "wear property" refers to damage to a solid surface, which includes gradual material loss as a result of relative motion between that surface and a contacting substance or substances, as shown in Figure (2.2). Recently, the primary concern for continued development of metallic implant materials has been the transfer of stress between hard tissue and metallic implant components in contact, since further bone degradation and adsorption should be prevented. Specifically, a significant discrepancy in the hardness and other mechanical and tribological properties of bone and metallic implant materials may result in more bone loss and deterioration[27]. The wear process has the potential to break the protective oxide film that is naturally present on the surface of the alloy, resulting in increased attack in the presence of a corrosive environment[28].

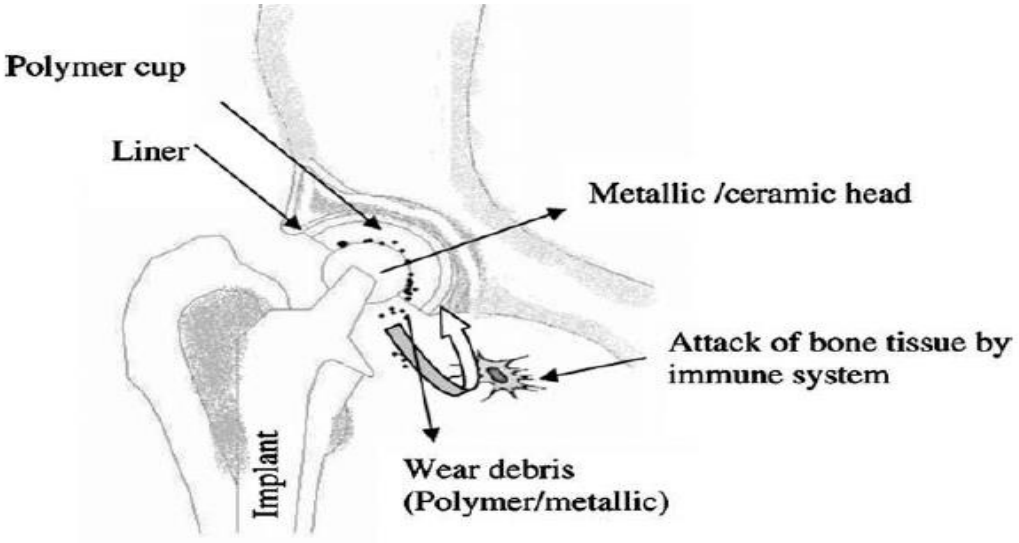

Figure (2.2): Wear of Total Joint Replacements[27].

2.6.4.1.1 Wear mechanisms

is critical for designing materials that are suitable for wear reduction [29].Wear mechanisms are broadly classified into six kinds:

1. Adhesive wear

The surface interaction and welding of the junctions at the sliding contact create adhesive wear. The kind of bonding (ionic, metallic, van der Waals and covalent) at the contact junction influences this wear process. If the bond at the junction is stronger than the bond in the bulk, the weaker part of the materials in contact is removed and transferred to the counter surface. Surface removal produces a rough appearance as well as a significant volume of worn material, followed by severe wear[29].

2.Delamination Wear

The debris is plates, the length to the thickness is ten times caused by forming and fracture such as cylinder in internal combustion machining may occur in abrasive wear. It is seen that the ductility increases strength of material against delimitation[30].

3.Erosion Wear

Caused by impact of solid or liquid or gaseous particles form losses in weight or removal of particles in which the fluid carry the particles .It is depended on the kinetic energy for particles and the emission of the energy on the surface.

4. Tribochemical wear

Tribochemical wear occurs as a consequence of the removal of reaction products/layers generated on the contacting surface during the reaction.

5.Fatigue Wear

Wear debris is created as a result of the contact being loaded cyclically. This process is identifiable by the formation of cracks and crevice of the surface material. [28].

6. abracive wear

The material removal by hard particles sliding between two surfaces is in relative motion. More than one type of mechanism can be involved in a wear situation. Also, these individual mechanisms can interact sequentially to form a more complex wear process. However, one mechanism generally is the controlling and primary mechanism. The relative importance or occurrence of individual mechanisms can change with changes in tribosystem parameters.

Therefore, materials can exhibit transitions in wear behavior as a result of changes in other operational parameters, such as load, velocity, and friction [31].

2.7 compsite materials

Composites, often known as composite materials, are engineered materials consisting of two or more constituent materials with significantly different physical, chemical, and mechanical characteristics. The individual properties of their constituent parts, as well as their relative volume fractions and arrangements in the material system, determine the typical attributes of these composites. Composites may be created to meet particular chemical , mechanical, geometrical , structural and even aesthetic criteria, depending on the intended use. These synthetic materials have applications in construction, such as bridges and buildings, the automotive sector, such as automobile bodywork, aeronautics, naval (boats and ships), and biological disciplines. Although polymeric, ceramic , and metallic biomaterials have been used for decades in medical treatments like tissue repair and replacement, composites are just now becoming known[32]. Because it has several advantages, the most important of which are corrosion resistance, design flexibility, durability, low weight, and strength[33].

2.7.1 Metal matrix compsites

Metal matrix composites have several advantages over monolithic metals, including higher specific strength, higher specific modulus, lower coefficients of thermal expansion, better high-temperature characteristics, and better wear resistance. Because of its features, metal matrix composites (MMCs) are being studied for a range of applications. Their hardness, however, is lower than that of monolithic metals, and they are now more costly[34].

In general, MMCs consist of at least two constituents: the matrix of metal and the reinforcement. The matrix is specified as a metal in all circumstances, however pure metal is seldom used: it is generally an alloy. Some MMC classes, like diamond tools, hard metals and cermetshave diverse and wide uses, and, although they may be called conventional materials, they are constantly evolving[35].

2.7.2 types of reniforcement

There are various classifications for metal matrix composites. The kind and extent to which reinforcing components are used in, fiber, layer, penetration composite (infiltration composite) and particles materials is one categorization. Continuous fiber composite materials and short fiber composite materials, both of which are sometimes referred to as whisker composite materials, are two different forms of fiber composite materials[36]. Fig (2.1) shows Classification of composite materials with metal matrixes.

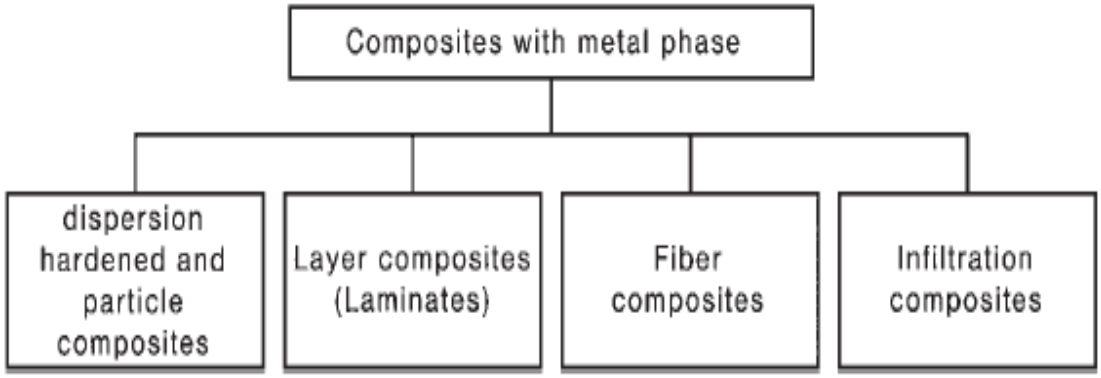

Fig(2.1). Classification of composite materials with metal matrixes[37].

2. 7.2.1 Particle-Reinforced Composites

1. Large-particle strengthened composites

The term large means that particle–matrix interactions cannot be treated at the atomic or molecular level, but must instead be treated using continuum mechanics. The particulate phase is harder and stiffer than the matrix in the most of these composites. These reinforcing particles tend to inhibit matrix phase movement in the vicinity of each particle. The matrix, in essence, passes some of the applied stress to the particles, which carry a portion of the load. Strong bonding at the matrix–particle interface determines the degree of reinforcement or improvement in mechanical behavior[37]. Shown in Fig(2.2 a).

2. Dispersion-strengthened composites

Dispersion-enhanced composites generally include particles much finer with sizes of between (10 and 100 nm) 0.01 and 0.1μm. Particle–matrix interactions lead to atomic or molecular strengthening levels. The strengthening mechanism is similar to that of precipitation hardening. Whereas the small scattered particles block or impede the dislocation's motion while the matrix

carries most of the applied load. Thus, plastic deformation is reduced, leading in a rise in yield, tensile strength, and hardness[37]. Shown in Fig(2.2 b).

Metal oxides (ZrO_2, Al_2O_2, ThO_2), metal borides (TaB_2, ZrB_2, TiB_2, WB), nitrides of metal (TaN, ZrN, Si3N4, TiN), and carbides of Metal (SiC, TaC, WC, B_4C) are used as reinforcing particles in the materials of a composite containing an alloy of metal matrix[38].

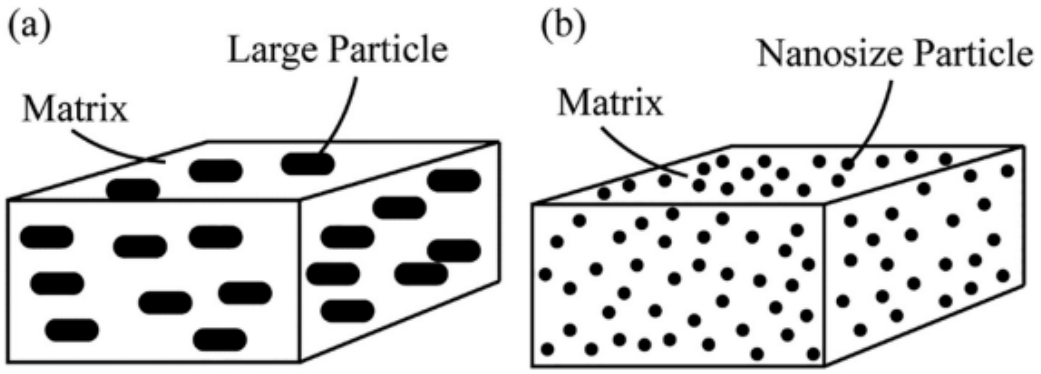

Fig (2.2): Types of particle reinforced composites (a) Large particle (b) Dispersion – strengthened[32].

2.8 Cobalt based alloy

In 1735, the Swedish chemist Brandt isolated the metal and initiated the scientific study of the element. Co-based alloys have been established, after extensively studied about 40 years by Bergman, since 1900s. The biomedical applications started in1930 and then developed in 1932 for dental prosthesis and medical applications by casting in wax models, Vitallium, for the reproduction of complex shapes by exactness lost-wax casting. The Co-Cr-Mo alloy extension to orthopedic application was in 1940[39].

Today, CoCrMo alloys are essential in a variety of applications due to their:

1. good mechanical properties[39].

2. good corrosion resistance[40].

3. the smallest ion released[41].

4. good biocompatibility[42].

5. good osteocompatibility as compared to other metal implants [40].

2.9 Types of Cobalt Chrome Alloys.

There are several Co–Cr alloys available, but only two are being utilized extensively as implant alloys[41]. These two are:

1. ASTM cobalt–chromium–molybdenum (CoCrMo)

a cast Co-28Cr-6Mo alloy. Protasul-2 (Sulzer AG), Vitallium (Howmedica, Inc.), Zimaloy are the trade names for this alloy (Zimmer) and Haynes Stellite 21 (Cabot Corporation). This alloy is notable for its superior resistance of corrosion, even in chloride conditions. This is mostly due to its high bulk chromium concentration and surface layer of chromium oxide (Cr_2O_3). This material is widely utilized in medicinal and aeronautical applications[6].

2. ASTM F562 cobalt–nickel–chromium– molybdenum (CoNiCrMo).

Other cobalt alloys permitted for implant usage include one containing iron (CoNiCrMoWFe, ASTM F563) and another containing tungsten (CoCrNiW, ASTM F90). While CoNiCrMo alloys with a high nickel content (25–37%) provide improved corrosion resistance, they create concerns regarding possible toxicity and/or immunogenic sensitivity due to released Ni. Under static circumstances, particularly due to their low frictional (wear) qualities, the biologic reactivity of nickel liberated from CoNiCr alloys is a source for concern. Additionally, CoNiCr alloys are unsuitable for imployed in joints components. As a consequence, CoCrMo(ASTM F75) is the most often utilized implant alloy for entire joint components[41].

2.10 phases diagrams of CoCrMo alloy.

2.10.1 Binary phase diagram of CoCr alloy

According to Thermo-Calculation, the five phases below are existed in the Co-Cr binary alloy up 800 °C , Fig (2.3).

•Liquid phase.
• α-Co-rich (FCC) phase.
• ε-Co-rich (HCP) phase.
•σ phase.
• α-Cr-rich (BCC) phase.

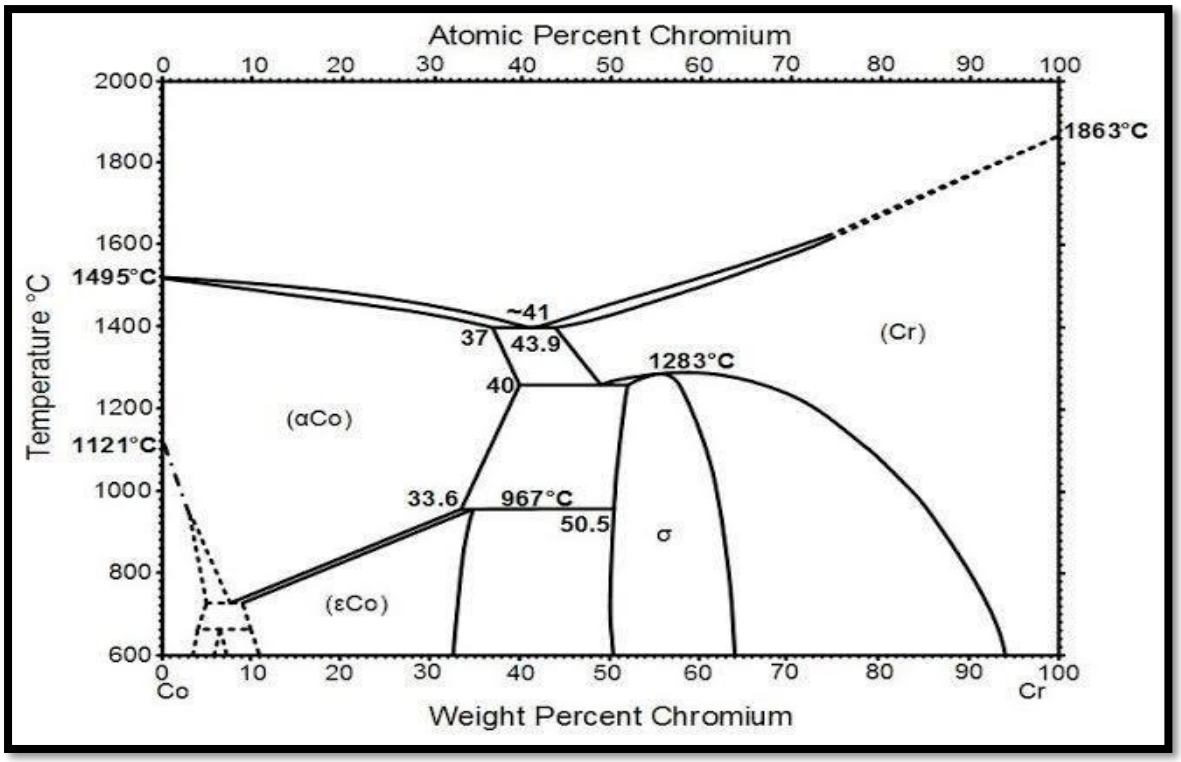

Fig (2.3) binary phase diagram of CoCr system[42].

At 1121°C, chromium solubility in cobalt (α- Co) begins at (0 wt. %) Cr and grows to (10 wt. %) Cr at 700°C. At 967°C, the dissolution of α- Co rises into (33.6 wt. percent) of Cr then increases to 40 wt. percent of Cr at 1260°C, indicating that chromium is soluble in cobalt to a maximum. α-Co dissolves about 37 wt.% at the eutectic temperature of 1395°C. At temperatures less than 967 °C for 33.6 wt. % of chromium the α-Co transfers to ε-Co and at less than 700°C for 10 wt. % of Cr. At a high temperature of more than 1283°C, α- Cr begins at 43.9 to 100 wt. % of Cr. The CoCrMo alloy sigma phase (σ) runs from 50.5 to 63 wt.% Cr when the temperature is less than 1283 °C[43].

The Cobalt-Chrome binary system possess four interactions, according to thermodynamic database[44]:

1- At 1397 °C and 42.2 % Cr $L \longrightarrow FCC + BCC$. (Eutectic reaction)

2- At 1281 °C and 58.3 % Cr $BCC \longrightarrow \sigma$. (Congruent reaction)

3- At 1269 °C and 52.5 % Cr $BCC \longrightarrow FCC + \sigma$. (Eutectoid reaction)

4- At 967 °C and 37.6 % Cr $FCC + \sigma \longrightarrow HCP$. (Peritectoid reaction)

At 417 ° C, pure cobalt exhibits an allotropic transformation from the high temperature (α- Co)phase with the (FCC) structure to the low temperature (ε-Co)phase with the (HCP) structure.[45].

2.10.2 Trinary phase diagram of Co Cr Mo alloy

Alloys are primarily composed of the γ phase (FCC) and ε phase (BCC). Additionally, they precipitate the σ phase (BCT) somewhat (intermetallic component with approximate chemical composition Co_2Cr_3). Created during cooling because of martensitic transition from γ to ε. In the case of Co-Cr-Mo alloys, the ratio of these phases has a major effect on the alloy's characteristics. The elongation of the Co-29Cr-6Mo alloy rises as the γ phase fraction increases[46,47].

Of the above characteristics, it can be illustrated that the alloy involving of the ε phase is promising for the application used in corrosion or wear condition, whereas alloy involving of the γ phase is suitable for plastic formation. However, the effect of C percentage and heat treatment on the steadiness of γ phase has been mentioned until now. The steadiness of the ε phase has not been inspected in details yet[46].

The ternary phase diagrams of the Cobalt-Chrome-Molybdenum alloy system at (a) 1200°C and (b) 927°C are shown in Fig (2.4). The solid circles in figure (2.4) depict the ASTM-F75 standard's composition (Cobalt-Chrome-Molybdenum). At the composition, the phase ε and σ phase presence are constant at 927 °, despite the fact that only the γ phase is constant at 1200 °C[48].

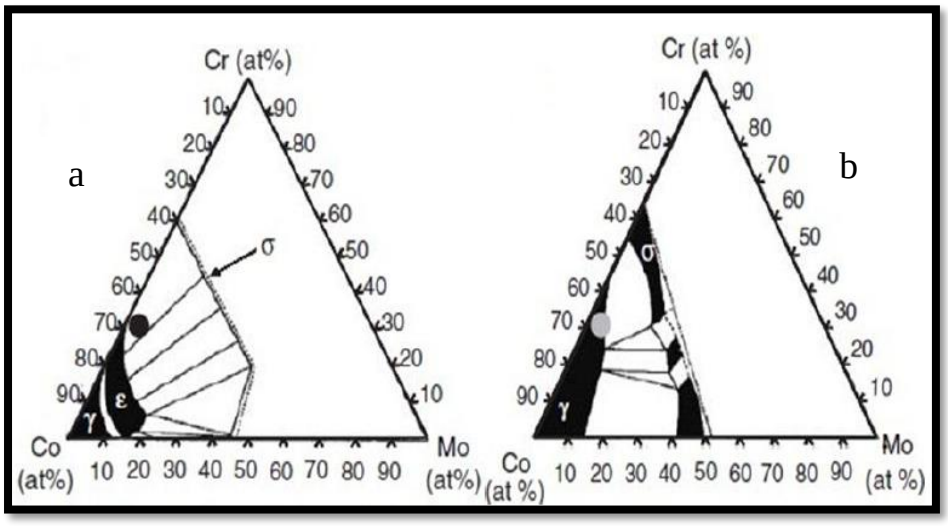

Fig(2.4): A ternary phase diagram of the CoCrMo alloy system at temperatures of (a) 1200°C and (b) 927°C[48].

CoCrMo alloy solidification begins with dendritic growth of γ-FCC crystals. Secondary phase precipitates formed at grain boundaries and interdendritic zones as temperature decreased. Sigma intermetallic compound is the first secondary phase to appear. Carbides form with further cooling, according to the global reaction $\sigma + C = M_{23}C_6$. It has also been observed that certain metastable carbides form during the process of solidification in a restricted temperature range, such as $M_{12}C$ and M_7C_3. $M_{23}C_6$ carbides are available in two characteristics: pearlite and blocky. At 990 °C, once the solidification is completed, under a slow cooling rate, pearlite is formed. According to one study, the volume fraction of both blocky carbides and the eutectoid phase rises dramatically with content of carbon. However, the cooling rate has little effect on the blocky carbide volume fraction[47]. Fig (2.5) shown (LOM) image of (ASTM F 75).

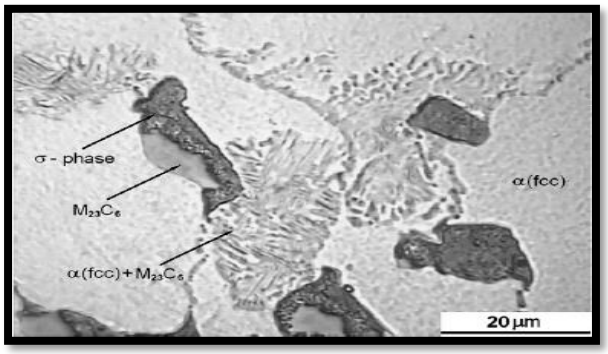

Figure (2.5) (LOM) image of (ASTM F 75)[47].

2.11 Chemical composition and effect of alloying elements of (F75) alloy.

According to American society of testing and material (ASTM) Co28CrMo alloy typically consist of (27-30) mass% chromium, (5-7) mass% Molybdenum, and in addition to some additive, table (2.2) is shown CoCr alloys chemical composition[49].

Table (2.2) CoCr alloys chemical composition [49].

Element	CoCrMo(F75)		CoCrWNi(F90)		CoNiCrMo(F562)		CoNiCrMoWFe(F563)	
	Min.	Max	Min.	Max.	Min.	Max.	Min.	Max.
Cr	27.0	30.0	19.0	21.0	19.0	21.0	18.00	22.00
Mo	5.0	7.0	—	—	9.0	10.5	3.00	4.00
Ni	—	2.5	9.0	11.0	33.0	37.0	15.00	25.00
Fe	—	0.75	—	3.0	—	1.0	4.00	6.00
C	—	0.35	0.05	0.15	—	0.025	—	0.05
Si	—	1.00	—	1.00	—	0.15	—	0.50
Mn	—	1.00	—	2.00	—	0.15	—	1.00
W	—	—	14.0	16.0	—	—	3.00	4.00
P	—	—	—	—	—	0.015	—	—
S	—	—	—	—	—	0.010	—	0.010
Ti	—	—	—	—	—	1.0	0.50	3.50
Co			Balance					

Cobalt adds rigidity, hardness, and strength to the material. By producing a solid solution with cobalt (α), chromium hardens alloys and enhances resistance of corrosion via a passivation action. Molybdenum fortifies alloys by hardening and solid solution, improves homogeneity, and inhibits intergranular corrosion and surface pitting and decreases grain size. Nickel lowers the alloy's melting point, making it softer and more ductile. Si and Mn improve cast ability and fluidity[50].

Carbon of $Co_{28}Cr_6Mo$ (F75) alloy has favorable formation of carbides[51], which produces varied outcomes for (ASTM F75)[3]. It strengthens the alloy, enhances wear resistance by precipitation of carbide, increases tribocorrosion resistance, and corrosion resistance[13]. Carbides, on the other hand, absorb chromium during the solidification process. This results in a Cr-depleted zone along with the carbide, which is known as sensitization, despite the fact that the molybdenum concentration reduces the depletion process. The surrounding carbide regions are therefore exposed to localized assault by pits and crevices corrosion, which accelerates the corrosion rate[3].

2.12 Physical Metallurgy

Co has an atomic number of 27, an atomic weight of 58, a number of electrons/protons of 27, a neutrons number of 32, with a density of 8.9 g/cm^3 on average. It has (HCP) crystal structure. When properly completed and polished, the color of ASTM (F75) alloy is silvery white glossy. Casting shrinkage is 2.3 %. The melting and boiling point is 1495°C and 2907°C respectively. The CoCrMo alloy has two microstructures: FCC, which is stable at elevated temperatures, and HCP, which is stable at low temperatures up to 417°C. Because the transition kinetic from (FCC phase) to (HCP phase) is extremely slow at ambient temperature, quick cooling limits the creation of an HCP structure, and the majority of CoCrMo alloys utilized in biomedical field have metastable (FCC) matrix structures, such as a hip joint replacement. The rate of transformation is affected by alloying components and particular thermal processing parameters. When Ni, Fe, and C decrease the transformation rate (FCC stabilizers), while (Cr, Mo, and W) are added, the transformation rate increases (HCP stabilizers) [3].

2.13 Mechanical properties

Co-28Cr-6Mo alloy has excellent mechanical properties and high wear resistance compared with Ti alloys and stainless steels 316L due to the chemical compositions and manufacturing process [56]. The mechanical properties depend on the manufacturing process as presented in tables (2.3) for cast Co-28Cr-6Mo alloy. The strengthening of Co- 28Cr-6Mo alloy is provided by solid-solution strengthening and by precipitation of carbides [52].

Table (2.3): Comparison the mechanical properties of implant alloys to those of human bone [53].

Material	Tensile strength (MN/m^2)	Yield strength (MN/m^2)	Young modulus (GN/m^2)	Elongation at fracture %	Vickers hardness (HV)	Fatigue limit (GN/m^2)
Human Bone	137.3	-	30	1.49	26.3	-
316L SS (annealed)	650	280	211	45	190	0.28
Wrought Co-Cr-Mo	1540	1050	541	9	450	0.49
Cast Co-Cr-Mo	690	490	241	8	300	0.30
Titanium	710	470	121	30	-	0.30

2.14 Biocompatibility and corrosion resistance of Co-28Cr-6Mo.

When compared to stainless steel, Co-28Cr-6Mo offers superior corrosion resistance, particularly in the human body. It combines with high chromium concentrations to generate a rich passive oxide of chromium (Cr_2O_3) thin film with a thickness of 1.8 nm [52]. The film, which develops spontaneously on the surface of ASTM (F75) alloy, acts as a barrier to processes of corrosion. It isolates the surface of metal from the surroundings, resulting in excellent corrosion resistance. Furthermore, molybdenum content is used to increase pitting corrosion resistance. In the absence of passive films, the driving force for implant corrosion is very strong. The mechanical and chemical stability of implants in human bodies is directly connected to the integrity of these films. The resistance of corrosion of ASTM(F75) alloy is strongly connected to its biocompatibility [53,54].

2.15 Applications in Biomedicine.

CoCrMo alloy is extensively utilized in the manufacture of many types of devices or implants that are surgically inserted in vivo. They are utilized in dentistry for like dental root implants, detachable partial dentures, dental implants, dental wire, and screws. Support structures heart valve, suture, and pacer. orthopedic prosthesis, mini plates, bone plates for fracture fixation, artificial joints such as knee and total hip prosthesis replacements as shown in Fig(2.6)[50,56,57].

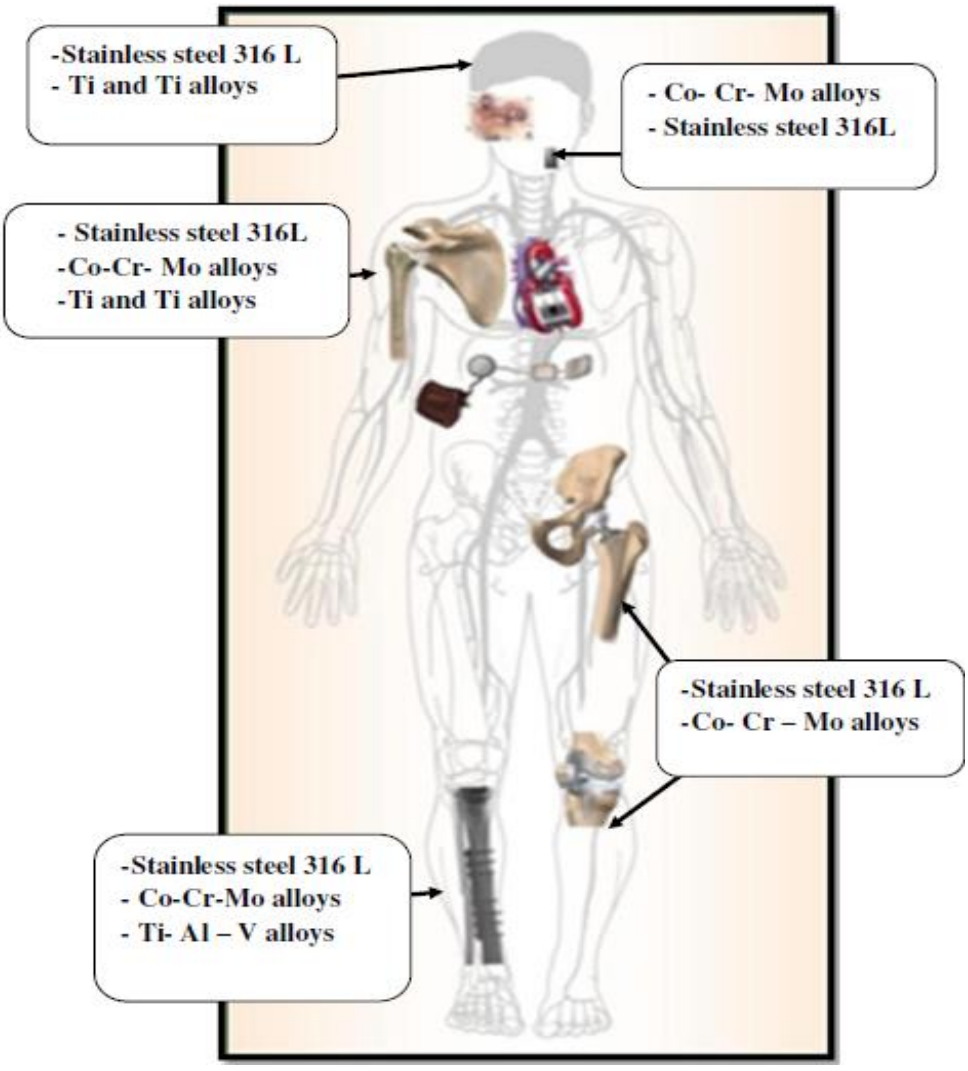

Figure (2.6): Alloys used in orthopedic implants in the human body [57].

2.16 Material of addition

2.16.1 Zirconia

Zirconium" (Zr) is a metal and the name comes from the Arabic word "Zargon," which means golden in colour. Zirconium dioxide (ZrO2) was accidentally identified by the German chemist Martin Heinrich Klaproth in 1789, while he was working with the heating of some gems. Zirconia has been used as biomaterial since the 1970s. It has been widely used as a hip replacement material and has been used in dentistry for crown and bridge applications since 2004[58]. It has high melting point 2900°C and low density value (5.68 g/cm^3) [59].

It has mechanical qualities comparable to metals and a hue akin to tooth color. The mechanical characteristics of zirconia are comparable to those of stainless steel. It has a traction resistance of up to 900-1200 MPa and a compression resistance of about 2000 MPa. This material can also withstand cyclical pressures. Cales discovered that applying an intermittent force of 28 kN to zirconia substrates required 50 billion cycles to break the samples, but with a force greater than 90 kN, structural breakdown of the samples happened after just 15 cycles. [60].

When combined with UHMWPE, zirconia showed excellent biocompatibility as well as good wear and friction. It is tough, abrasive, and corrosion resistant[61].

Some mechanical properties comparable to or better than those of alumina ceramic. Zirconia, like other ceramics, is very biocompatible and may be used to make big implants such as the femoral head and acetabular cup in total hip replacement[1]. Crowns and bridges, prosthetic knees, bone screws and plates[62].

Zirconia's decreased modulus of elasticity and increased strength make it an attractive material for load-bearing prostheses. There is insufficient evidence to evaluate if these features will result in increased clinical success rates over an extended period of time (>15 years)[63].

2.17 CoCrMo (F75) alloy manufacturing process.

2.17.1 Investment casting.

This alloy is widely utilized in biomedical and aeronautical applications. It is often formed into the final device via an investment casting method, which includes the use of wax as an initial mold for the final device. The wax mold is then covered with ceramic before being melted, resulting in a ceramic mold. At 1350–1450 °C, the alloy is melted and poured into this ceramic mold. The ceramic is torn away after solidification, and the metal is further treated to produce the finished gadget. Depending on the casting circumstances of F75 alloy, three distinct microstructural characteristics that tend to degrade the alloy's mechanical qualities have been found. (a) Co-rich matrix including interdendritic and grain boundary carbides such as $Mo_{23}C_6$, $Cr_{23}C_6$, or $Co_{23}C_6$. There may also be interdendritic Co- and Mo-rich sigma inter-metallic and Co-based gamma-phases. (b) The grain sizes are large. This is a major limitation since it decreases the tensile strength of the alloy. (c) There are casting flaws. Under in vivo circumstances, such flaws might result in implant fatigue fracture[6].

2.17.2 Powder metallurgy

Powder Metallurgy (PM) is a well-known method for producing small, complex shapes. This might be one of the most significant application domains for this technology, where recently, the great majority of industrial components have been manufactured using PM manufacturing technologies, which create a simple production pathway by compressing the powder in dies followed by a sintering phase. This manufacturing approach might be referred to as the mass production PM technique, in which cost is the primary consideration and properties, which are always subordinate to technical requirements, are the second level of request[65].

The processing performance of metal powders and the qualities of the products are reliant on the parameters of the metal powders utilized, such as particle size, particle size distribution, particle shape, compressibility of powders, apparent density, and purity of powders[66].

The main steps to manufacture parts by PM process shown in Figure (2.7). The steps include: blending and mixing of powders, cold compaction, and sintering [67].

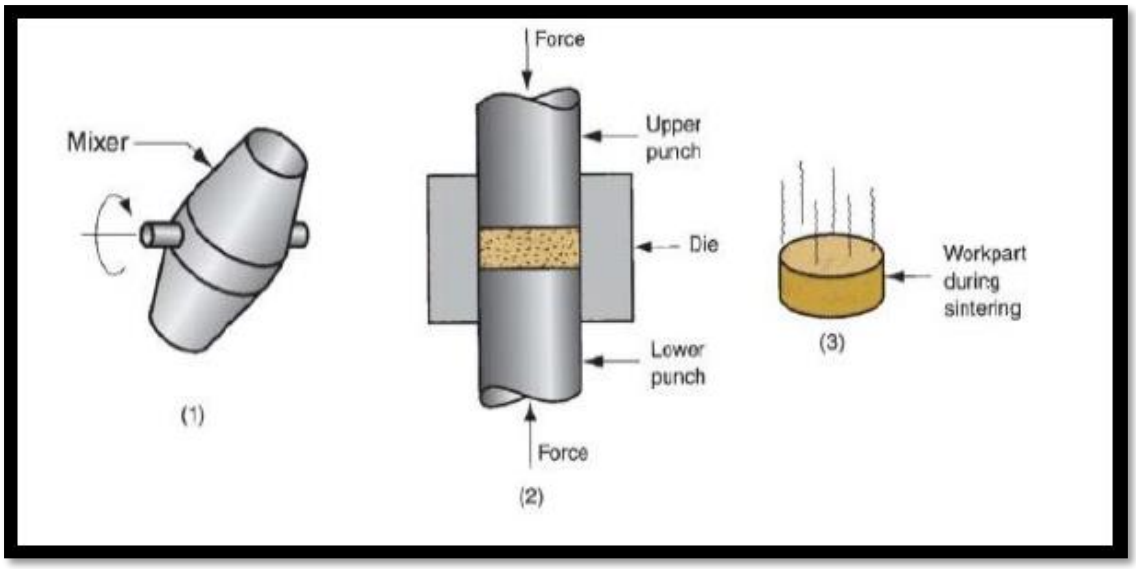

Figure (2.7): Basic Steps of Powder Metallurgy Technique: (1) Mixing of Powders, (2) Pressing of Powders, (3) Sintering[67].

1. Powders blending and mixing

Metallic powders must be properly homogenized prior to compaction and sintering in order to get optimal results. Blending is a process that involves the mixing of powders that have the same content or material but may have varying particle sizes. Distinct particle sizes are often combined to minimize porosity, whereas mixing is described as the process of combining powders of two or more different materials[68].

The mixing procedure is used to achieve the most homogenous distribution of powders in the shortest amount of time feasible. The time required for mixing might range from a few minutes to 24 hours or even many days, depending on the intended outcome. Prolonged mixing results in particle work hardening, which must be avoided. Mixing may be either dry or wet. Wet mixing is used to produce a uniform mixture of powder particles. It may be produced by adding sufficient alcohol, benzene, or acetone as a liquid medium to the powder to give it the consistency of a thin paste. Following completion of the mixing operation, benzene or acetone is removed by the air or heated to 50°C in a controlled oven[69].

2. Compacting of the Powders

Compaction is the shaping stage that allows for the creation of very complicated geometries with adequate strength to resist ejection from the tools and subsequent handling up to the point of sintering completion without breaking or damage. The pressure is necessary to compress the green compact where

determined by the material and the properties of the powder employed. The compacting process must be structured in such a way that pressure is distributed uniformly over the affected region[70]. The portion of the compact after compacting is referred to as a green compact and it has a density known as the green density. Figure (2.8) depicts the impact of the compaction pressure[68].

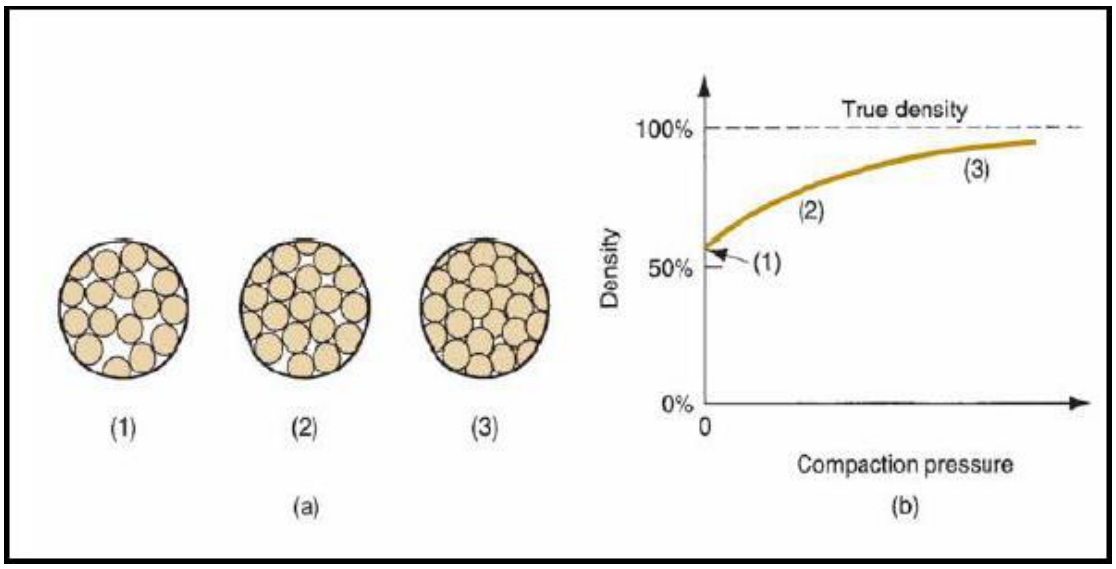

Figure (2.8): (A) Effect of Pressure on Particles Arrangement during Compaction; (B) Powders Density as a Function of Pressure [68].

3. Sintering

Sintering is a heat treatment procedure used to bond the metallic particles in the green compact in order to strengthen its strength and hardness. The treatment is typically carried out at temperatures between 0.7 and 0.9 of the metal's melting point. There are two kinds of sintering processes: Sintering in the solid state and sintering in the liquid phase. The solid-state sintering, which termed when the metal remains un-melted at the treatment temperatures. The liquid-state sintering termed when a minor constituents become molten at the treatment temperature, the amount of liquid phase must be limited so that the part retains in shape[71]. Figure (2.9) shows depicts the changes that occur during the sintering of metallic particles on a microscopic scale[68].

The difference in chemical or potential free energy between the free surface of the particles and the contact sites of connected particles is the driving factor for solid state sintering[72].

The rate of particle bonding during sintering depends on temperature, materials, particle size. Small particles are more energetic, so they sinter faster.

Parameters such as surface area and particle size, time temperature, pressure and atmosphere, green density, are effective parameters during sintering[73].

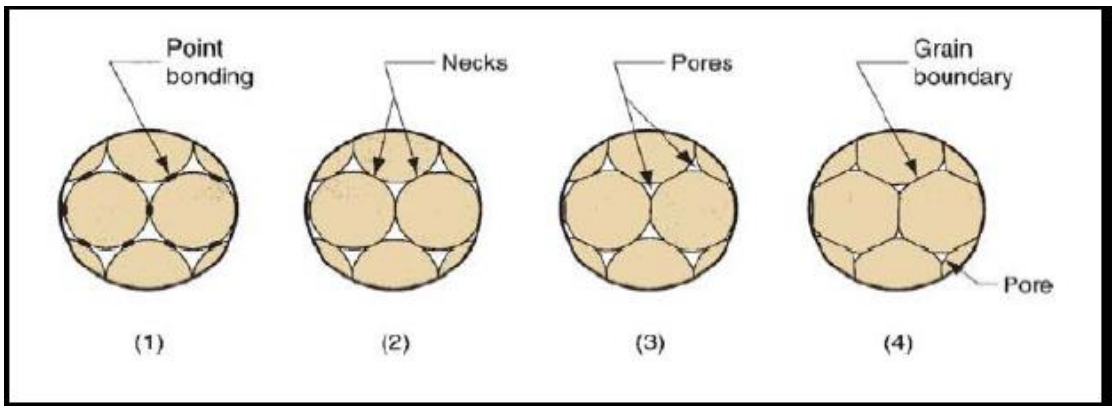

Figure (2.9): Changes that occur during the sintering of metallic powders: (1) Particles begin to bond at the Contact Region; (2) Contact Regions develop into Necks; (3) Pores between Particles get smaller; and (4) Grain Boundaries between Particles develop in place of Necked Regions [68].

2.18 Advantages and limitations of powder metallurgy

PM is an important commercial technology and this because of the following considerations:

1. PM components may be accumulated and manufactured in net or near-net shape, obviating or reducing the need for future machining [74].
2. PM is one of the most advantageous casting methods in terms of dimensional control, with regular tolerances of + 0.13 mm[68].
3. With PM parts, a certain amount of porosity may be achieved in the fabrication of porous metal components such as gears, filters, and oil-impregnated bearings [75].
4. Certain metals that are difficult to form using conventional processes may be shaped using powder metallurgy, for example, tungsten filaments for incandescent light bulbs [76].
5. PM differentiates via its manufacturing process, since some alloy combinations and cermet manufactured by PM cannot be fashioned in any other manner. [77].
6. The PM process wastes little ingredients; about 97 % of the starting powders are transformed to product. This compares well to casting procedures that use sprues, runners, and risers[68].
7. Powder metallurgy manufacturing processes may be mechanical for economical manufacturing [75].

There are certain limitations to PM processing[78]:

1. Due to the fact that the compacted components must be evacuated from the die without fracture, the forms that may be created using this process are restricted.

2. Due to the relatively high compacting pressures necessary to press the powder, the dies are subject to significant wear.

3. Due to the high rate of die wear and the expensive cost of dies and presses, this technique is uneconomical for short runs.4. A completely dense product is not possible without heating the product after pressing operation.

5. The equipment required is highly expensive.

6. This method produces physical properties that less than those produced by other methods.

7. Occasionally, thermal difficulties occur with low melting powders such as zinc, tin, and cadmium.

8. Many metal powder is explosive at room temperature.

2.19 Literature Review

Biomaterials were presented to the scientific community at Clemson University and garnered significant interest due to their potential to improve people's health. For example, complete hip replacement is advised for those who have medical difficulties due to severe acetabular wear, osteoarthritis, an accident, or advanced age. Annually, around 230000 total hip arthroplasties are performed, expected to climb over the next several decades. Degeneration happens in human joints due to specific events such as the lack of a biological self-healing mechanism, wear, or severe loading. According to reports, the number of persons affected by these issues grew sevenfold between 2002 and 2010. By the end of 2030, it is anticipated that demand for hip and knee constructed of Co and Ti-based alloys will grow by 174 percent (57200 operations) and 673 percent (3.48 billion operations), respectively [79].

In 2004, Aleksadra Kocijan et.al [80]] used X-ray photoelectron spectroscopy to investigate the passive layer's composition (formed by electrochemical oxidation at different passivation potentials on CoCrMo and CoNiCrMo alloys in simulated physiological solution with and without the complexing agent (EDTA)). Where was determine the composition as a function of depth, cationic fraction and thickness of the passive film. On both CoCrMo and CNiCrMo alloys, chromium oxide is found to be the major component of the passive layer. The passive layers' minor constituents, Co and Mo oxides in the case of Co-Cr-Mo alloys and Ni, Co, and Mo oxides in the case of Co-Ni-Cr-Mo alloys, are also present in the layer's outermost part. EDTA has an effect on the formation of the passive layer on each alloy. In the presence of EDTA, the stability of the passive layer is reduced.

In, 2004 Hanawa et.al[81]**.** Conducted a study on the metal ion release from biometallic implanted into the human body, including Co Cr alloy, titanium, and titanium alloys and stainless steel. The review demonstrates that surface oxide films on metallic objects act such a blocker of release of ion and they transform with the release in human body. Additionally, the research concluded that metal ion release might be hastened by the inorganic ions, low concentrations of dissolved oxygen, cells, and proteins. The review concludes by stating that an active ion rapidly reacts with a molecule of water or a nearby anion to generate a hydroxide, oxide, or inorganic salt. This is because the ions of metal released do not always react with biomolecules to produce toxicity. As a result, cytoxicity,

allergies, and other biological impacts have a minimal probability of combining with biomolecules and causing these effects.

In 2005, Robert Wen et al. [82]**.** Investigated the electrochemical corrosion of cast Co28Cr6Mo ASTM (F75) implant alloys in several the body fluids (urine, joint fluid and serum) using a potentiodynamic scan, cyclic voltammeter and impedance spectroscopy. In three biological solutions, current densities of corrosion of the CoCrMo implant ranged between 1.65 and 2.59 A/cm2. The findings of the impedance and Tafel analysis plots revealed the same results. It is determined that the corrosion resistance of the CoCrMo implant alloy is superior to that of urine in serum and joint fluid at 37°C.

In 2005, Lucien Reclaru et al.[52]**.** Investigated the corrosion resistance of Co28Cr6Mo alloy ASTM F75 prosthesis implants coated with Ti plasma spray. Electrochemical methods were used to determine the open circuit voltage, polarization resistance and corrosion current density. Ti coatings applied by vacuum plasma spraying or sintering had a unique porous morphology, and the implants displayed significant corrosion activity.

In 2008, Dourandish et al.[83] Investigated the progressive sintering of biocompatible CoCrMo alloys for composite structures of porosity graded. The structure of composite has a porous layer that promotes tissue development and a strong core. 19 and 63 μm as an average of particle size were utilized to evaluate the process. The sintered specimens' microstructures were characterized. The findings suggested that a sintering temperature of 1280C° for 120 minutes combined with the use of argon might be used to create composite layers with varying porosity, such as a solid core (5% porosity) surrounded by a porous layer (33 %porosity).

In (2008), Valero Vidal and Lgual Munozet al.[84]. Studied compared the electrochemical corrosion behavior of Co28Cr6Mo and AISI 316 L alloy in different simulated fluids to assess the corrosion of biomaterial alloys for surgical implants, and simulated fluids was KCl + NaCl + KH_2PO_4 + Na_2HPO_4, albumi +NaCl, KCl + albumi + KH2PO4 +NaCl + Na_2HPO_4, albumi +NaCl, KCl + albumi + KH_2PO4 +NaCl + Na_2HPO_4. The purpose of this comparative is to examine the effect of immersion duration (5, 10, 15, 20, 25 hr.) and solution chemistry on passive behavior when electrochemical methods are applied. The corrosion resistance of AISI 316L declines with age, but the resistance of corrosion of the Co28Cr6Mo alloy rises.

In (2010), George Bellefontaine et al.[3]**.** Studied the corrosion behavior of Co28Cr6Mo ASTM (F75) alloy for hip joints replacement. The influence of cast and double heat treatment on the behavior of corrosion and microstructure of Co28Cr6Mo alloy were compared. A software simulator was used to investigate corrosion behavior. For the hip simulator, open circuit potential. and potentiostatic techniques were also used, utilize 3.5 % sodium chloride and 28 % bovine. In an articulating hip simulator under load, 28 % bovine serum is less corrosive than 3.5% NaCl. The Open circuit potential test revealed that there is no discernible varies between the double heat treated and cast condition

In 2015,H.jamal Al-deen et al. [85]**.** Investigated the effects of the addition (0.5, 1, and 1.5) of Y on the wear, corrosion, and compressive strength behavior of CoCrMo (F75) alloys, which were prepared by P/M. This research revealed that increasing the amount of Y results in a decrease in hardness, an increase in porosity and a decrease in compressive strength. The addition of Y improves wear resistance, and the improvement increases as the Y content increases. The addition of Y enhanced the corrosion resistance of F75 alloy in both artificial saliva and Hank's solution, the improvement increased as the amount of Y added increased.

In 2018, H. Jamal Al-Deen et al.[86]**.** Studied the influence of adding indium (0.5, 1, 1.5, and 2%) on the properties of the ASTM (F75) alloy, which was made by powder metallurgy method. wear behavior and the rate of corrosion were studied by mechanical and electrochemical tests. The study found a decrease in the porosity an increase in hardness, improved wear resistance, and improved corrosion resistance in both solutions (Hank's solution and synthetic saliva) with increased indium addition.

In 2014, Z. Doni et al.[87]**.** Studied effect of adding Al_2O_3 (5 and 10 %) on the triboelectrochemically characterize of CoCrMo alloy by powder metallurgy method. Corrosion and tribocorrosion behavior of the composites were investigated in 8 g/L NaCl solution at body temperature.Corroded and worn surfaces were investigated by a field emission gun scanning electron microscope equipped with energy dispersive X-ray spectroscopy. After tribocorrosion experiments, wear rates were calculated using a profilometer. Results suggest that Al_2O_3 particle addition decreased the tendency of CoCrMo alloy to corrosion under both static and tribocorrosion conditions. However, no significant influence on the corrosion and wear rates was observed in composites mainly due to increased porosity and insufficient matrix/reinforcement bonding.

2.19 Summary of literature review

For the importance of CoCr alloys in medical fields, there are many scientific research to strengthening such alloys and improve their properties. Many researchers improved the mechanical and Chemical properties of CoCr alloys especially Co28Cr6Mo(F75) alloy however each study is looking at different topic that is not specifically related to the current study investigation by heat treatment, forming, coating or Nano ceramic particles.

Most of the literature review studies highlight the importance of CoCrMo alloy and its specialties and what are the main characteristics about such an alloy. The collection of the previous studies selected in this chapter looked at variety of aspects including different elements, techniques and even different topics, which give a broader understanding and a general picture about the whole subject.

CHAPTER THREE

Experimental Work

Chapter Three

Expe rimental Work

3.1 Introduction

This part explain empirical procedure and work equipment used in this research. Preparation samples style, surface operation and tests like XRD and microstructure characterizations, hardness, wear and corrosion resistance elucidated in detail.

3.2 Materials

The materials that it was used to prepare CoCrMo ally (F75) are listed in the table (3.1) that show powders and its purities with average particle size.

Table (3.1): Purities and average practical size of powders.

Powders	Average particle size(μ)	Purity%
cobalt	4.873	99.95
Chromium	10.93	99.95
Molybdenum	12.76	99.9
Nickle	52.31	99.44
Manganese	43.26	99.39
Silicon	51.47	99.11
Iron	59.34	99.78
Carbon	37.44	99.44
Zirconia	0.495	99

3.3 Design and procedure of experimental work.

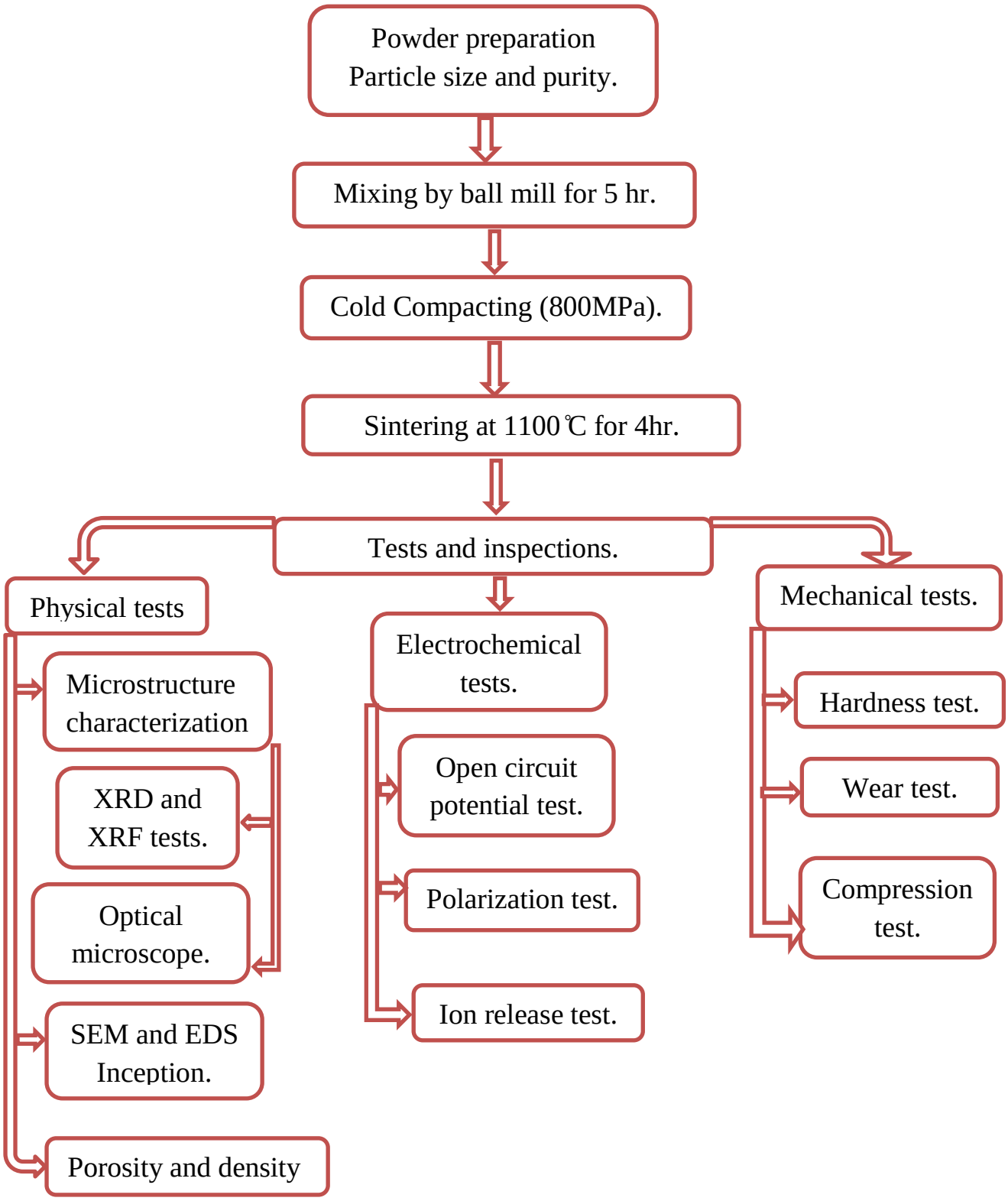

Fig (3.1) depicts the Experimental Procedures Diagram.

3.4 Analyzer of particles size

The Bettersize 2000 laser particles size-measuring instrument was used to determine the average particles size. The powder placed in the dispersed liquid and then placed in the measuring device, which gives the average particle size of the powder as shown in Fig (3.2). Located in the college of engineering materials Laboratories of the Department of ceramic - University of Babylon. The red curve shows the normal distribution for particles size and the blue curve shows accumulated distribution for particles size.

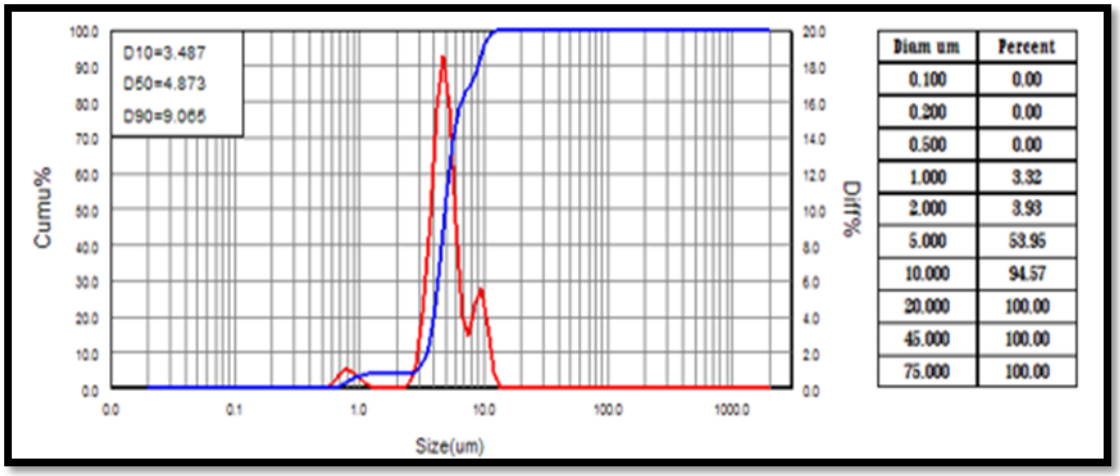

Diam um	Percent
0.100	0.00
0.200	0.00
0.500	0.00
1.000	3.32
2.000	3.93
5.000	53.95
10.000	94.57
20.000	100.00
45.000	100.00
75.000	100.00

(a)

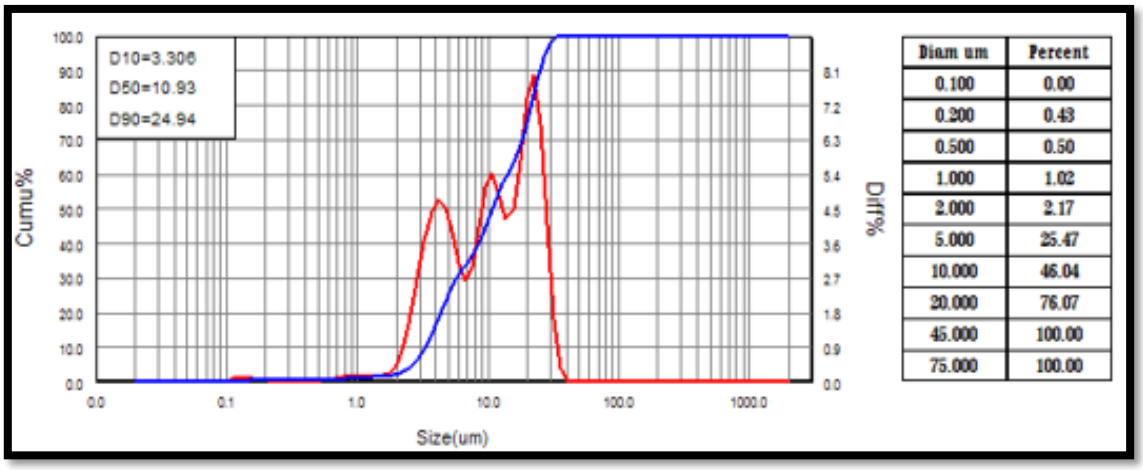

Diam um	Percent
0.100	0.00
0.200	0.43
0.500	0.50
1.000	1.02
2.000	2.17
5.000	25.47
10.000	46.04
20.000	76.07
45.000	100.00
75.000	100.00

(b)

Fig (3.2): average of size particle for material (a) Co, (b) Cr, (c) Mo and (d) ZrO_2.

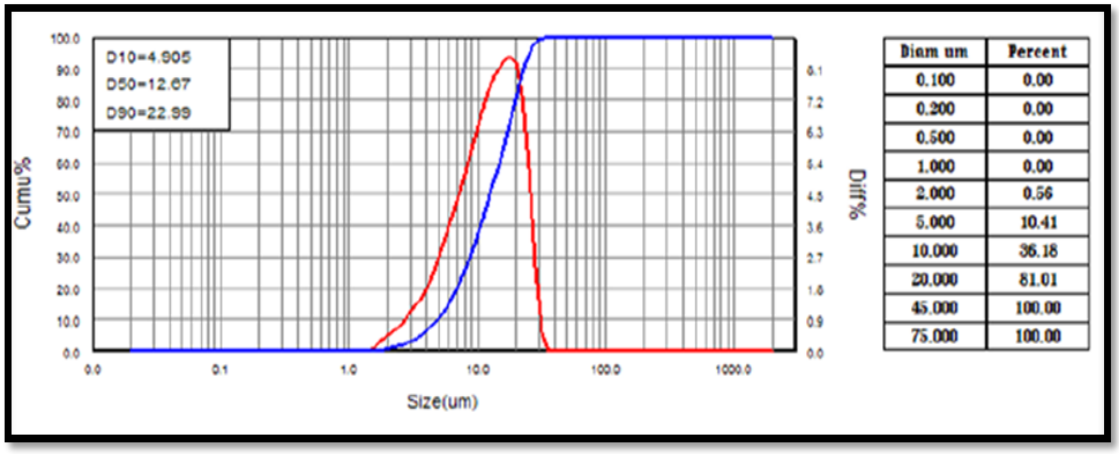

(c)

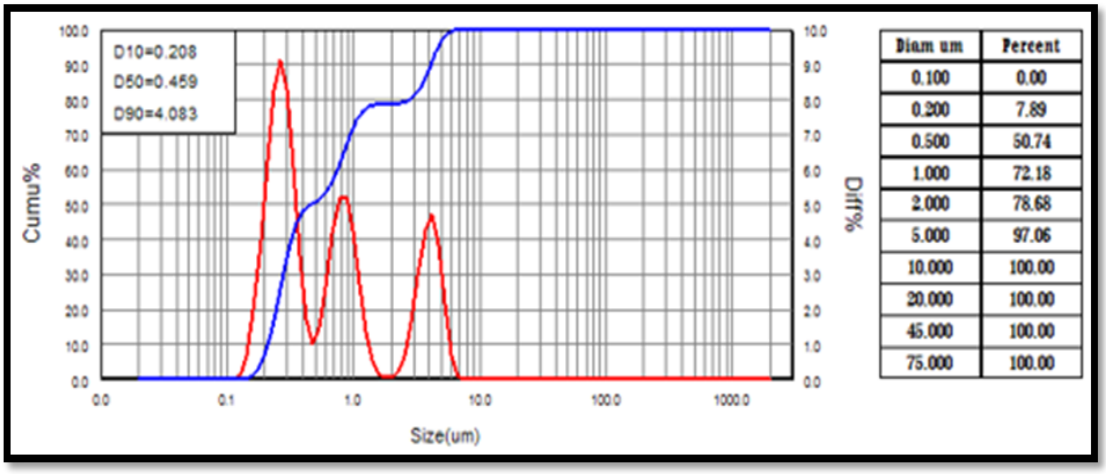

(d)

Continues

3.5 powders weight

Delicate Balance type (L220S– D), with (± 0.0001 accuracy) (German made) was utilized to weight each amount of powders before mixing. These powders were used to prepare CrCrMo (F75) alloy (28%Cr, 6%MO, 2.5 %Ni, 1%Mn, 1%Si, 0.75%Fe, 0.35C and balance Co), the composition and code of the alloys, which are utilized in this study, are shown in Table (3.2).

Table (3.2): The Composition and Code of the Alloys

Sample coding	Alloy Compositions %								
	Cr	Mo	Ni	Mn	Si	Fe	C	ZrO_2	Co
B	28	6	2.5	1	1	0.75	0.35	-----	Balance
A1	28	6	2.5	1	1	0.75	0.35	0.5	
A2	28	6	2.5	1	1	0.75	0.35	1	
A3	28	6	2.5	1	1	0.75	0.35	1.5	
A4	28	6	2.5	1	1	0.75	0.35	2	
A5	28	6	2.5	1	1	0.75	0.35	2.5	
A6	28	6	2.5	1	1	0.75	0.35	3	
A7	28	6	2.5	1	1	0.75	0.35	3.5	
A8	28	6	2.5	1	1	0.75	0.35	4	
A9	28	6	2.5	1	1	0.75	0.35	4.5	
A10	28	6	2.5	1	1	0.75	0.35	5	

3.6 Mixing of powders

Wet mixing of powders was accomplished using a planetary automated ball mill and stainless steel balls of varied sizes were employed for 5 hours to provide an even and homogeneous distribution of powder particles. Acetone was added to wet the medium of mixing.

3.7 Powders compacting.

Mould (12mm) diameter made from stainless steel was employed to execution of the process of compacting as shown in (3.3a), and by electric-hydraulic press one channel device, type: CT340-CT440, American as shown in Fig (3.4). (3g) of mixture was compacted with pressure (800Mpa) [88]. The holding time was (4min) to create a disk spaceman with a diameter and thickness of 12mm and 4.5mm, respectively are shown in (3.3b). Graphite is used as a lubricant in the pressing process to minimize friction.

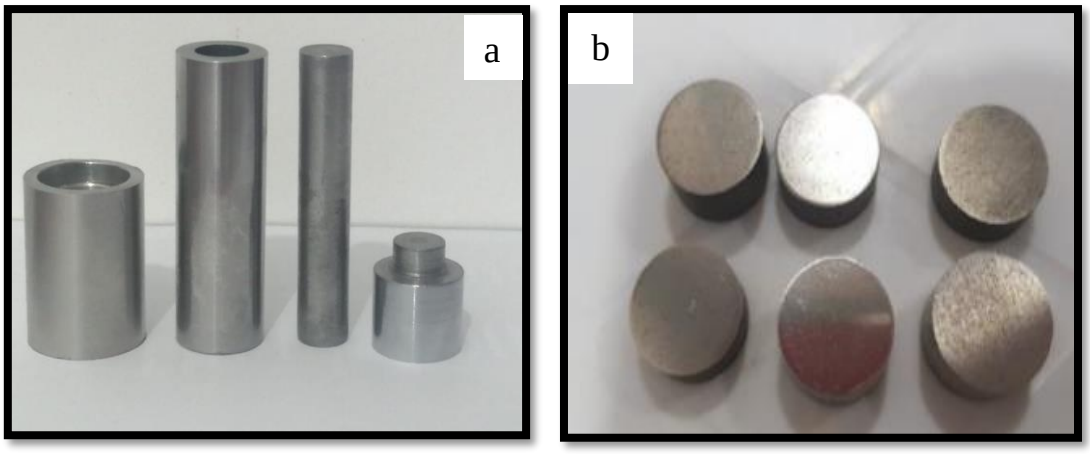

Figure (3.3): (a) Mould used in the compacting process. (b) Green compacts.

Figure (3.4): Electric Hydraulic. Press One Channel, CT430-CT440.

3.8 Sintering process.

A tube furnace was used to conduct the sintering procedure, which included heating the material from ambient temperature to 1100 °C with heating rate 5°C per minute and stay time for 4 h in an argon atmosphere to inhibit the specimen's oxidation. Afterwards, slow cooling in the furnace with continues argon circumstances to the room temperature. As shown in Fig (3.5). The samples after sintering process are shown in Fig (3.6).

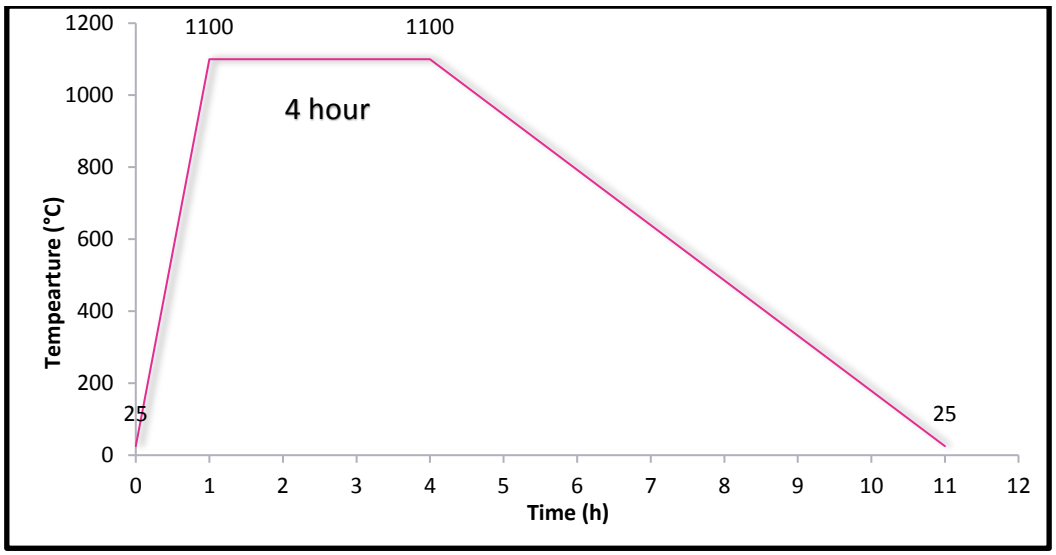

Figure (3.5): Heating Cycle in Sintering Process.

Fig (3.6): the specimens after sintering process.

3.9 The preparation of specimens for testing

Following the sintering process, the samples were grinded using silicon carbide papers with grits of (320, 400, 600,800, 1200, 1500, 2000, 3000), and then polished using a 3µm diamond past and polishing pads to achieve a bright surface for the final stage.

The following solutions were used to etch the specimens as shown in table (3.3). The prepared specimens swabbed for 20 seconds in the etching solution, then rinsed with ionic water and dried, providing them for microstructure studies.

Table (3.3): Etching Solution Chemical Composition[89].

Number	Constituent	ML
1	Acetic acid	15
2	water	15
3	HCl	60
4	HNO_3	15

3.11 Microstructure characterization

3.11.1 X-Ray Diffraction (XRD).

An XRD machine (type XRD-6000 Shimadzu) was used to know the composition and determine the phase of each sample, as shown in fig (3.8). The XRD generator was set to (40) kV and (30) mA, with a speed of scanning 5° /min. The rate of scanning ranged from 30 to 100. This test was conducted at the Ministry of Science and Technology.

3.11.2 Light Optical Microscope (LOM)

The microscopic structure was studied using optical microscopy in order to identify the existing phases and to see the shape and size of the grains, after grinding, polishing and etched in a solution (swab). This test was done at specimen's preparation laboratory, the microscope is type (BEL PHOTONICS), Located in the college of engineering materials Laboratories of the Department of Metallurgical - University of Babylon.

3.11.3 SEM& EDS inception

The surface composition and topography of alloys were obtained using SEM, where the specimen was imaged using a high-pack of electrons, and the analytical technique that was used for chemical analysis and elemental analysis of the implant's surface after sintering was done using Energy-dispersive spectroscopy EDS. The EDS device was linked to the SEM, and the inspection took place concurrently with the SEM observation. The test was carried out at Babylon University/College of Pharmacy.

3.11.4 Sintered Samples' True Density and Porosity.

1- After 5 hours of drying at 100 °C in a drying oven, the samples are cooled to room temperature while they are inside the oven. The dry mass of the sample is Y.
2- At ambient temperature, utilizing an evacuation pump that specifically designed for this purpose. For 30 minutes, the pressure was reduced over the specimen while it was submerged in oil.
3- The specimen was totally submerged and weighted. As mass, X.
4- Weighting the sample in water as mass F.
5- Finally, the porosity is calculated as[90]:

$$p = [\frac{X-Y}{(x-F)D^{\circ}} * 100]Dw \quad \text{(3-1)}$$

$$\rho = \left(\frac{Y}{X-F}\right)Dw \quad \text{(3-2)}$$

Where:

Dw = water density (1 g/cm^3)

D^0= oil density (0.8 g/cm^3)

ρ= true density

3.12 Mechanical tests.

3.12.1 macro-hardness test

The hardness of the samples was determined using a Macro-hardness Brinell tester (Germany made) with an applied load of (*31.25*) kg/mm^2 and a diameter ball of 2.5 mm, with an implantation duration of (10 sec) in the condition of applied weight. Three measurements were collected for each specimen, and the average value is utilized to analysis the alloys' behavior. This device located in the metals laboratory in the Laboratories of the Department of Metallurgical Engineering -University of Babylon.

3.12.2 Dry sliding wear test.

After one hour of drying in a drying oven set to 100 °C, the specimens were stored in well-knit boxes lined with material of silica gel to ensure complete drying. This test was conducted employing the pin on disk concept with (350 rpm) and a constant radius (*8 mm*) with various sliding distances and loads (*20N, 25N, and 30N).* Prior to testing, the sample was weighted using a (*0.0001*) precision electric balance. The samples tested were weighted after a period of (*5, 10, 15, 20, 25, 30, 35 and 40*) min, and the volume loss was computed using

equation (3-2). Figure (3.7) depicts the device used in this work, located in the metals laboratory in the Laboratories of the Department of Metallurgical Engineering -University of Babylon. The test procedure has been validated in accordance with ASTM G 99[91].

Volume loss= $\frac{weight\ loss(g)}{\rho(\frac{g}{cm^3})}$ …….. (3-2).

Where:

Loss of weight (g) = loss quantity after (5, 10, 15, 20, 25, 30, 35and 40) min.

ρ = *True density.*

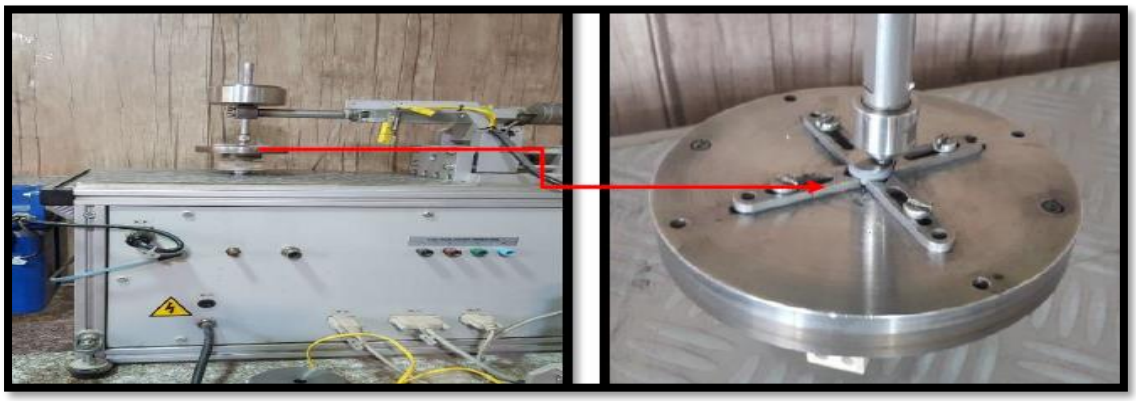

Figure (3.7): Pin –on – Disk Wear Instrument.

3.12.3 Compression test

Compression testing was performed in line with ASTM standards at room temperature (D695-85). Using a computerized electronic universal testing equipment, type (WDW 200, No. W1124), located in the metals laboratory in the Laboratories of the Department of Metallurgical Engineering -University of Babylon. The specimen dimensions are (12 *mm* in diameter and 18 *mm* in height), and the specimens were vertically positioned between the jaws to determine compression strength. The experiment was conducted at a constant loading rate of one millimeter per minute. Compressive strength is determined using the following calculations[92]:

$comperssive\ strength = \frac{\max force(N)}{cross\ sectional\ area(mm^2)}$…… (3-3).

3.13 Electrochemical tests

The corrosive behavior of CoCrMo was studied in various solutions (Hank's solution and synthetic saliva). Tables (3.4) and (3.5) show the chemical compositions of Hank's solution and synthetic saliva, respectively. Synthetic saliva and Hank's solution had PH 6.7 and 7.4, respectively, at 37 °C.

Table (3.4) Chemical composition of artificial saliva solution[93].

No.	Constituent	Constituent/L.
1	NaCl	0.4
2	KCl	0.4
3	$NaH_2PO_4.2H_2O$	0.906
4	$Na_2S.9H_2O$	0.005
5	urea	1

Table (3.5) Hank's solution's composition[94].

Number.	Constituent.	Constituent/L.
1	*KCl*	0.4
2	$Na_2HPO_4.2H_2O$	0.06
3	*NaCl*	8
4	$NaHCO_3$	0.35
5	$MgSO_4.7H_2O$	0.06
6	$MgC_{12}.6H_2O$	0.1
7	$CaCl_2$	0.14
8	KH_2PO_2	0.06
9	*Glucose*	1

3.13.1 Open circuit potential (OCP)

In a cell 500-ml electrolytic glass cell, specimens were immersed in synthetic saliva and again in Hank's solution. The potential difference between the working and reference electrodes (saturated calomel electrode) was measured by connecting a voltmeter between them and reading the information every 5 minutes after the first reading until the voltage was stable for each specimen.

3.13.2 Potentiodaynamic polarization.

The experiment took place in a three-electrode cell filled with synthetic saliva, then with Hank's solution. According to ASTM F746-04, used (reference, counter and work) electrodes are SCE, platinum and the specimen respectively. Potentiodynamic polarization charts have been drawn, as well as (I_{corr}.) and (E_{corr}.) were calculated using Tafel plots with anodic and cathodic polarization with

range (±350mv) and rate of scanning 1mv/sec. The rate of corrosion may be determined using the following equation[85].

$$corrosion\ rate = \frac{0.13\ icorr(Ew)}{\rho}$$

Where:

E. w= Weight of equivalent (g/eq.).

ρ= True density.

$i_{corr.}$ = Corrosion current density ($\mu A/ cm^2$).

0.13 = Metric and time conversion factor.

3.13.3 Metals Ions Release (Static Immersion Tests)

The test of ion release was carried out of alloys (F75, A4, A10) by immersing in the simulated body fluid (synthetic saliva and Hank's solution) at the temperature 37±1°C for 21 days[95]. The samples were immersed in small containers containing 50ml of each solution, and these containers are immersed in a larger container with a controlled water temperature to maintain a temperature of 37°C±1. This test was carried out in accordance with the current JIS T- 0304 metallic biomaterial requirements[96].

Assessing the metals ion (Co) concentrations by Atomic Absorption flame.

CHAPTER FOUR

Results and Discussion

Chapter Four

Results & Discussion

4.1 Introduction

Experimental results have been demonstrated in this chapter which involve the properties related to the specimens that were prepared by powder metallurgy technique.The physical tests which incloude phase's analysis from XRD technique, microstrcture characteristic from light optical microscope, SEM and EDS, porosity and true density of sinterd samples. The mechanical tests that include hardness and dry sliding wear tests and compression test. Electrocemical test that invlove open circuit potential test, polarization test. ion release test. Biolegical tests and which include antibacterial test.

4.2 Powder characterization

Its conatin the follwing tests:

4.2.1 X-Ray Diffraction (XRD) of pure powders

Figures (4.1), (4.2), (4.3) and (4.4) illustrate the X-ray diffraction for the used Cobalt, Chromium, Molybdenum and zirconia powders respectively. The shown patterns matched to the standard patterns for mentioned powders, to make sure that the powders used in this research are within the required phase specification.

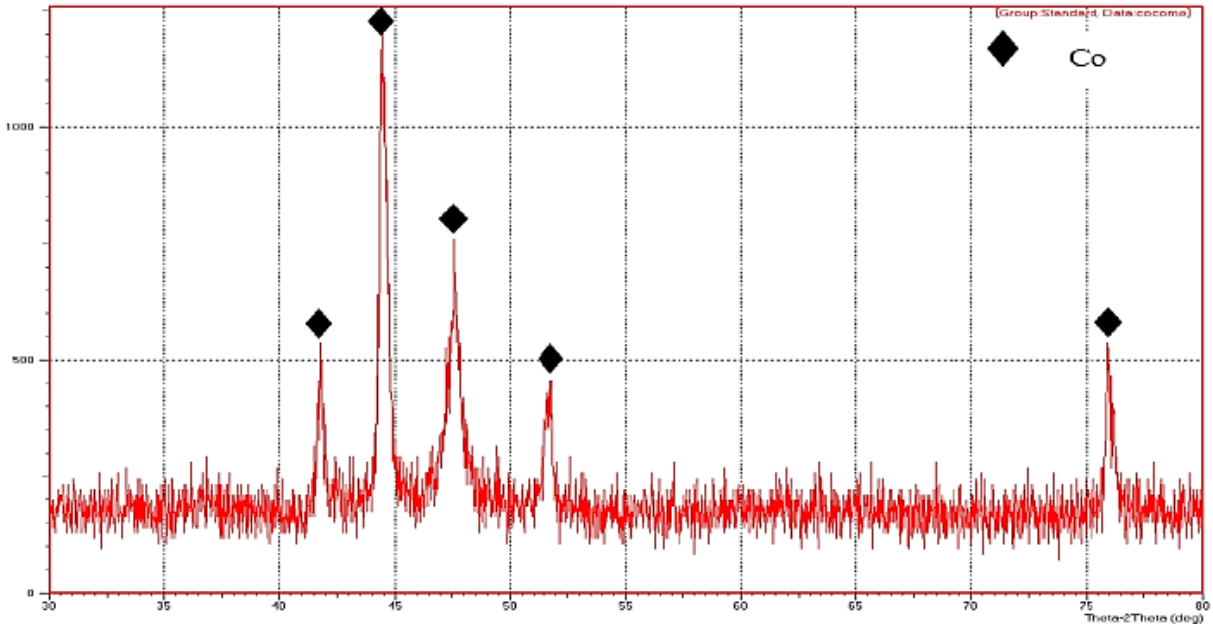

Fig (4.1): XRD pattern of Co powder.

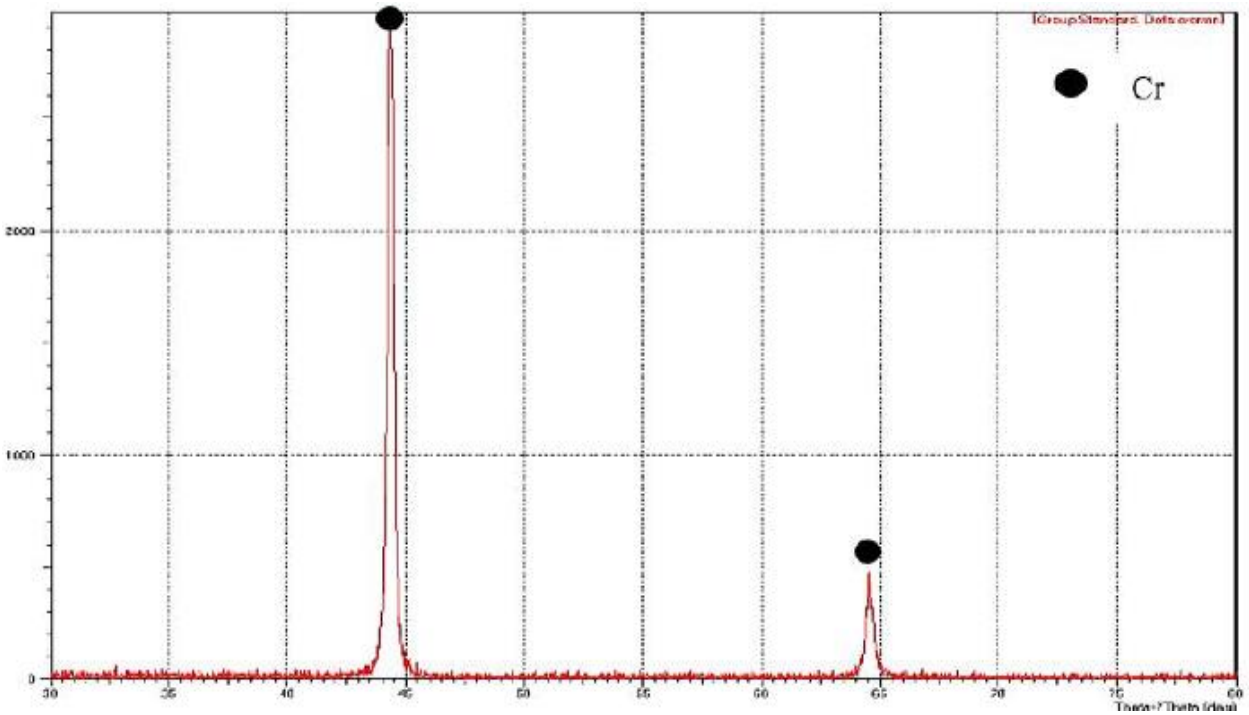

Fig (4.2): XRD pattern of Cr powder

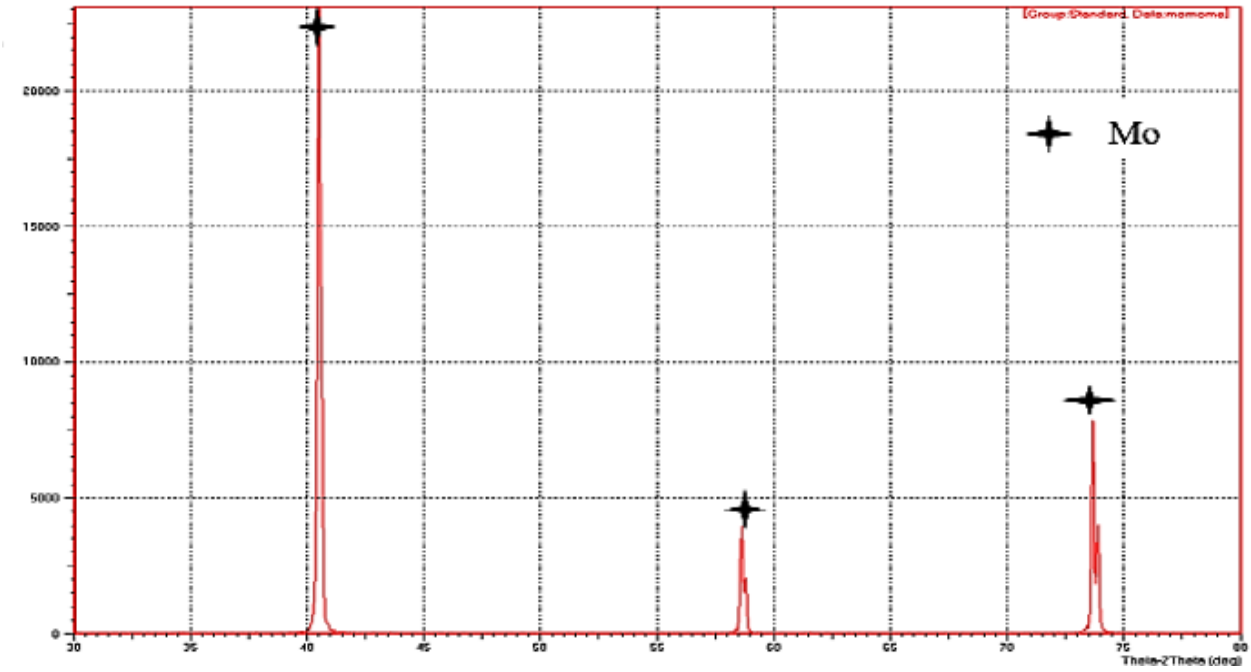

Fig (4.3): XRD pattern of Mo powder

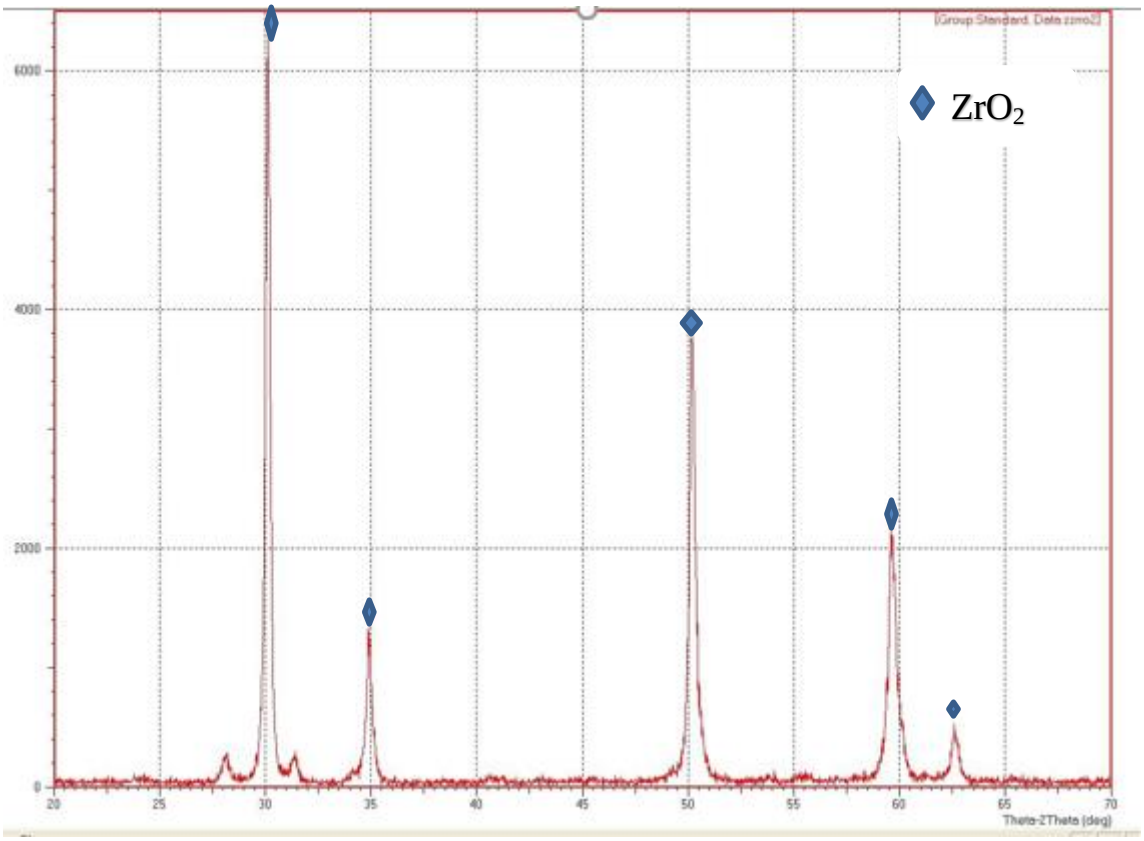

Fig (4.4) XRD pattern of ZrO_2 powder.

4.3 Characterization of Microstructure of alloys

4.3.1 X-Ray Diffraction Analysis

The main objective to analyze X-ray diffraction was to determine the phases present in sintered specimens to analyze the microstructure of the studied CoCrMo base alloy and CoCrMo-XZrO_2 after sintering process, because in general, the mechanical and physical properties of the alloys are affected by phase transition [101].

Figure (4.5). Illustrated the XRD pattern for sintered CoCrMo base alloy. It can be observe that all Co, Cr and Mo transformed to (CoCrMo), (CoCr) and (Co_2Mo_3) phases. This means that 1100°C for 4h under Argon gas was enough to complete the sintering process due to the enhancement of the inter diffusion between Co, Cr, and Mo, where phase transformation is a diffusion process and needs a high temperature to occur.

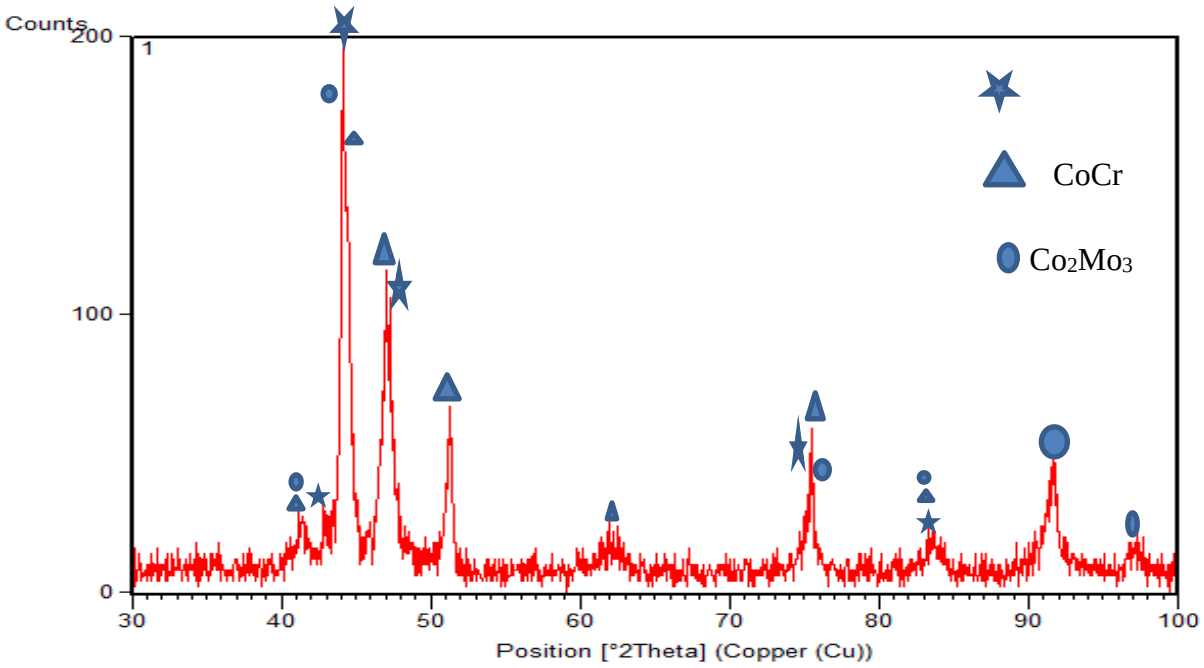

Fig (4.5): XRD pattern of M alloy

Figure (4.6). Indicate the XRD pattern for sintered CoCrMo alloy with zirconium oxide additive to it. The all amount of Co, Cr and Mo transformed to (CoCrMo), (CoCr) and (Co_2Mo_3) phases. The absence of free element is necessary in the alloys, which used as biomaterials due to its toxicity effect into living body.

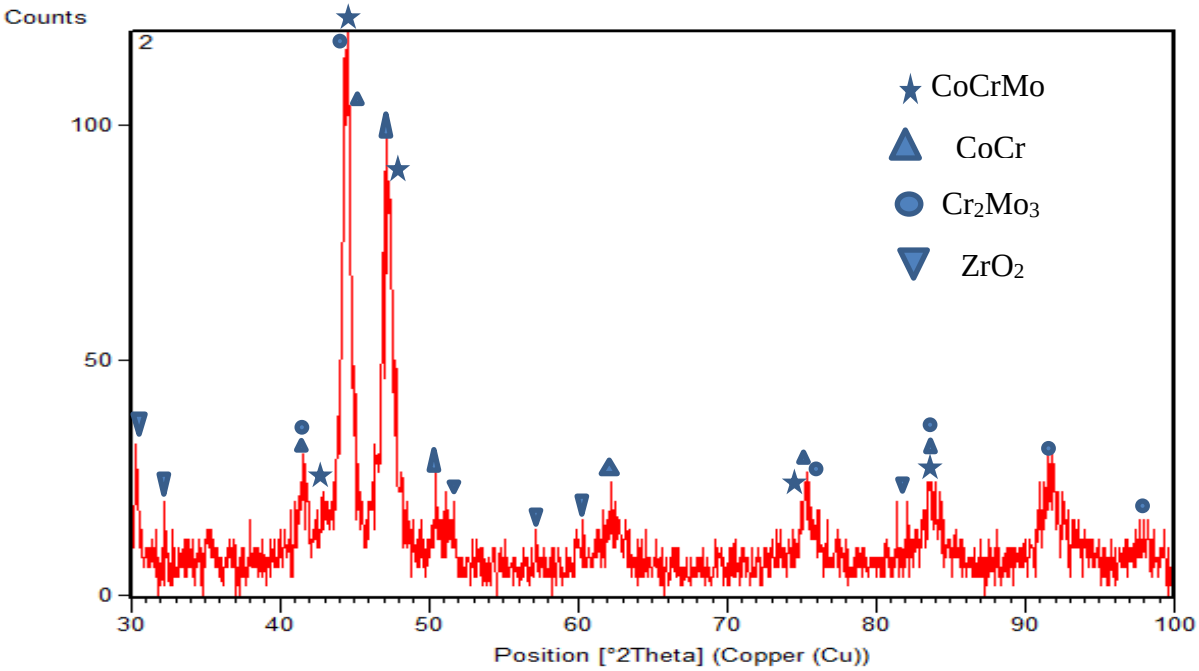

Fig (4.6): XRD pattern of A10 alloy

4.3.1.2 Light optical microscope

The microstructure of an alloy is an essential parameter that determines its mechanical, physics and electrochemical properties as hardness, wear and corrosion resistance. The grain boundaries in the microstructure of alloys were detected by etching of samples. Figure (4.7) shows the microstructure images that have been taken by using optical microscope for etched alloy after sintering process with magnification of 400x. The microstructure showed grain boundaries, pores in different size and insures the formation of the phases, all specimens of alloys consisting of two regions (a duplex microstructure), represents the regions of the light (CoCr phase) and the other regions are dark which indicates the (CoCrMo) phase. There are many pores in different size can be seen on the surface and it is expected because the samples are prepared by powder metallurgy technique.

Compared with the base alloy, it is noted that the grain size has reduction with the zirconia additive, due to the distribution of the particles of zirconia in the matrix and at the grain boundaries that lead to preventing them from growing.

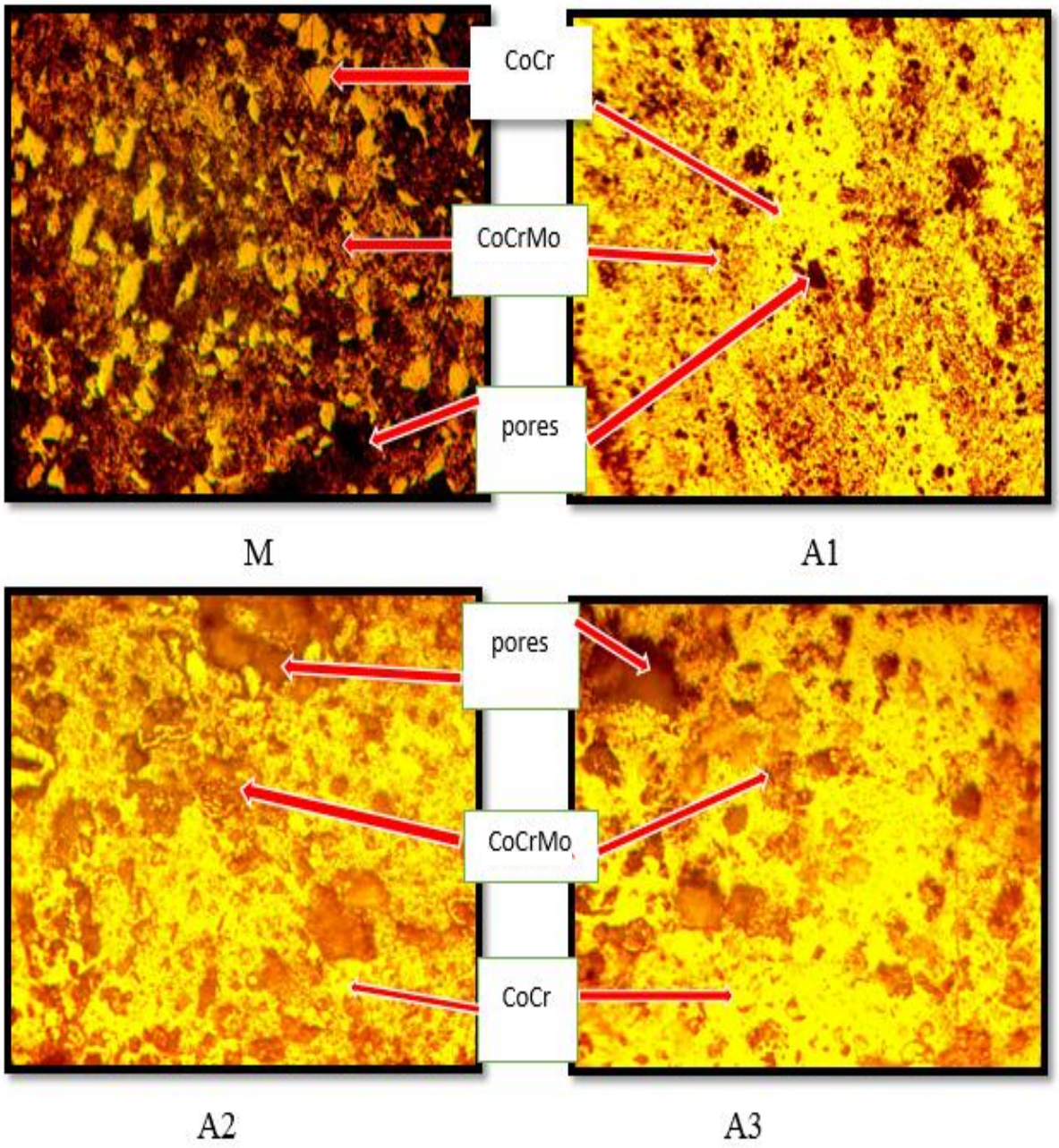

Fig (4.7) Microstructure of CoCrMo alloy (with and without ZrO_2 additions) with magnification 400X.

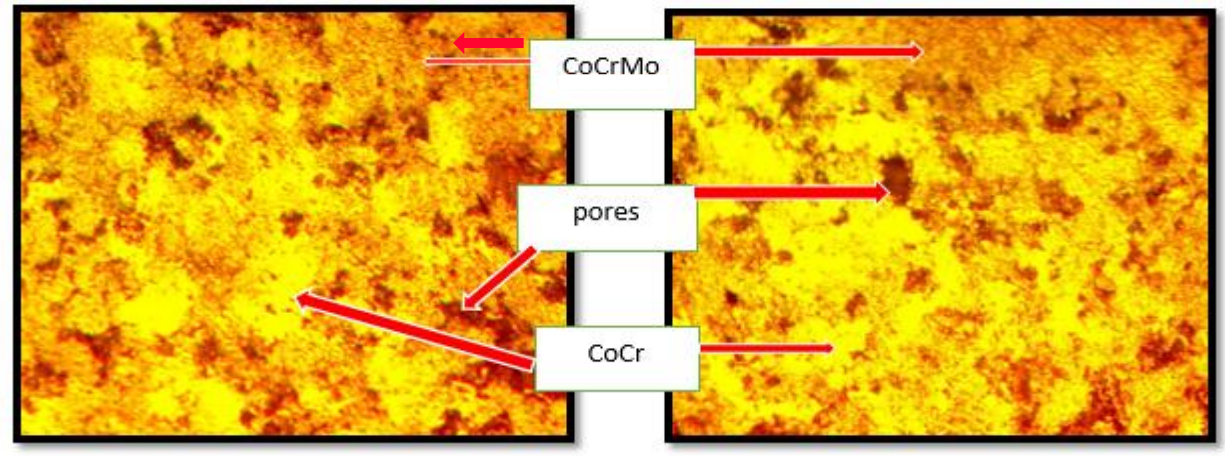

A5 A6

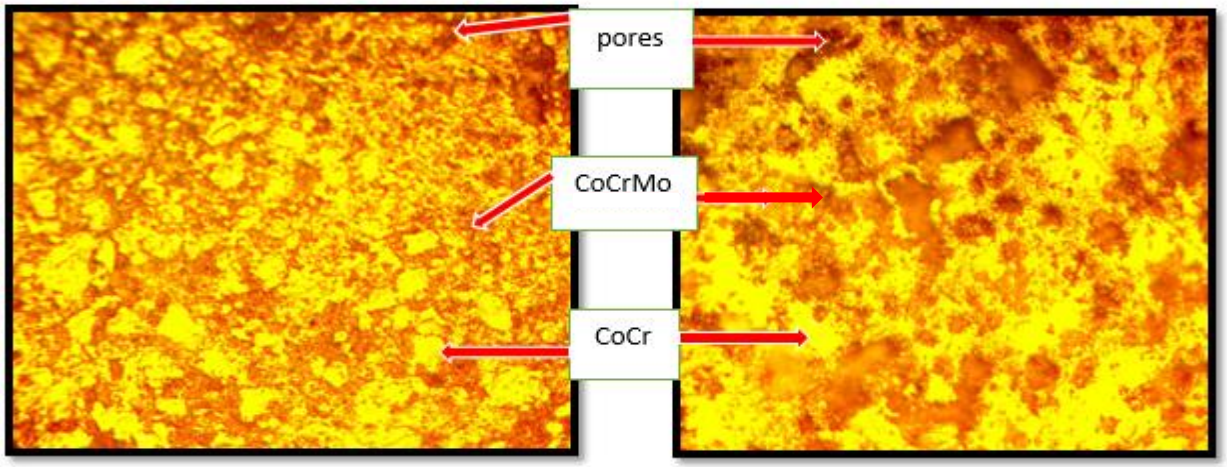

A7 A8

Continuous.

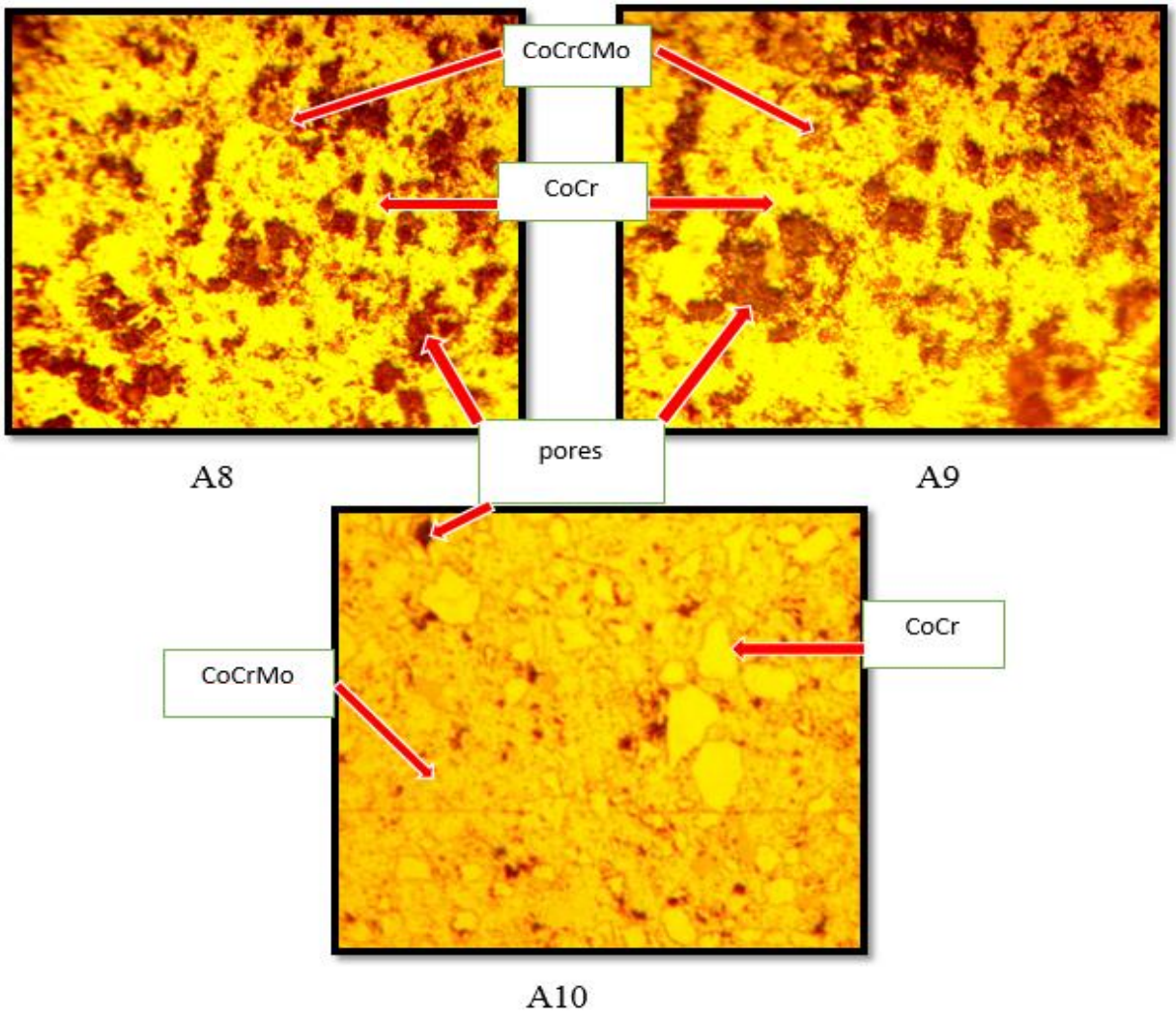

Continues.

4.3.1.3 Scanning Electron Microscope (SEM) and Energy Dispersive X-ray Spectroscopy (EDS)

Figures (4.8) and (4.9) shows SEM of base alloy (B) and alloy with zirconium oxide addition (A10) respectively.

As shown from figure (4.8) and (4.9) that SEM are very sensitive to chemical composition as a result, the microstructure of sintered specimens showed a multiphase structure in which the two phases (CoCr and Co_2Mo_3) are embedded in uniformly matrix (CoCrMo –F.C.C), thus confirming the XRD results.
SEM images of etched alloys showed grain boundaries and pores in different sizes.

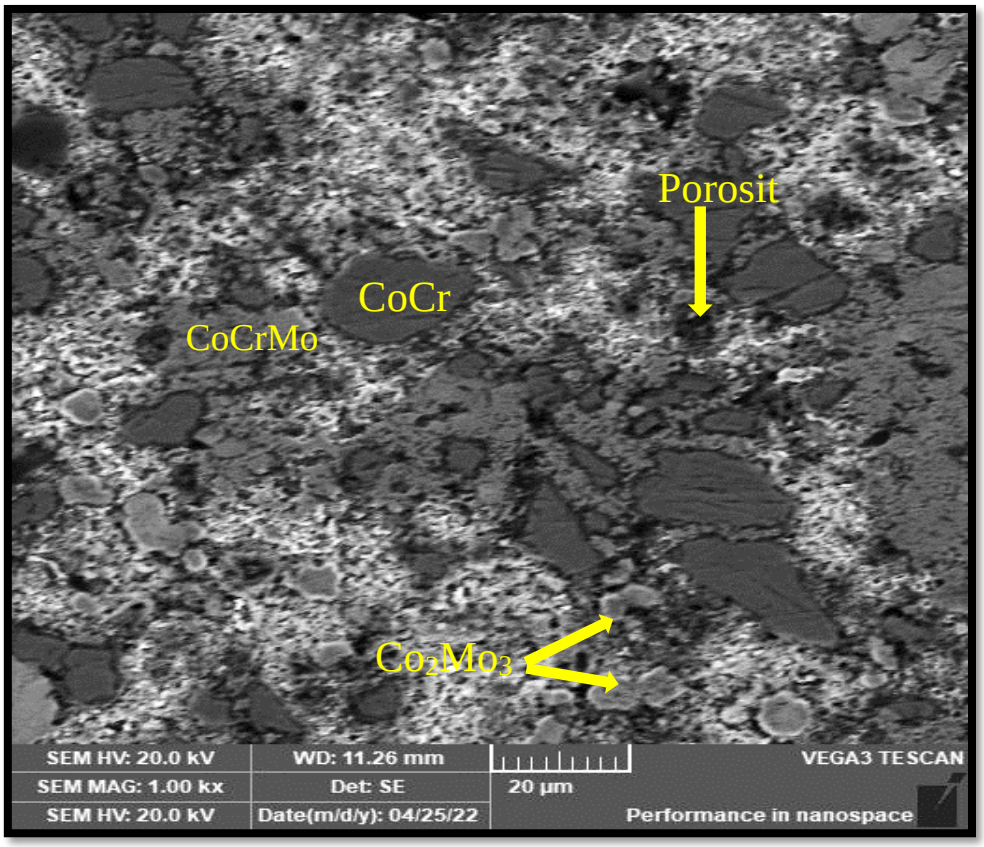

Fig (4.8): SEM for B alloy

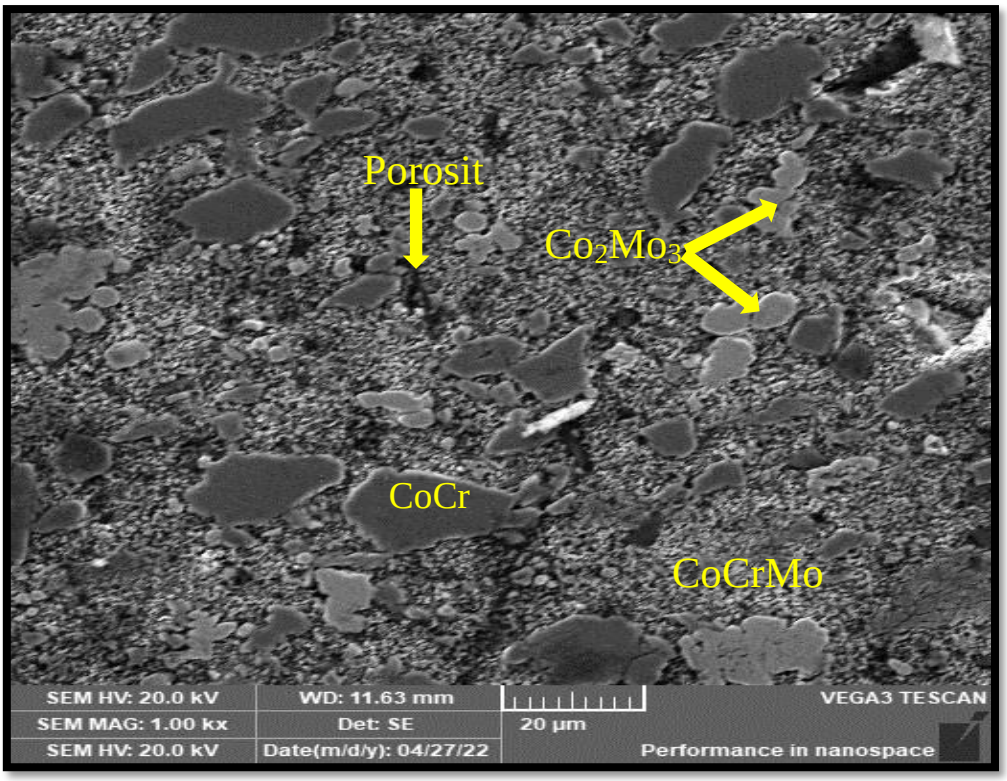

Fig (4.9): SEM image for A10 alloy.

The constituent elements of the alloy detected by Energy Dispersive X-ray Spectroscopy (EDS), where two alloys were analyzed, one prepared from the (CoCrMo) base and the rest from the base, adding different proportions of zirconium oxide done this test by used etching solution. Figure (4.10) shows the EDS spectrum of elements found in base CoCrMo alloys. The chemical analysis consist of cobalt, chromium, and molybdenum where quantified because the basic components of the alloy consist of these elements with the presence of other elements present in very small percentages. On the other hand, the EDS analysis for the prepared specimen with ZrO_2 (5%) are shown in Fig (4.11) It seems clear from the chemical analysis ZrO_2 is present in the composition the chemist of prepared alloys. In addition to the main elements in the alloy (cobalt, chromium and molybdenum) with the presence of other elements present in very small percentages. As can be seen, the results of EDS analysis were relatively close from the percentage of addition , because the values gained from EDS analysis do not cover the total area , only the spot where the electron stroke.

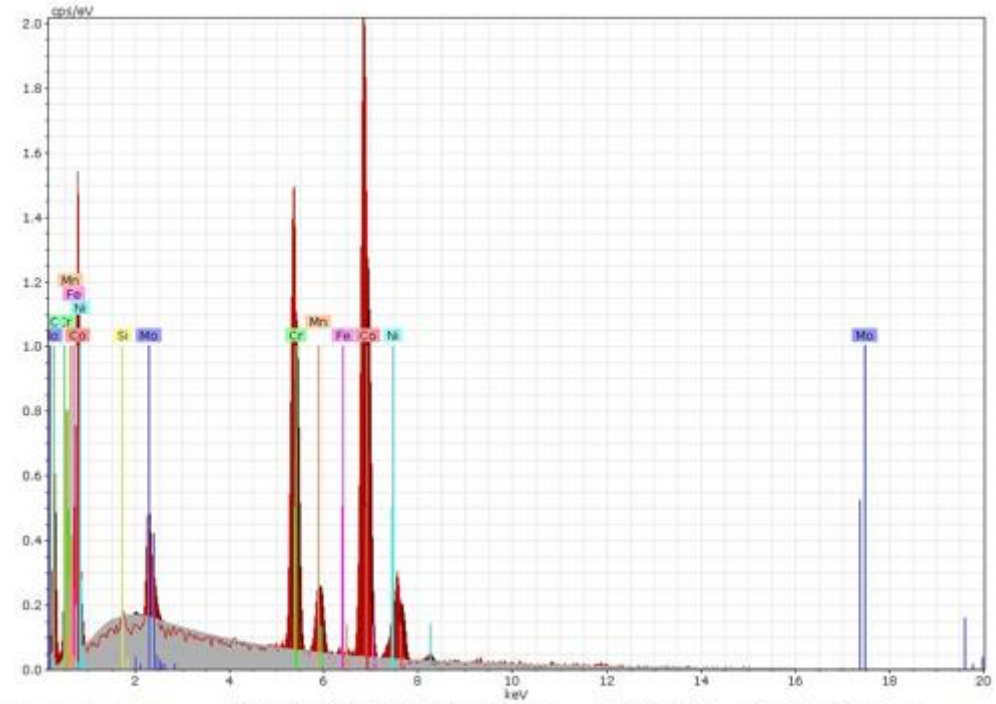

Spectrum: Acquisition

Element	Series	unn. C [wt.%]	norm. C [wt.%]	Atom. C [at.%]	Error (1 Sigma) [wt.%]
Cobalt	K-series	37.09	55.47	55.32	1.13
Chromium	K-series	15.15	22.65	25.60	0.49
Molybdenum	L-series	6.50	9.72	5.95	0.31
Nickel	K-series	6.38	9.54	9.55	0.30
Iron	K-series	0.00	0.00	0.00	0.00
Silicon	K-series	0.50	0.75	1.56	0.07
Manganese	K-series	1.26	1.88	2.01	0.10
	Total:	66.88	100.00	100.00	

a

Fig (4.10): EDS for (B) alloy

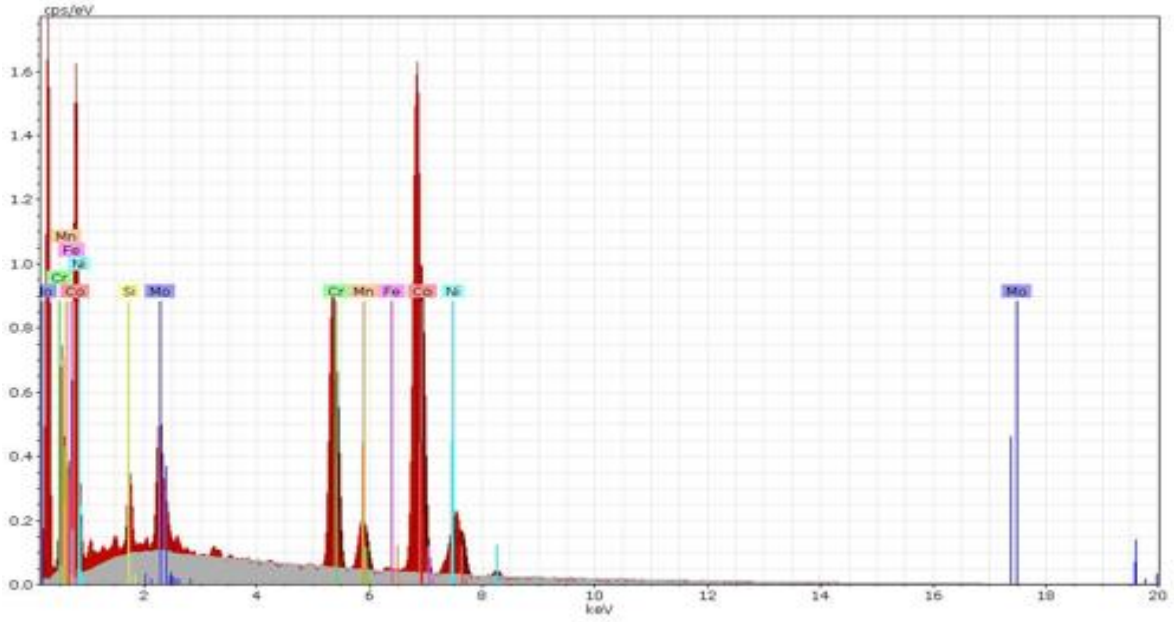

Spectrum: Acquisition

Element	Series	unn. C [wt.%]	norm. C [wt.%]	Atom. C [at.%]	Error (1 Sigma) [wt.%]
Cobalt	K-series	36.05	55.46	54.91	1.06
Chromium	K-series	11.66	17.93	20.12	0.38
Molybdenum	L-series	7.92	12.19	7.41	0.35
Nickel	K-series	6.06	9.32	9.27	0.26
Iron	K-series	0.00	0.00	0.00	0.00
Silicon	K-series	1.84	2.84	5.90	0.13
Manganese	K-series	1.47	2.25	2.39	0.10
	Total:	65.00	100.00	100.00	

b

Continues.

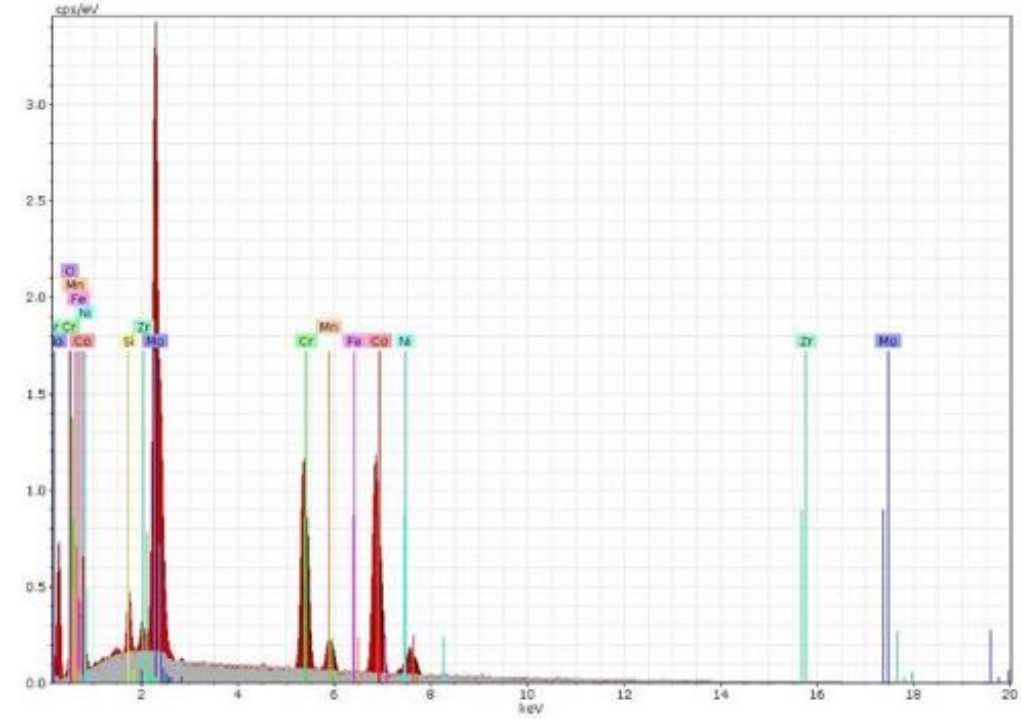

Spectrum: Acquisition

Element	Series	unn. C [wt.%]	norm. C [wt.%]	Atom. C [at.%]	Error (1 Sigma) [wt.%]
Cobalt	K-series	19.69	23.64	23.42	0.66
Chromium	K-series	12.45	14.95	16.79	0.43
Molybdenum	L-series	40.06	48.09	29.27	1.50
Nickel	K-series	2.96	3.55	3.53	0.18
Iron	K-series	0.00	0.00	0.00	0.00
Silicon	K-series	1.55	1.86	3.87	0.12
Manganese	K-series	1.23	1.47	1.56	0.10
Zirconium	L-series	0.53	0.64	0.41	0.07
Oxygen	K-series	4.83	5.80	21.16	1.57
	Total:	83.29	100.00	100.00	

a

Fig (4.11): EDS for A10 alloy

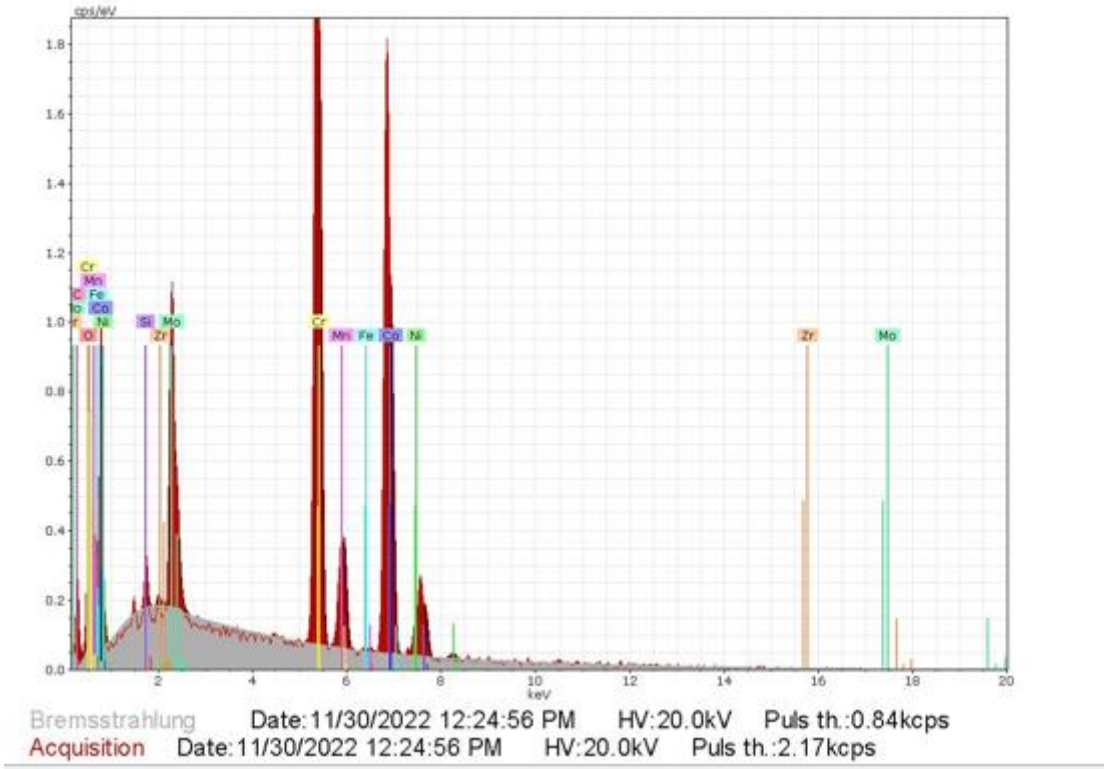

Spectrum: Acquisition

Element	Series	unn. C [wt.%]	norm. C [wt.%]	Atom. C [at.%]	Error (1 Sigma) [wt.%]
Oxygen	K-series	0.68	0.92	3.33	0.36
Nickel	K-series	4.22	5.75	5.65	0.22
Cobalt	K-series	30.21	41.14	40.26	0.92
Iron	K-series	0.00	0.00	0.00	0.00
Manganese	K-series	1.84	2.51	2.63	0.12
Chromium	K-series	23.63	32.18	35.69	0.71
Zirconium	L-series	0.00	0.00	0.00	0.00
Molybdenum	L-series	11.89	16.19	9.73	0.50
Silicon	K-series	0.97	1.32	2.71	0.09
	Total:	73.43	100.00	100.00	

b

Continues.

4.3.2 Porosity and density after sintering process.

The porosity of all used samples after sintering at 1100 c° for 4 h have been measured. Effect addition of zirconia on porosity values shows in Fig (4.12). Where observed there was a decrease in the porosity values with an increase in zirconia addition. This is due to the dispersion of ceramic particles (ZrO_2) in the matrix of alloy, which led to the closure of the pores in the structure, where the

decrease in the porosity was directly proportional to the increase in the addition of zirconia

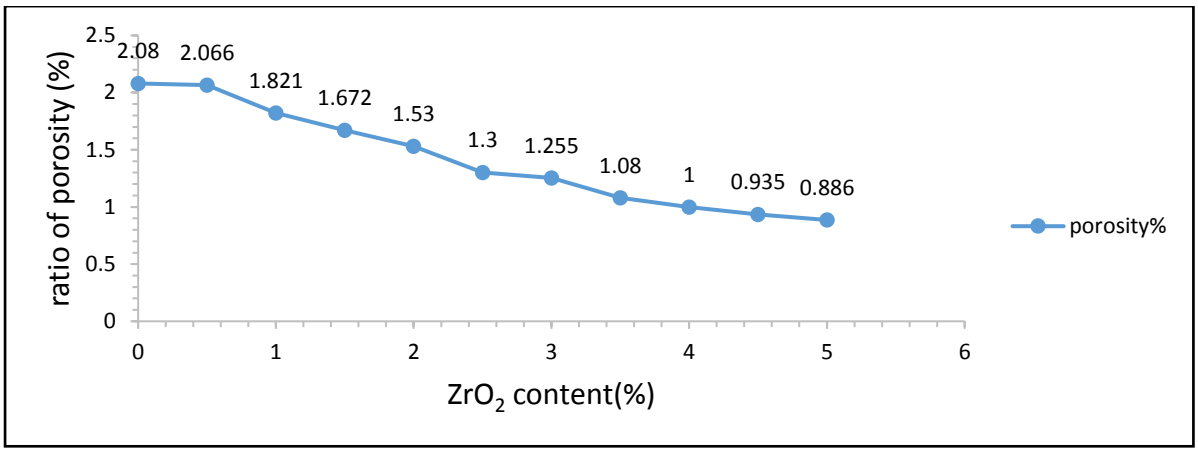

Fig (4.12) effect of ZrO_2 addition on porosity values.

Figure (4.13) shows a slight decrease in the density of the alloy with the addition of zirconia because it low density (5.68 g / cm^3) and added at the expense of the relatively high-density cobalt element (8.9 g / cm^3).

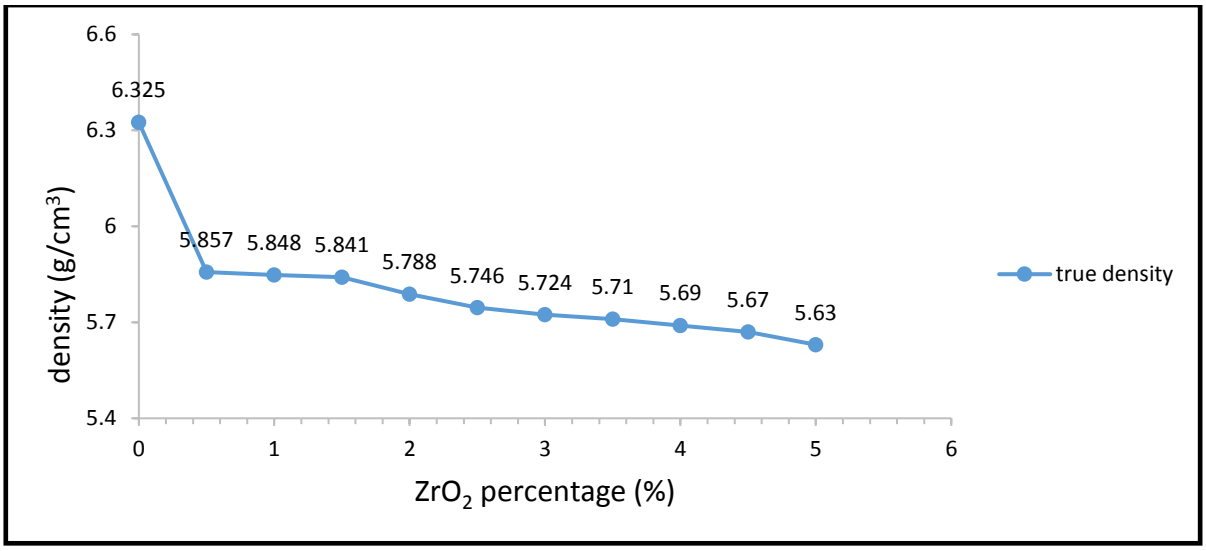

Fig (4.13) effect of ZrO_2 addition on the density values of samples.

4.5Mechanical tests results

4.5.1 Macro-hardness test

The macro-hardness results of all alloy samples are shown in Figure (4.14). Figure (4.14) show that CoCrMo base alloy without and with zirconium oxide additive, showed significantly higher values of hardness in comparison with CoCrMo base alloys, values of hardness shown increased gradually with the gradual increased in the addition of ZrO_2. The higher hardness is due to the role of (ZrO_2) distribution into matrix in the strengthening mechanism whereby these reinforcement particles tend to restrict the matrix phase movement in the vicinity of each particle. In essence, the matrix transfers some of the applied stress to the particles, which bear a fraction of the load[37]. Thus, it reduces the movement of the matrix. The hardness also increased with the addition of zirconium oxide due to the decrease in the porosity of the alloy.

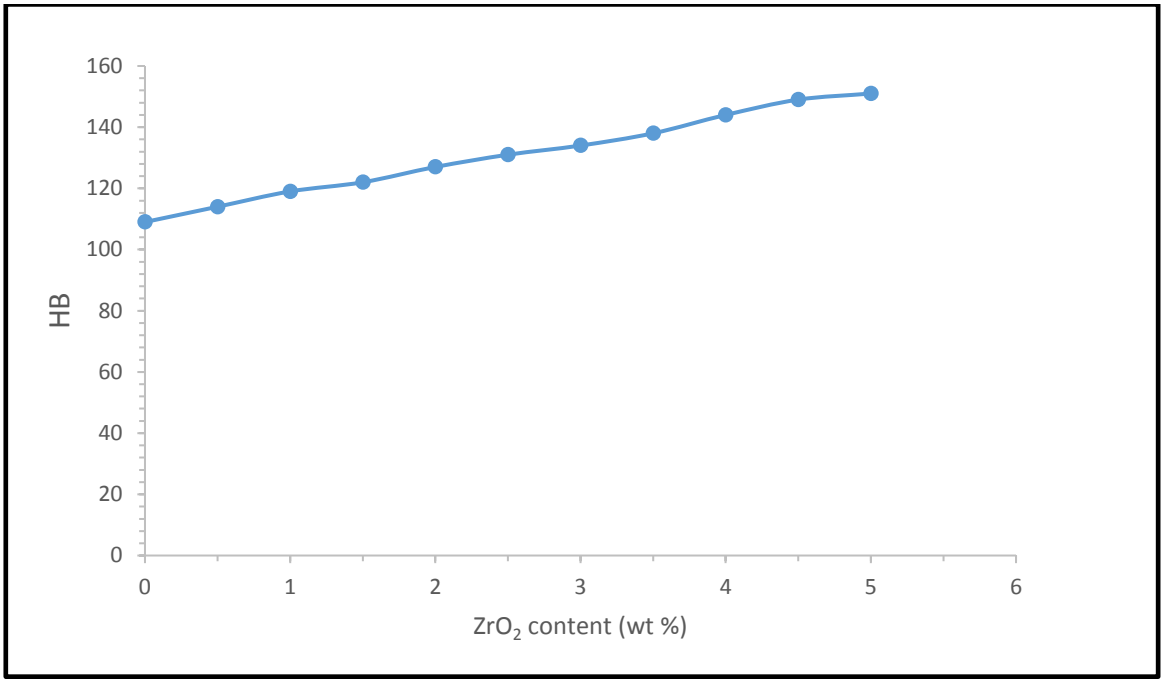

Fig (4.14): Effect zirconia content on hardness for CoCrMo alloy.

The table (4.2) shows the improvement percentage in the hardness values of the alloy CoCrMo with and without zirconium oxide. The improvement percentage of hardness is increase with the addition of zirconia. The highest percentage of improvement at the highest percentage of zirconia addition due to the relatively high percentage of ceramic particles (ZrO_2) present in the alloy.

Table (4.2): Macro-hardness and improvement percentage of all alloy.

Alloys	Hardness	Improvement percentage %
B	109	-----
A1	112	2.75
A2	116	6.4
A3	122	11.9
A4	127	16.5
A5	131	20.1
A6	134	22.9
A7	138	26.6
A8	144	32.1
A9	149	36.6
A10	151	38.5

4.6.2 Dry sliding wear test

The samples with a diameter of (*12*) mm are subjected to dry wear test under various load *20, 25* and *30* N for various times (*5*, *10*, *15*, *20*, *25*, *30*, *35*, *40*) min, were chosen constant load and different times according to several experiments. The Figures (4.15) are show the relationship between the volume loss of CoCrMo base alloy with and without additions (0.5, 1, 1.5, 2, 2.5, 3, 3.5, 4, 4.5, 5% wt. ZrO_2). From this figure versus time under various load (20,25 and 30 N), it's clear that weight loss gradually increased with increasing time regardless of the chemical composition and microstructure of alloys, this because of the increasing of friction at the surface as the load increase[97]. In addition, increasing of wear rate with time of all samples is because more friction time leads to remove more material from the surface. It can be noted the behavior of the volume curve with time, the volume loss increase initially with time until reach study state, the asperities of the surface will be removed during sliding indicating the increase in the volume loss (wear rate) of the specimens and the increasing in the frication coefficient, when all asperities removed the friction coefficient reach constant value, consequently the volume loss reach constant value with time.

From Figures (4.15) it is possible to note the lower volume loss of CoCrMo alloy with the ZrO_2 additives compared to the base alloy, this attributed to restricts of matrix movement and grain boundaries by zirconium oxide particles added to base alloy, which caused increase hardness, thus increase wear resistance and decrease volume loss.

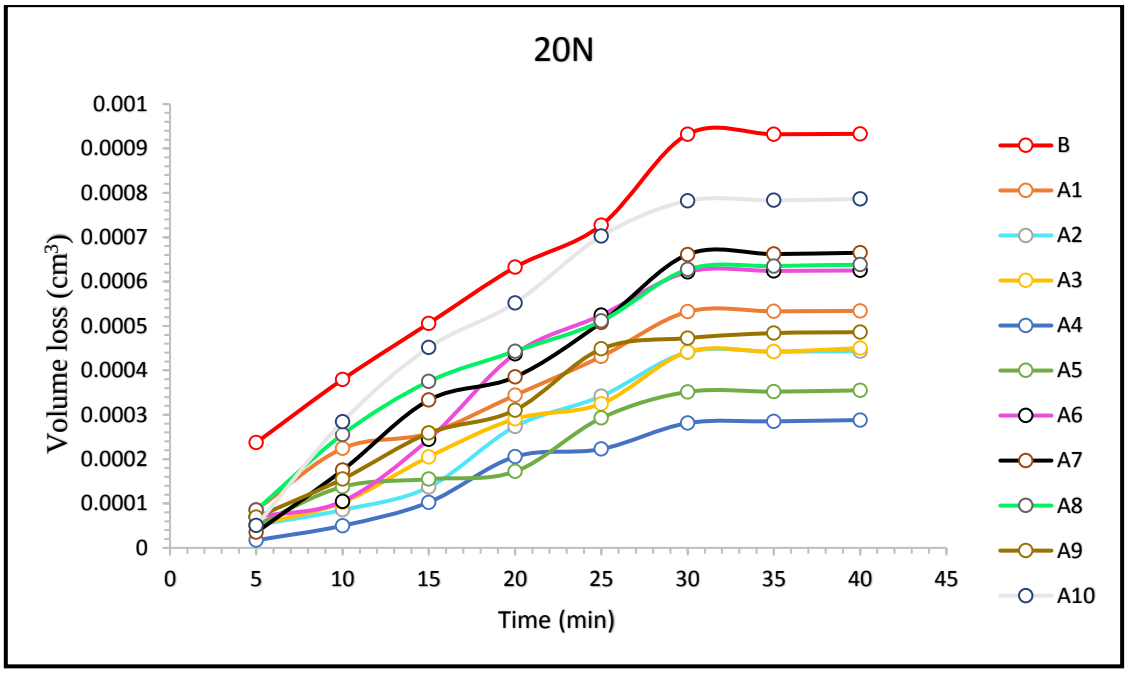

a

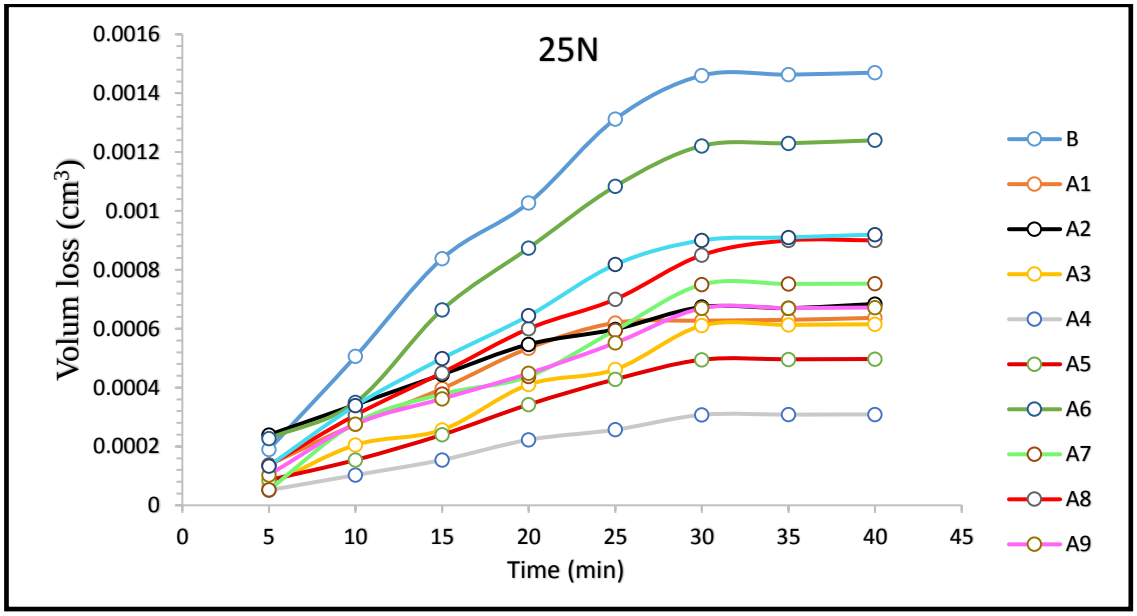

b

Fig (4.15): Volume Losses vs. Time for CoCrMo base Alloys and CoCrMo – $xZrO_2$ under (20, 30 and 30N) Loads.

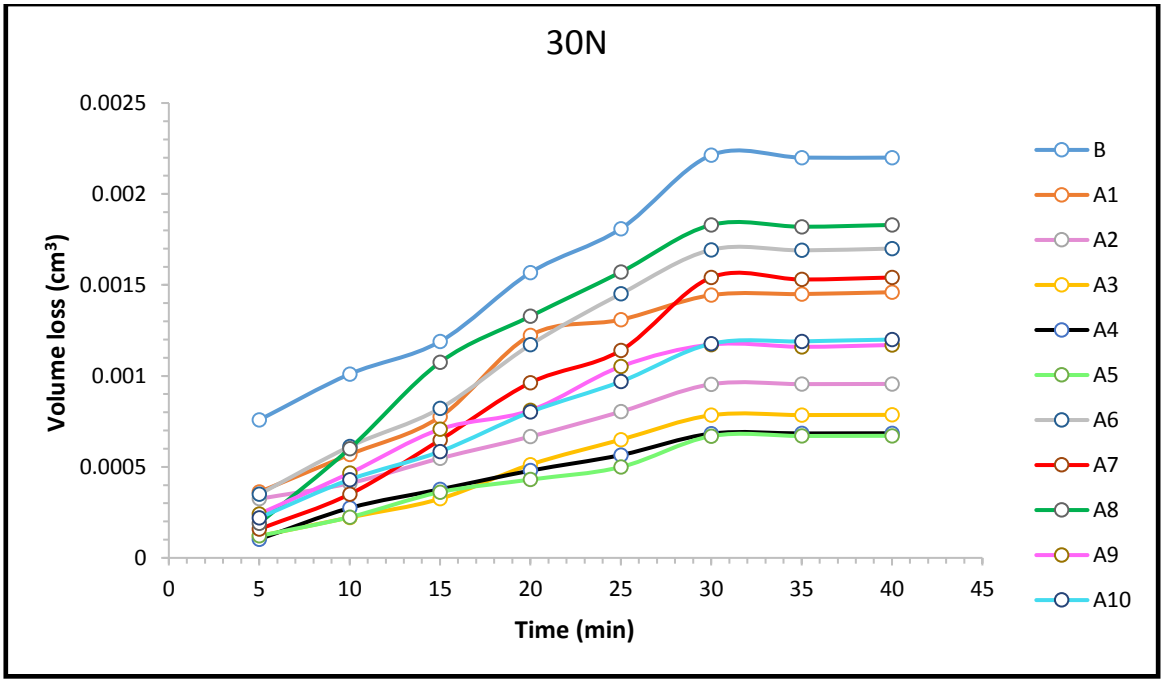

c

Continues.

Table (4.3) shows the volume loss values of base CoCrMo alloy with and without zirconia and improvement percentage of base alloy with (ZrO_2) addition. Volume loss of base alloy is (0.002 cm^3), which decrease with adding zirconium oxide particles to it. The volume loss of CoCrMo-0.5ZrO_2 alloy is (0.00146 cm^3) with improvement percentage (33.6%), decreasing continuous with gradual increased addition of ZrO_2 even arrives addition percentage to 2.5% of zirconia (A5 alloy) with minimum volume loss (0.000671cm^3) and improvement percentage(69.5), then occur drop in the wear resistance where increase volume loss with decreasing improvement percentage after pass this addition.

Table (4.3): Volume loss and Improvement percentage of all alloy

alloy	Volume loss (cm^3)	Improvement percentage %
B	0.0022	------
A1	0.00146	33.6
A2	0.000956	56.5
A3	0.000786	64.2
A4	0.000685	68.8
A5	0.000671	69.5
A6	0.0017	22.7
A7	0.00154	30
A8	0.00183	16.8
A9	0.00117	46.8
A10	0.001	54.5

4.6.3 Compressive test

The results of the compressive strength test are illustrated in Figure (4.16). The strength of compressive values of the CoCrMo alloy with the addition of zirconia are higher than its value for the base alloy, due to the reinforcement mechanism by large particulate composite. The hard and stiff zirconium oxide particles, dispersed in the ductile matrix bear a fraction of supply load which restrain matrix movement around each particle[37], also decreases of porosity when zirconia additive to base alloy leads to increase compressive strength.

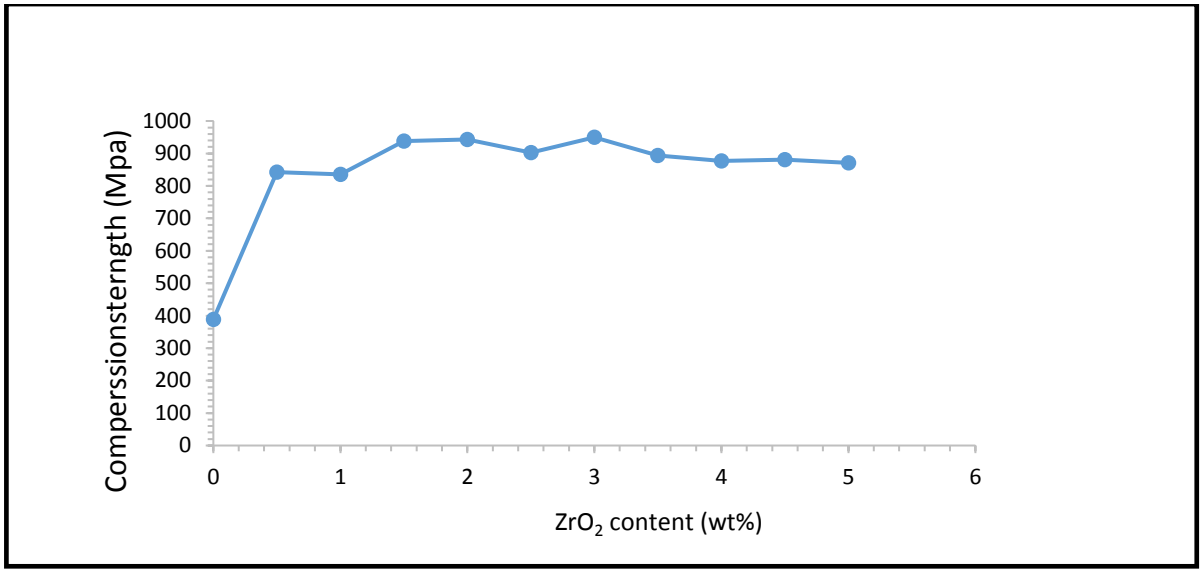

Fig (4.16): compressive strength for CoCrMo alloy (without and with ZrO_2).

Table (4.4) demonstrates the compressive strength magnitudes of base alloy without and with zirconia, addition and improvement percentage compared with base alloy. (388.41Mpa) value of compressive strength of base alloy. Trace addition of zirconium oxide particles Increase this value to (841.99Mpa) at (0.5%) with high improvement percentage (116.5%), and increasing continuous with gradual increased addition of ZrO_2 particles even arrives addition percentage to 3% of zirconia (A6 alloy) with maximum compressive strength(949Mpa) and improvement (144.4%). Occur drop in the values of compressive strength and decreasing improvement percentage after pass this addition.

Table (4.4): The compressive strength and improvement percentage of all alloy.

samples	Compressive strength(MPa)	Improvement percentage %
B	388.41	------
A1	841.99	116.7
A2	835.10	115
A3	937.75	141.4
A4	942.97	142.7
A5	902.31	132.3
A6	949.6	144.4
A7	893.8	130.11
A8	877.09	125.8
A9	880.6	126.7
A10	871	124.2

4.7 Electrochemical tests

4.7.1 Open circuit potential test

In order to understand the stability of an alloy CoCrMo in the solutions of the living body, it is necessary to know its behavior in the environment that simulates of body fluids to know the biocompatibility of these alloys. This is done by the open-circuit potential for by time during immersion until the tendency to a steady-state value; it is one of the typical methods for studying the formation of a protective layer and passivation of implants in Hank's and saliva solutions and compared the stability of (CoCrMo-X ZrO_2) alloy with the stability of the base alloy.

The OCP-time curves for all alloys in two various solutions (synthetic saliva and solution of Hank) at 37°C±1 are shown in Fig (4.17). In case of synthetic saliva and Hank's solution the test period is (125 to 260) and (150 to 350) min respectively. From Fig (4.17), it can be noted that the potential of some specimens move to negative direction is due to the continuous dissolution of the alloys, while the potential of another specimens moves towards the positive direction because continuous deposition of alloys. When deposition and dissolution are in equilibrium, the OCP will be nearly in constant value[98].

Fig (4.17) illustrates the behavior of CoCrMo alloy with and without zirconia additive in both (Saliva and Hank's) solutions. The CoCrMo alloy with addition zirconium oxide particles more noble than base alloy where the open circuit potential of alloys moving in the positive direction with respect to that of base alloy. This behavior is due to the presence of stable zirconium oxide particles dispersed in the matrix, which occupies a space of the surface of the alloy and the formation of a protective layer added to the layer of chromium oxide formed on the surface, which leads to making the alloy with the addition nobler than the base alloy. The final potential values of all alloys tested in the synthetic saliva and Hank's solution with improvement percentage of alloy with zirconium oxide particles are shown in the tables (4.5) and (4.6) respectively. The OCP of base alloy in artificial saliva is (-430 mV) and potential values decrease with zirconia particles addition to the base alloy with improvement percentage range from 107.67% as the maximum at A1 alloy to 4.18% as minimum at A6 alloy with potential (+33mV) and (-412mV) respectively. OCP of base alloy in Hank's solution is (-397mV) it possible noted this value less than OCP in artificial saliva is due to the pH value for each solution, where more number of pH represent more positive potential. PH of Hank's solution was (7.4) and for synthetic saliva (6.62) respectively, and enhanced the OCP of alloy with addition of zirconium oxide particles where range from (-93mV) at A1 alloy with maximum

improvement (76.57%) to (-370mV) at A2 alloy with minimum improvement percentage (6.8 %).

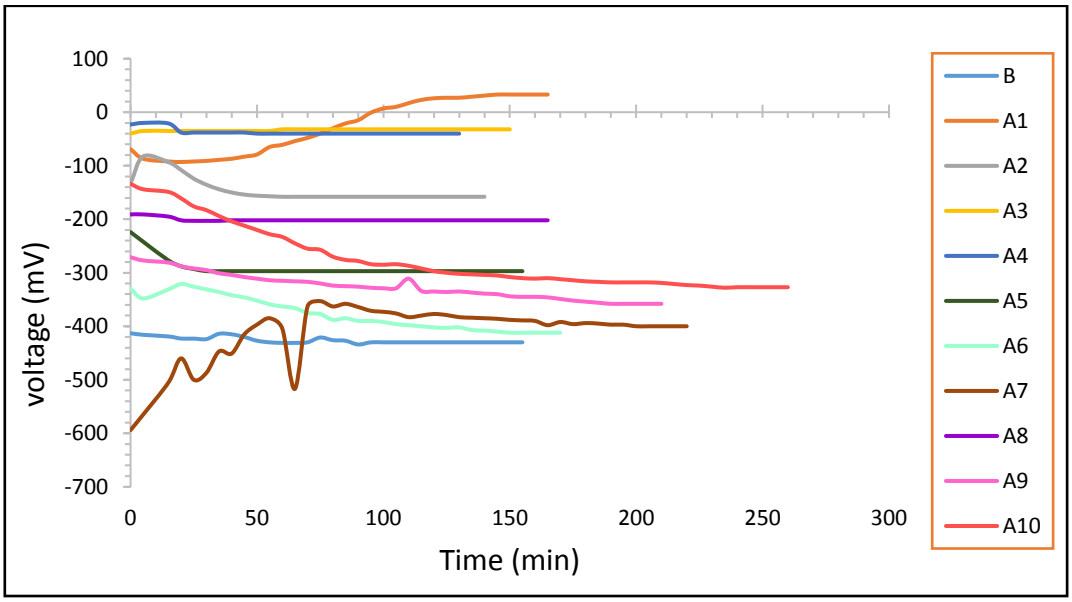

(a)

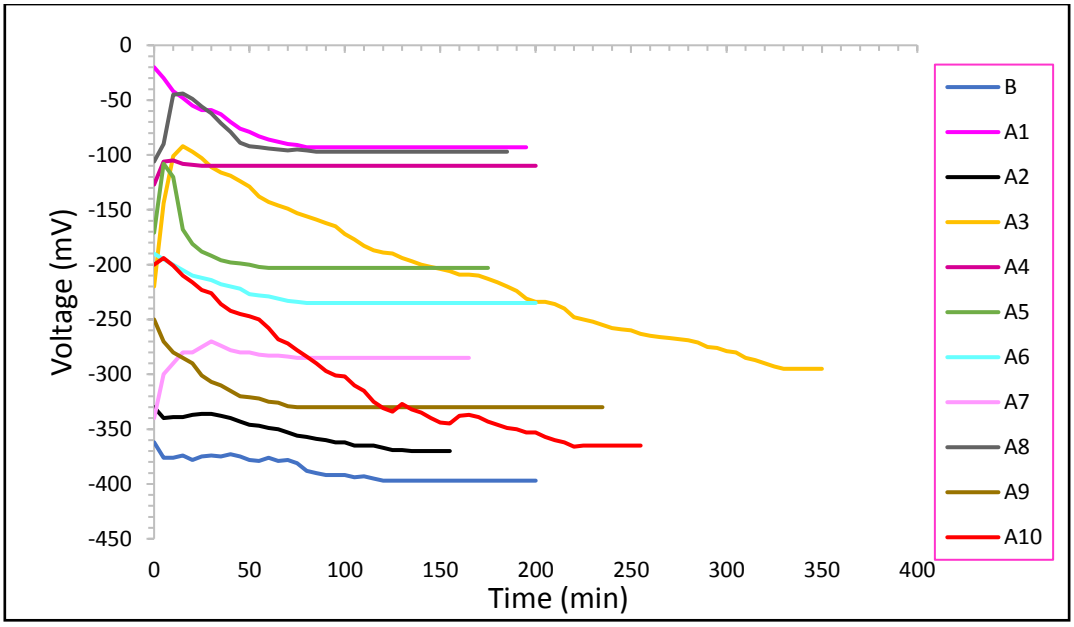

(b)

Fig (4.17): OCP-Time of alloys in A: prostheses saliva, b: Hank's solution at 37±1ºC.

Table (4.5): E_{OCP} and Improvement Percentage % for All Alloys in artificial saliva.

Alloy	$E._{OCP}$ (mV)	Improvement percentage %
M	-430	-----
A1	+33	107.67
A2	-158	63.25
A3	-35	91.86
A4	-38	91.16
A5	-297	30.93
A6	-412	4.18
A7	-400	6.97
A8	-202	53.02
A9	-358	16.74
A10	-327	23.95

Table (4.6): E_{OCP} and Percentage Improvement for All Alloys in Hank's Solution.

alloys	E_{OCP} (mV)	Improve percentage%
M	-397	----------
A1	-93	76.57
A2	-370	6.80
A3	-295	25.69
A4	-110	72.29
A5	-203	48.86
A6	-235	40.8
A7	-285	28.2
A8	-97	75.56
A9	-330	16.87
A10	-365	8.06

4.7.2 Potentiodynamic polarization

The corrosion behavior of all alloys used in Hank's solutions and synthetic saliva have been studied, by utilizing potentiodynamic polarization to give estimation about behavior of the corrosion of alloys.

The parameters of corrosion are the current of corrosion density ($i_{corr.}$), corrosion potential ($E_{corr.}$) and rate of corrosion resulted from corrosion test for the specimens in mentioned solutions at 37 ± 1C were showed in tables (4.7) and (4.8).

Figure (4.18) illustrates polarization tests of CoCrMo in (synthetic saliva and Hank's) solutions at 37°C ±1. In cathodic polarization, current density decreases with increasing potential until corrosion potential reached, increasing potential will starts active anodic polarization, where current density increases with increasing potential (explain the dissolution of CoCrMo alloys)[98].

From figure (4.18 a and b), it can have noted the polarization curve of base alloy more negative compared to base alloy with zirconia additives. Zirconium oxide particles, which made the polarization curve, move in the positive direction, it made the alloy nobler than the base alloy and this gives an indication of a low rate of corrosion and an increase in its resistance.

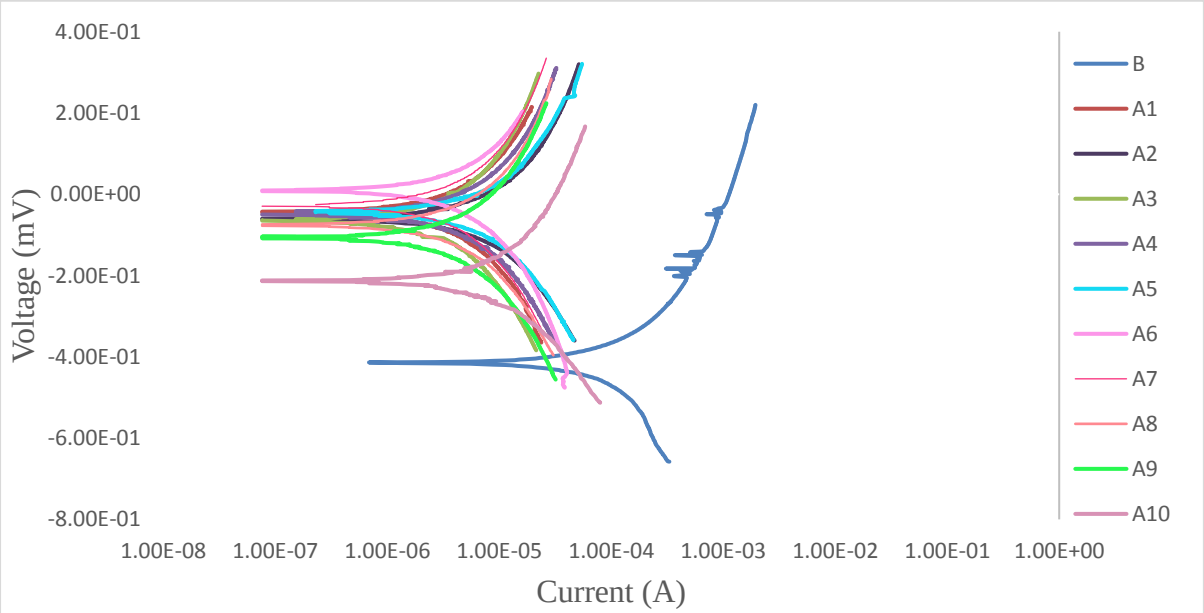

(a)

Fig (4.18): Potentiodynamic Polarization Curves of CoCrMo base alloy a CoCrMo-XZrO_2 and in a: synthetic saliva, b: Hank's solution at 37°C±1.

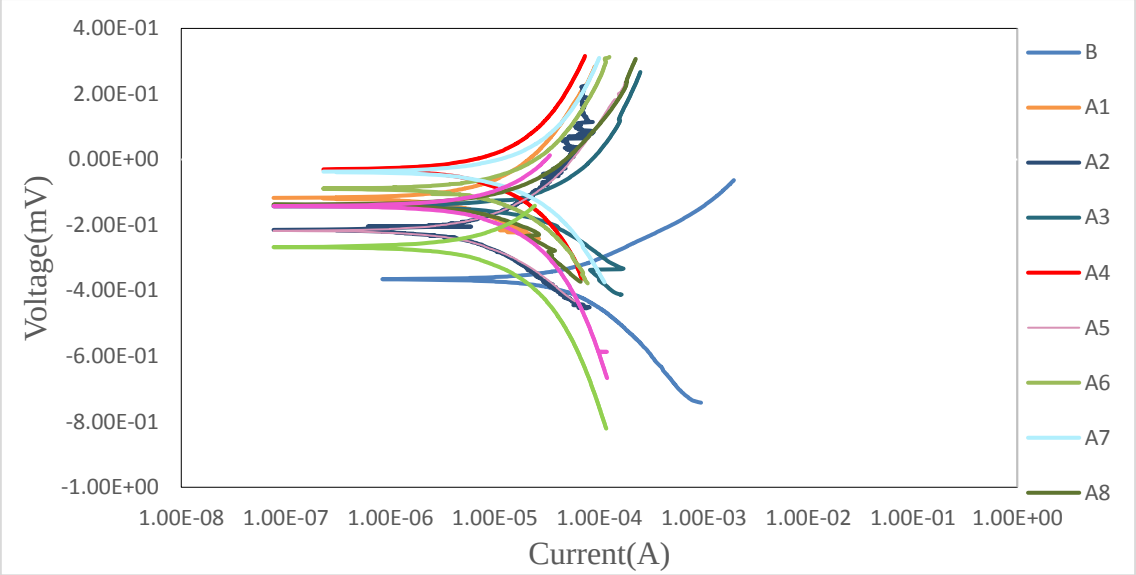

(b)

Continues.

From table (4.7), it can be noted that the density of corrosion current (I_{corr}) values of base alloy in synthetic saliva is (3.911µA/cm^2) with corrosion rate (1.582 mpy) which are decreased significantly with the addition of zirconia particles for base alloy, and thus increase corrosion resistance of these alloys. This improvement in corrosion resistance (decreasing the corrosion current density and corrosion rate) due to the presence of stable zirconium oxide particles dispersed in the matrix of CoCrMo alloy, Which occupies an area of the surface of the alloy and which works to reinforce the chromium oxide layer formed on the surface. This lead to making the alloy with the addition nobler than the base alloy and this indicates decrease of alloy dissolution. The lowest value of the corrosion current density (0.116µA/cm^2) when adding (1% ZrO_2), which gave the highest percentage of improvement in corrosion resistance (96.7%), with the lowest corrosion rate (0.051mpy).

Table (4.7): Potential of Corrosion (E_{corr}), The Density of Corrosion Current (i_{corr}) and Corrosion of rate for Alloy Utilized in this study at (37 °C ±1) in synthetic Saliva

samples	i_{corr} µ/cm^2	E_{corr} (mV)	Corrosion rate(mpy)	Improvement percentage %
B	3.911	-414	1.582	------
A1	0.144	-45	0.064	95.9
A2	0.116	-63	0.051	96.7
A3	0.225	-60	0.095	93.9
A4	0.169	-45	0.075	95.2
A5	0.259	-50	0.117	92.6
A6	0.145	9	0.067	95.7
A7	0.177	-26	0.082	94.8
A8	0.159	-75	0.0725	95.4
A9	0.169	-106	0.0784	95
A10	0.320	-213	0.144	90

Table (4.8). Illustrate the corrosion of current density, corrosion potential, corrosion rate and improvement percentage of (CoCrMo-XZrO_2) alloys in Hank's solution. Compared with base alloy which give current density (2.863µA/cm^2) and corrosion rate (1.158mpy), where the lowest value of the density of corrosion current (0.318µA/cm^2), corrosion rate (0.14mpy) and the maximum improvement percentage (87.83 %) at additive 0.5% of zirconium oxide particles to base alloy, which indicates decrease of alloys dissolution with adding ZrO_2 (corrosion resistance improvement).

Table (4.8): Potential of Corrosion (E_{corr}), The Density of Corrosion Current (i_{corr}) and rate of corrosion for Alloys utilized in this study at (37 °C ±1) in solution of Hank's.

samples	i_{corr} $\mu A/cm^2$	E_{corr} (mV)	corrosion Rate (mpy)	Improvement percentage %
B	2.863	-365	1.158	-----
A1	0.318	-118	0.140	87.83
A2	0.336	-215	0.143	87.17
A3	0.9	-134	0.383	66.8
A4	0.394	-31	0.176	84.8
A5	0.341	-218	0.153	86.7
A6	0.536	-88	0.247	78.6
A7	0.572	-38	0.265	77.1
A8	0.561	-138	0.254	77.9
A9	0.415	-148	0.191	83.5
A10	0.377	-213	0.169	85.4

The microstructure for the corroded surface has been taken by using SEM in order to study the corrosion effect on the surface of the alloy.
Figure (4.19) shows the corroded base alloy under a scanning electron microscope, showing cracking of the protective oxide layer, which indicates the weakness of the chromium oxide layer in the base alloy compared to the alloy with addition, as shown in the figures (4.20) and (4.21).

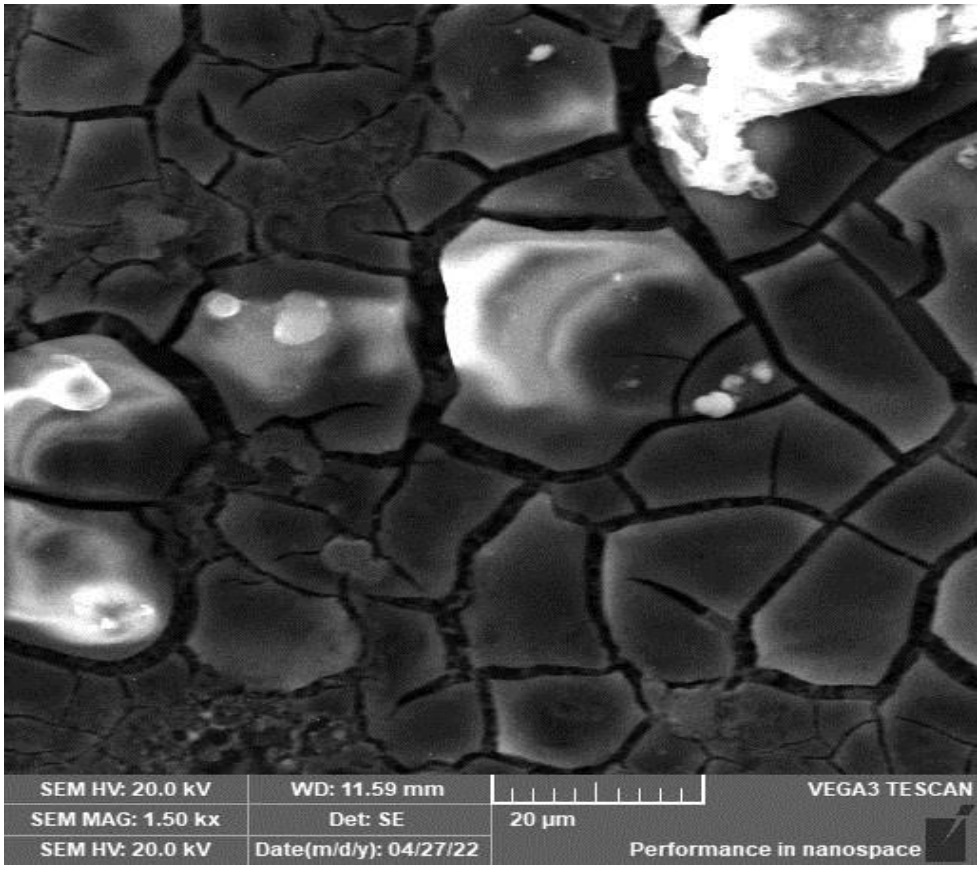

Fig (4.19): SEM for B alloy corroded in Hanks solution

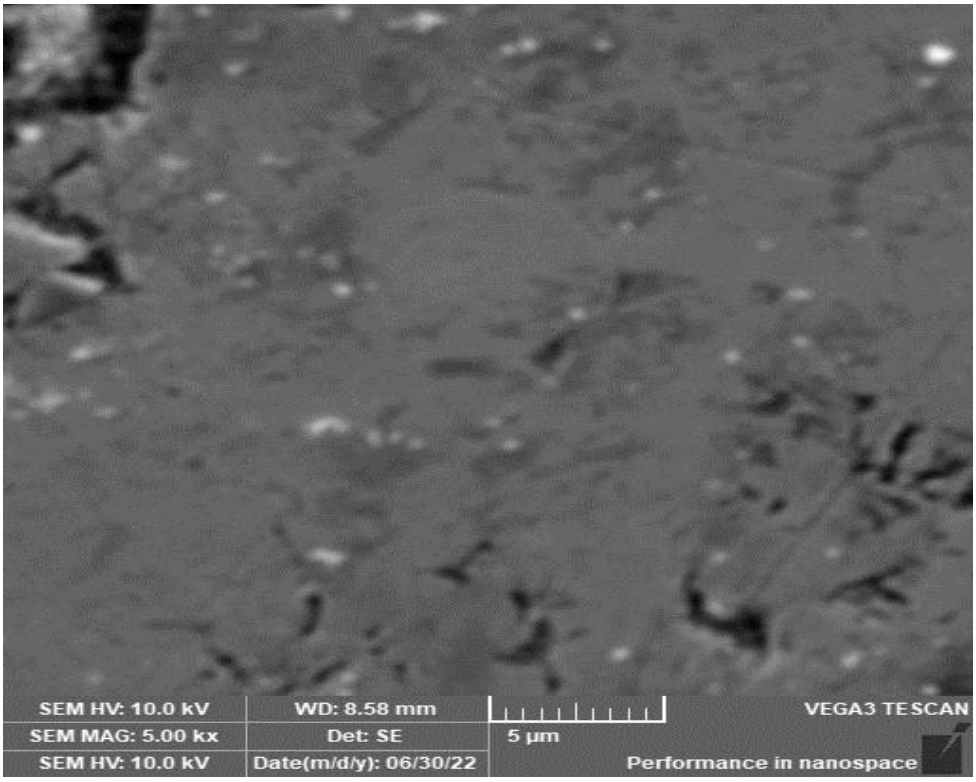

Fig (4.20): SEM for A5 alloy corroded in Hanks solution

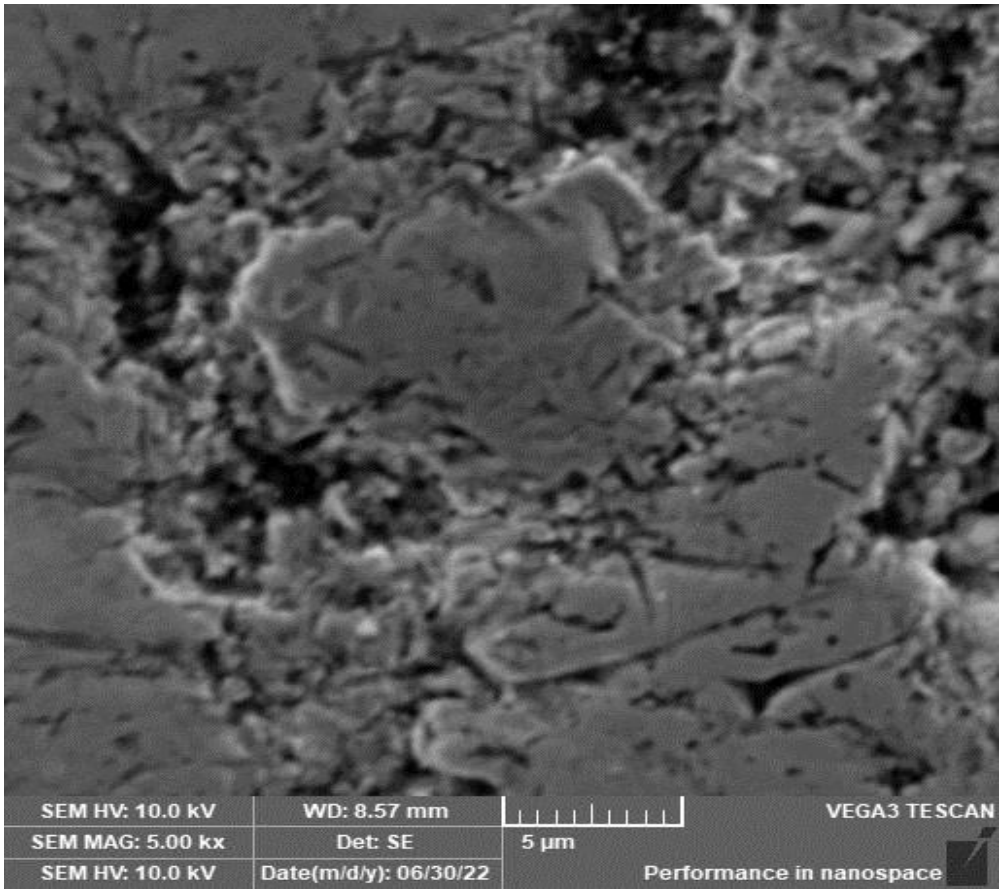

Fig (4.21): SEM for A5 alloy corroded in Hanks solution

4.8 Ion release test

Released ions of metals from the surgical implant within surrounding tissue by a various of mechanisms, consist of corrosion and wear like fretting corrosion, stress corrosion and corrosion fatigue etc.

This metal ion release has been related with clinical implants deterioration, osteolysis and cause allergic reaction. There requirement for lengthened use for implant, with fewer metals ions release. Therefore, the behavior of metal ion release of each from base alloy and alloys with zirconium oxide particles addition is being studied by using different solutions from Hank's and artificial saliva.

The stability of passive film is strongly affected the metals ions release, when the film undergoes corrosion, through this degraded film, metal will release. The configuration of pits is associated with the stability potentials of (passive) film, which represent as a guide for the happened activities.

Where the use of two solutions (synthetic saliva and Hank’s solution) to be performed immersion test with CoCrMo alloy to known the ion release concentration quantitative data, and that is to known the biocompatibility of

materials to the select the appropriate biomaterials for different medical applications.

From figures, (4.22) and (4.23) it possible noted cobalt ions release in the base alloy in both solutions (saliva and hank's solutions) higher than alloy with zirconium oxide particles addition. The ions release in artificial saliva and Hank's solution (0.26 and 14.22. ppm) of base alloy respectively, while the ions release of CoCrMo alloy with (2.5% and 5% ZrO_2) is very negligible (device insensitive) in synthetic saliva, while cobalt ion release (0.89 for A5 and 1.84 for A10) in Hank's solution as shown in table (4.9).

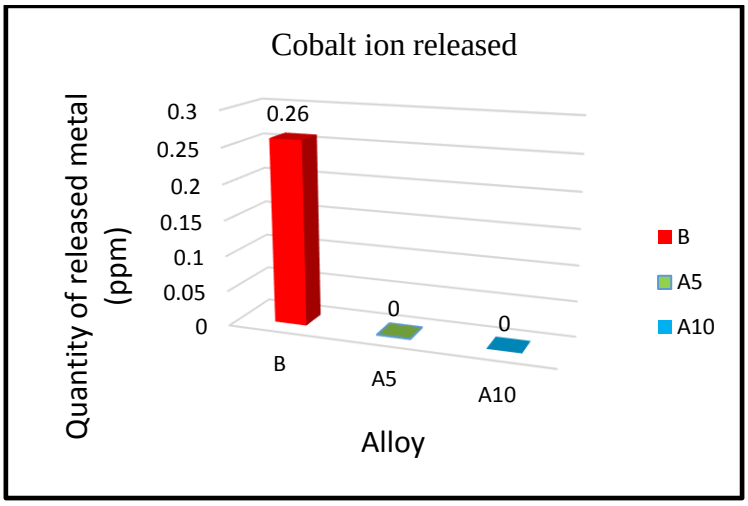

Figure (4.22): Quantity of each metal ion released from B, A5and A10 alloy in artificial saliva solutions and 37°C ±1 after 21 days.

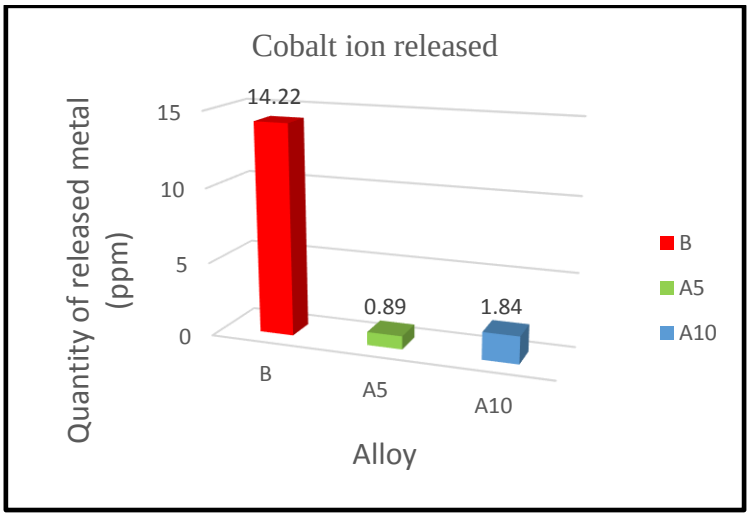

Figure (4.23): Quantity of each metal ion released from B, A5and A10 alloy in Hank's solutions and 37°C ±1 after 21 days.

In Hank's solution, the values of ions release were higher than in artificial saliva, as was observed in the potentiodynamic polarization test where the rate of corrosion in Hank’s solution higher than synthetic saliva.

This result illustrates that the resistance of corrosion of the (COCrMo-XZrO_2) alloys was higher than the corrosion resistance of base COCrMo alloy, coincide with the results of the potentiodynamic polarization.

Table (4.9): cobalt ions release concentrations in Hank's solution & saliva solutions at 37^{o}C±1.

Alloy	Hank’s solution (ppm)	Synthetic saliva (ppm)
B	14.22	0.26
A5	0.89	nil
A10	1.84	nil

CHAPTER FIVE

Conclusions & Recommendations

Chapter Five

Conclusions & recommendations

5.1 Conclusions

According to the obtained results, the following conclusions are made and some suggestions or recommendations mentioned for future work: -

1- CoCrMo base alloy (with and without ZrO_2), was prepared by powder metallurgy (P/M) method. XRD results showed that the sintering temperature was 1100°C for 4 hours enough to ensure the transformation of the used elements into alloy structure.

2- Zirconium oxide addition to CoCrMo alloy led to decrease the density and porosity of the sintered specimens.

3- Zirconium oxide addition to CoCrMo alloy led to an increase in the hardness compared to the base alloy.

4- Zirconium oxide addition to CoCrMo alloy led to an increase in wear resistance compared to the base alloy.

5- Zirconium oxide addition to CoCrMo alloy led to an increase in the compressive strength compared to the base alloy.

6- Zirconium oxide addition to CoCrMo alloy led to an increase in the corrosion resistance in both artificial and hanks solution.

7- Zirconium oxide addition to CoCrMo alloy led to decrease Cobalt ion release compared to the base alloy in the both synthetic saliva and Hank's solution.

5.2 Recommendations for future

1- Study the effect of yttrium oxide addition on the mechanical and electrochemical properties of CoCrMo alloy.
2- Study the effect of Al_2O_3 on physical, mechanical and electrochemical properties of CoCrMo alloy.
3- Study the effect of anodizing process on properties of CoCrMo alloy.

References

Reference

[1] J. Park and R. S. Lakes, *Biomaterials: an introduction*. Springer Science & Business Media, 2007.

[2] E. By and L. L. H. and J. R. Jones, *Biomaterials, artificial organs and tissue engineering*. Woodhead, 2005.

[3] H. Hermawan, D. Ramdan, and J. R. P. Djuansjah, "Metals for biomedical applications," *Biomed. Eng. theory to Appl.*, vol. 1, pp. 411–430, 2011.

[4] B. E. Abali and I. Giorgio, *Developments and Novel Approaches in Biomechanics and Metamaterials*. Springer, 2020.

[5] K. Prasad *et al.*, "Metallic biomaterials: Current challenges and opportunities," *Materials*, vol. 10, no. 8. MDPI AG, Jul. 31, 2017, doi: 10.3390/ma10080884.

[6] C. M. Agrawal, J. L. Ong, M. R. Appleford, and G. Mani, *Introduction to Biomaterials: Introduction; 2. Basic properties of materials; 3. Biological systems; 4. Characterization of biomaterials; 5. Metals: structure and properties; 6. Polymers; 7. Ceramics; 8. Natural biomaterials; 9. Surface modification; 10. Sterilization of biomedical implants; 11. Cell-biomaterial interactions; 12. Drug delivery systems; 13. Tissue engineering; 14. Clinical applications*. Cambridge University Press, 2014.

[7] Q. Chen and G. THOUAS, *Biomaterials A BASIC INTRODUCTION*. Woodhead Pub. and Maney Pub. on behalf of Institute of Materials, Minerals & Mining, 2008.

[8] J. Y. Wong, J. D. Bronzino, and D. R. Peterson, "Biomaterials—Principles and Practices. Vol. 1." Taylor & Francis Group, Boca Raton, 2013.

[9] G. L. Winters and M. J. Nutt, *Stainless steels for medical and surgical applications*. ASTM International, 2003.

[10] K. L. Ong, S. Lovald, and J. Black, *Orthopaedic biomaterials in research and practice*. CRC press, 2014.

[11] M. Kyomoto *et al.*, "High lubricious surface of cobalt–chromium–molybdenum alloy prepared by grafting poly (2-methacryloyloxyethyl phosphorylcholine)," *Biomaterials*, vol. 28, no. 20, pp. 3121–3130, 2007.

[12] R. F. Allen, "Standard specification for wrought 18 chromium-14 nickle-2.5 molybdenum stainless steel bar and wire for surgical implants (F138)," *Annu. B. ASTM Stand. Med. Devices Serv.*, 1998.

[13] J. Lutz and S. Mändl, "Reduced tribocorrosion of CoCr alloys in simulated

body fluid after nitrogen insertion," *Surf. Coatings Technol.*, vol. 204, no. 18–19, pp. 3043–3046, 2010.

[14] M. K. Abbass, S. A. Ajeel, and H. M. Wadullah, "Study of Corrosion Resistance of Co-Cr-Mo Surgical Implants Alloy in Artificial Saliva," *Eng. Technol. J.*, vol. 32, no. 10 Part (A) Engineering, 2014.

[15] R. Kotoka, "Functionalized Thin Film Coatings for Medical Implant Applications." North Carolina Agricultural and Technical State University, 2013.

[16] A. Aherwar, A. K. Singh, and A. Patnaik, "Cobalt based alloy: A better choice biomaterial for hip implants," *Trends Biomater. Artif. Organs*, vol. 30, no. 1, pp. 50–55, 2016.

[17] R. Mehta, S. Pande, S. Nanda, and T. Nanda, "Implant Surface Modification and Osseo Integration- Past , Present and Future," vol. 1, no. 5, pp. 20–25, 2014.

[18] R. A. Gittens, R. Olivares-Navarrete, Z. Schwartz, and B. D. Boyan, "Implant osseointegration and the role of microroughness and nanostructures: lessons for spine implants," *Acta Biomater.*, vol. 10, no. 8, pp. 3363–3371, 2014.

[19] A. W. Nugroho, "Investigation of the Production and Mechanical Properties of Porous Beta Titanium Alloy Compacts Prepared by Powder Metallurgy Processes for Biomedical Applications," no. April, 2013.

[20] R. A. Antunes and M. C. L. de Oliveira, "Corrosion fatigue of biomedical metallic alloys: mechanisms and mitigation," *Acta Biomater.*, vol. 8, no. 3, pp. 937–962, 2012.

[21] R. W. Schutz, "Understanding and preventing crevice corrosion of titanium alloys. Part I," *Mater. Perform.*, vol. 31, no. 10, pp. 57–62, 1992.

[22] X. G. Zhang, "Galvanic corrosion," *Uhlig's Corros. Handb.*, vol. 51, p. 123, 2011.

[23] M. G. Fontana and N. D. Greene, *Corrosion engineering*. McGraw-hill, 2018.

[24] G. S. Frankel, "Pitting corrosion," *ASM Handb.*, vol. 13, pp. 236–241, 2003.

[25] D. J. Blackwood, "Biomaterials: past successes and future problems," *Corros. Rev.*, vol. 21, no. 2–3, pp. 97–124, 2003.

[26] J. L. Katz and A. Meunier, "The elastic anisotropy of bone," *J. Biomech.*, vol. 20, no. 11–12, pp. 1063–1070, 1987.

[27] M. T. Mohammed, Z. A. Khan, and A. N. Siddiquee, “Influence of microstructural features on wear resistance of biomedical titanium materials,” *Int. J. Biomed. Biol. Eng.*, vol. 7, no. 1, pp. 49–53, 2013.

[28] L. Tane, W. C. Cronee, E. H. Wilson, and K. Sridharan, “Experimental Investigation of the Wear Behavior in Surface Modified NiTi,” *Materials Science Program*. Citeseer, pp. 562–565, 2001.

[29] M. Valefi, “Wear and friction of self-lubricating CuO-TZP composites,” 2012.

[30] B. Bhushan, *Introduction to tribology*. John Wiley & Sons, 2013.

[31] R. G. Bayer, “Fundamentals of wear failures,” *ASM Handb. Vol. 11, Fail. Anal. Prev.*, pp. 901–905, 2002.

[32] M. K. Egbo, “A fundamental review on composite materials and some of their applications in biomedical engineering,” *J. King Saud Univ. - Eng. Sci.*, vol. 33, no. 8, pp. 557–568, 2021, doi: 10.1016/j.jksues.2020.07.007.

[33] T.-D. Ngo, “Introduction to composite materials,” *Compos. Nanocomposite Mater. Knowl. to Ind. Appl.*, 2020.

[34] F. L. Matthews and R. D. Rawlings, *Composite materials: engineering and science*. Woodhead Publishing, 1999.

[35] M. Rosso, “Ceramic and metal matrix composites: Routes and properties,” *J. Mater. Process. Technol.*, vol. 175, no. 1–3, pp. 364–375, 2006.

[36] K. U. Kainer, “Basics of metal matrix composites,” *Met. Matrix Compos. Cust. Mater. Automot. Aerosp. Eng.*, pp. 1–54, 2006.

[37] W. D. Callister Jr and D. G. Rethwisch, *Materials science and engineering: an introduction*. wiley, 2020.

[38] J. W. Kaczmar and K. Pietrzak, “The production and application of metal matrix composite materials,” vol. 106, pp. 58–67, 2000.

[39] D. S. Finch, T. Oreskovic, K. Ramadurai, C. F. Herrmann, S. M. George, and R. L. Mahajan, “Biocompatibility of atomic layer- deposited alumina thin films,” *J. Biomed. Mater. Res. Part A An Off. J. Soc. Biomater. Japanese Soc. Biomater. Aust. Soc. Biomater. Korean Soc. Biomater.*, vol. 87, no. 1, pp. 100–106, 2008.

[40] P. N. Rojas and S. E. Rodil, “Corrosion behaviour of amorphous niobium oxide coatings,” *Int J Electrochem Sci*, vol. 7, pp. 1443–1458, 2012.

[41] B. D. Ratner, “The Nature of Matter and Materials,” in *Biomaterials*

Science: An Introduction to Materials: Third Edition, Elsevier Inc., 2013, pp. 6–9.

[42] G. F. Vander Voort *et al.*, "ASM handbook," *Metallogr. Microstruct.*, vol. 9, pp. 40002–44073, 2004.

[43] H. M. Wadullah, "Characterization of Structure and Corrosion Behavior," no. October, 2015, doi: 10.13140/RG.2.1.3461.1921.

[44] H. Fujii, T. Asano, Y. Matsuo, and Y. Sugie, "Effect of Heat-Treatment on Localized Corrosion Behavior of Duplex Stainless Steels in 3.5% NaCl Solution," *J. Mater. Sci. Eng. A*, vol. 1, no. 7A, p. 899, 2011.

[45] M. Takayukiinarushima and M. Editors, "Springer Series in Biomaterials Science and Engineering 3 Advances in Metallic Biomaterials Tissues, Materials and Biological Reactions." [Online]. Available: http://www.springer.com/series/10955.

[46] S. Kurosu, N. Nomura, and A. Chiba, "Effect of sigma phase in Co-29Cr-6Mo alloy on corrosion behavior in saline solution," *Mater. Trans.*, vol. 47, no. 8, pp. 1961–1964, 2006, doi: 10.2320/matertrans.47.1961.

[47] R. M. Namus, "CoCrMo alloys in hip and knee replacements application," no. September, 2018.

[48] S. Kurosu, N. Nomura, and A. Chiba, "Effect of Sigma Phase in Co-29Cr-6Mo Alloy on Corrosion and Mechanical Properties," *Adv. Mater. Res.*, vol. 26–28, pp. 777–780, 2007, doi: 10.4028/www.scientific.net/amr.26-28.777.

[49] M. G. Kamardan, N. H. A. Zaidi, M. N. Dalimin, A. M. A. Zaidi, S. B. Jamaludin, and M. M. A. Jamil, "The sintering temperature effect on the shrinkage behavior of cobalt chromium alloy," *Am. J. Appl. Sci.*, vol. 7, no. 11, p. 1443, 2010.

[50] A. P. Alekhin, G. I. Lapushkin, A. M. Markeev, A. A. Sigarev, and V. F. Toknova, "Atomic layer deposition of the titanium dioxide thin film from tetraethoxytitanium and water," *Russ. J. Gen. Chem.*, vol. 80, no. 6, pp. 1091–1096, 2010.

[51] J. V Giacchi, C. N. Morando, O. Fornaro, and H. A. Palacio, "Microstructural characterization of as-cast biocompatible Co–Cr–Mo alloys," *Mater. Charact.*, vol. 62, no. 1, pp. 53–61, 2011.

[52] L. Reclaru, P.-Y. Eschler, R. Lerf, and A. Blatter, "Electrochemical corrosion and metal ion release from Co-Cr-Mo prosthesis with titanium plasma spray coating," *Biomaterials*, vol. 26, no. 23, pp. 4747–4756, 2005.

[53] U. Türkan, *Biocompatibility and microstructural characterization of PVD coated and nitrogen implanted Co-Cr alloy*. Izmir Institute of Technology (Turkey), 2004.

[54] T. Kääriäinen, D. Cameron, M.-L. Kääriäinen, and A. Sherman, *Atomic layer deposition: principles, characteristics, and nanotechnology applications*. John Wiley & Sons, 2013.

[55] M. Yu, *Microstructure, corrosion behavior, mechanical property and biocompatibility of compression-molded zinc-nanodiamond composites as a bio-implant material*. Drexel University, 2014.

[56] P. E. Sinnett-Jones, J. A. Wharton, and R. J. K. Wood, "Micro-abrasion–corrosion of a CoCrMo alloy in simulated artificial hip joint environments," *Wear*, vol. 259, no. 7–12, pp. 898–909, 2005.

[57] G. Manivasagam, D. Dhinasekaran, and A. Rajamanickam, "Biomedical Implants: Corrosion and its Prevention - A Review," *Recent Patents Corros. Sci.*, vol. 2, no. 1, pp. 40–54, 2010, doi: 10.2174/1877610801002010040.

[58] P. Pittayachawan, "Dissertations," *J. Daoist Stud.*, vol. 1, no. 1, pp. 209–211, 2008, doi: 10.1353/dao.2008.0013.

[59] M. Y. Chou, P. K. Lam, and M. L. Cohen, "Ab initio study of structural and electronic properties of beryllium," *Phys. Rev. B*, vol. 28, no. 8, pp. 4179–4185, 1983, doi: 10.1103/PhysRevB.28.4179.

[60] P. F. Manicone, P. R. Iommetti, and L. Raffaelli, "An Overview of Zirconia Ceramics : Basic Properties and Clinical Applications An overview of zirconia ceramics : Basic properties and clinical applications," no. December, 2017, doi: 10.1016/j.jdent.2007.07.008.

[61] T. Blanquart, J. Niinistö, M. Ritala, and M. Leskelä, "Atomic layer deposition of groups 4 and 5 transition metal oxide thin films: focus on heteroleptic precursors," *Chem. Vap. Depos.*, vol. 20, no. 7-8–9, pp. 189–208, 2014.

[62] A. Henschke, *Ethics in an age of surveillance: personal information and virtual identities*. Cambridge University Press, 2017.

[63] B. D. Ratner, A. S. Hoffman, F. J. Schoen, and J. E. Lemons, *Biomaterials science: an introduction to materials in medicine*. Elsevier, 2004.

[64] O. Erdem, "The Development and Applications of Powder Metallurgy Manufacturing Methods in Automotive Industry," *Int. J. Eng. Res. Dev.*, vol. 9, no. 3, pp. 100–112, 2017.

[65] J. M. Torralba Castelló and M. Campos Gómez, "Toward high performance in Powder Metallurgy," 2014.

[66] A. Šalak, M. Selecká, and H. Danninger, *Machinability of powder metallurgy steels*. Cambridge Int Science Publishing, 2005.

[67] Y. Hammi, T. W. Stone, P. G. Allison, and M. F. Horstemeyer, "Fatigue Modeling of a Powder Metallurgy Main Bearing Cap," 2010.

[68] M. P. Groover, *Fundamentals of modern manufacturing: materials, processes, and systems*. John Wiley & Sons, 2020.

[69] K. V. Rao, *Manufacturing Science and Technology-Manufacturing Processess and Machine Tools*. New Age International, 2002.

[70] C. Shang, I. C. Sinka, and J. Pan, "Material data for modelling density distributions in green parts," in *Materials Science Forum*, 2011, vol. 672, pp. 207–214.

[71] V. Shatokha, *Sintering: Methods and products*. BoD–Books on Demand, 2012.

[72] L. Meluch, "Warm compaction of aluminium alloy Alumix 123." University of Birmingham, 2010.

[73] Z. Z. Fang, *Sintering of advanced materials*. Elsevier, 2010.

[74] G. J. Kipouros, W. F. Caley, and D. P. Bishop, "On the advantages of using powder metallurgy in new light metal alloy design," *Metall. Mater. Trans. A*, vol. 37, no. 12, pp. 3429–3436, 2006.

[75] P. C. Sharma, *A Textbook of Production Technology (Manufacturing Processes): Manufacturing Processes*. S. Chand Publishing, 2007.

[76] M. P. Groover, "Part II Engineering Materials," *Fundam. Mod. Manuf. Mater.*, pp. 98–132, 210AD.

[77] M. P. Groover, *Fundamentals of modern manufacturing*. Wiley-Blackwell, 2022.

[78] R. K. Rajput, *A textbook of manufacturing technology: Manufacturing processes*. Firewall Media, 2007.

[79] A. M. Khorasani, M. Goldberg, E. H. Doeven, and G. Littlefair, "Titanium in biomedical applications—properties and fabrication: a review," *J. Biomater. Tissue Eng.*, vol. 5, no. 8, pp. 593–619, 2015.

[80] A. Kocijan, I. Milošev, and B. Pihlar, "Cobalt-based alloys for orthopaedic applications studied by electrochemical and XPS analysis," *J. Mater. Sci.*

Mater. Med., vol. 15, no. 6, pp. 643–650, 2004.

[81] T. Hanawa, "Metal ion release from metal implants," *Mater. Sci. Eng. C*, vol. 24, no. 6–8, pp. 745–752, 2004.

[82] R. W.-W. Hsu, C.-C. Yang, C.-A. Huang, and Y.-S. Chen, "Electrochemical corrosion studies on Co–Cr–Mo implant alloy in biological solutions," *Mater. Chem. Phys.*, vol. 93, no. 2–3, pp. 531–538, 2005.

[83] M. Dourandish, D. Godlinski, A. Simchi, and V. Firouzdor, "Sintering of biocompatible P/M Co–Cr–Mo alloy (F-75) for fabrication of porosity-graded composite structures," *Mater. Sci. Eng. A*, vol. 472, no. 1–2, pp. 338–346, 2008.

[84] C. V. Vidal and A. I. Muñoz, "Electrochemical characterisation of biomedical alloys for surgical implants in simulated body fluids," *Corros. Sci.*, vol. 50, no. 7, pp. 1954–1961, 2008.

[85] D. H. J. J. AL-DEEN, A. L. I. HOBIHALEEM, and A. H. KHILFE, "STUDYING THE PROPERTIES OF COCRMO (F75) DOPED Y USING (PM)," *Carbon N. Y.*, vol. 99, no. 37.44, pp. 0–35.

[86] H. Jamal Al-Deen and E. Hassani, *Effect of In addition on the properties of CoCrMo (F75) alloy using P/M Technique*. 2018.

[87] Z. Doni *et al.*, "Tribocorrosion behaviour of hot pressed CoCrMo− Al2O3 composites for biomedical applications," *Tribol. Surfaces Interfaces*, vol. 8, no. 4, pp. 201–208, 2014.

[88] H. H. J. J. Al-Deen and E. A. R. Hassani, "Effect of in addition on the properties of CoCrMo (F75) alloy using P/M technique," *J. Eng. Appl. Sci.*, vol. 13, no. Specialissue12, pp. 9497–9502, 2018, doi: 10.3923/jeasci.2018.9497.9502.

[89] T. Odahara, H. Matsumoto, and A. Chiba, "Mechanical properties of biomedical Co-33Cr-5Mo-0.3 N alloy at elevated temperatures," *Mater. Trans.*, vol. 49, no. 9, pp. 1963–1969, 2008.

[90] A. A. Atiyah, A.-R. K. A. Ali, and N. M. Dawood, "Characterization of NiTi and NiTiCu porous shape memory alloys prepared by powder metallurgy (Part I)," *Arab. J. Sci. Eng.*, vol. 40, no. 3, pp. 901–913, 2015.

[91] A. Standard, "G99, Standard test method for wear testing with a pin-on-disk apparatus," *ASTM Int. West Conshohocken, PA*, 2006.

[92] A. H. Khilfa, "Effect of Y and Ge addition on Mechanical properties and

Corrosion behavior of Biomedical CoCrMo Alloy (F75).” master thesis, Materials engineering, University of Babylon, 2015.

[93] P. C. Fazio, “Annual Book of ASTM Standards, Wear and Erosion; Metal Corrosion,” *ASTM G102-89. Stand. Pract. Calc. Corros. Rates Relat. Inf. from Electrochem. Meas. ASTM, Philadelphia*, 2004.

[94] N. M. Dawood, “Preparation And Characterization of Bio Nitinol With Addition of Copper.” Ph. D. thesis, Materials Engineering Department, University Of Technology, Iraq, 2014.

[95] A. Amer and M. Mohammed, “Improvement of Mechanical and Electrochemical Properties of Biomedical Ti6Al4V alloy by Ta and Zr addition.”

[96] S. C. Gad and S. Gad-McDonald, *Biomaterials, medical devices, and combination products: Biocompatibility testing and safety assessment*. CRC Press, 2015.

[97] I. Tripathy, “Effect of microstructure on sliding wear behaviour of modified 9Cr-1Mo steel.” 2011.

[98] H. H. J. Al-Deen, “Improvement of Corrosion Resistance of Aluminum–Bronze Alloys In (3.5% NaCL and 2m HCl) Solutions by Indium Additions,” *J. Mech. Eng. Res. Dev.*, vol. 43, no. 2, pp. 218–225, 2020.

Appendices

Appendices

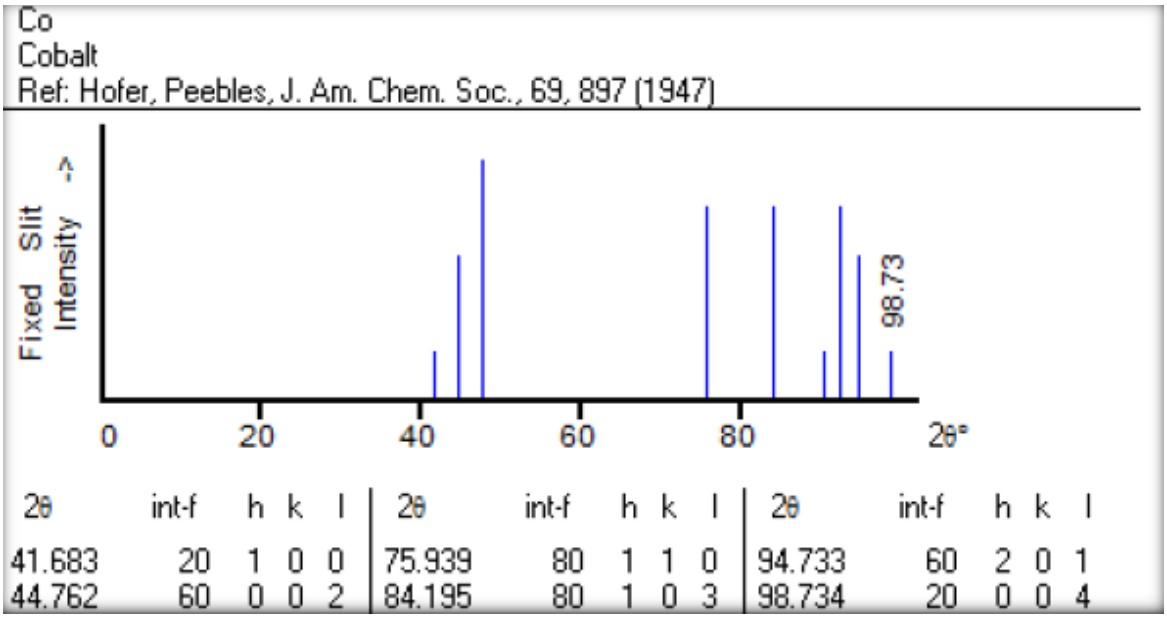

2θ	int-f	h	k	l	2θ	int-f	h	k	l	2θ	int-f	h	k	l
41.683	20	1	0	0	75.939	80	1	1	0	94.733	60	2	0	1
44.762	60	0	0	2	84.195	80	1	0	3	98.734	20	0	0	4

Fig (1): Chart for Pure Cobalt

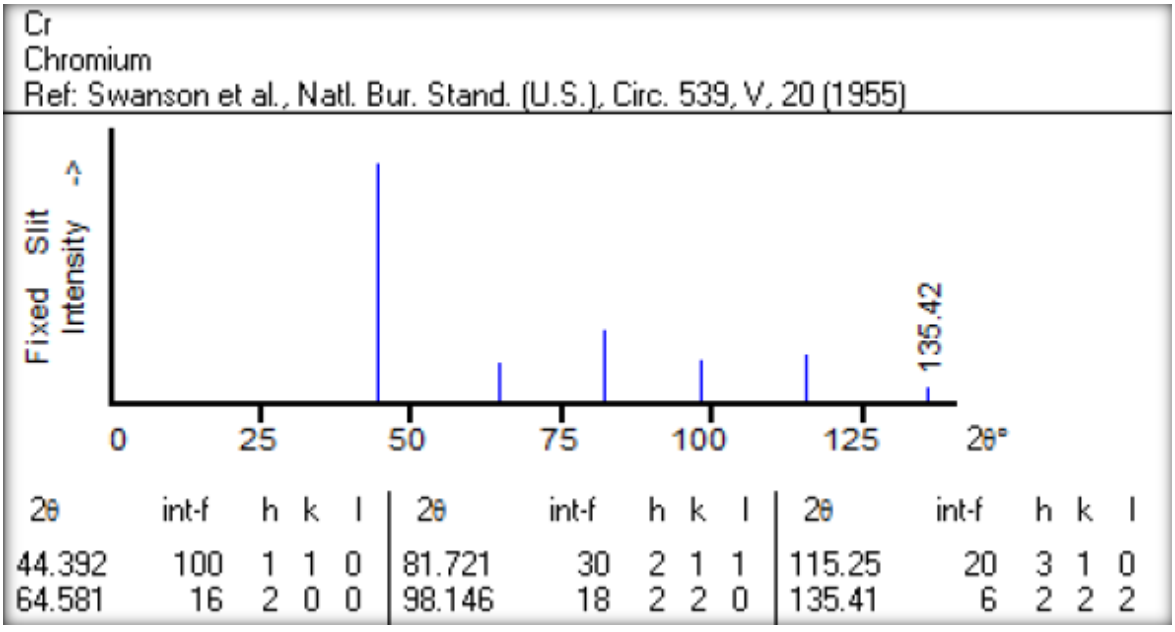

2θ	int-f	h	k	l	2θ	int-f	h	k	l	2θ	int-f	h	k	l
44.392	100	1	1	0	81.721	30	2	1	1	115.25	20	3	1	0
64.581	16	2	0	0	98.146	18	2	2	0	135.41	6	2	2	2

Fig (2): Chart for Pure Chromium

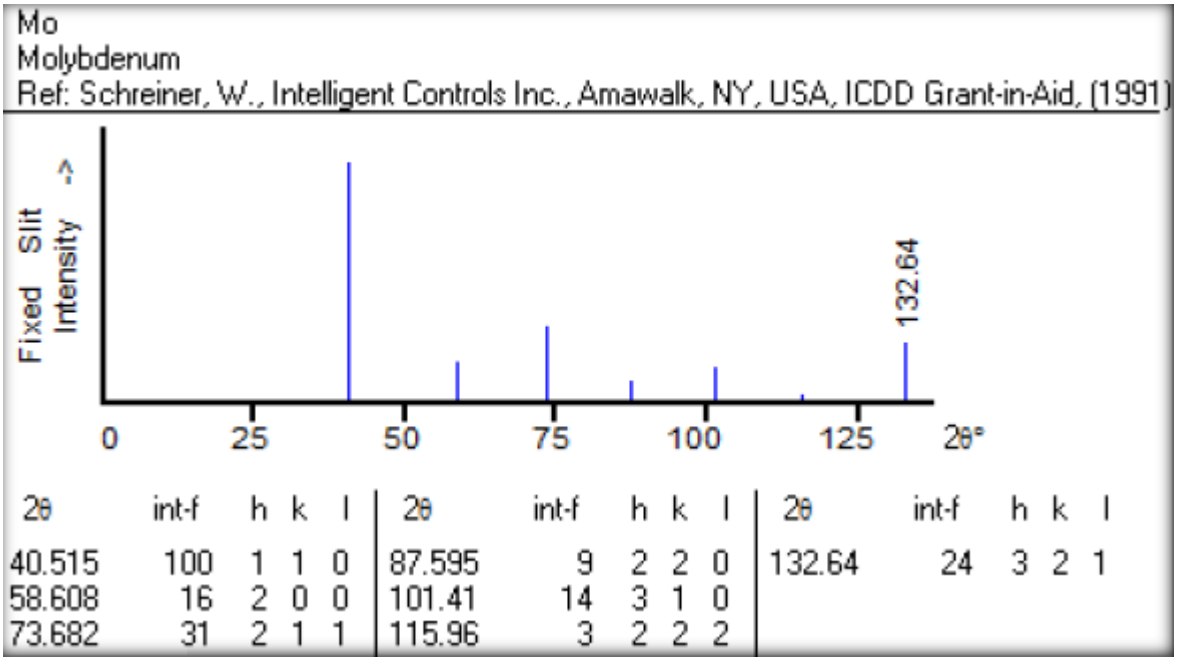

2θ	int-f	h	k	l	2θ	int-f	h	k	l	2θ	int-f	h	k	l
40.515	100	1	1	0	87.595	9	2	2	0	132.64	24	3	2	1
58.608	16	2	0	0	101.41	14	3	1	0					
73.682	31	2	1	1	115.96	3	2	2	2					

Fig (3): Chart for Pure Molybdenum

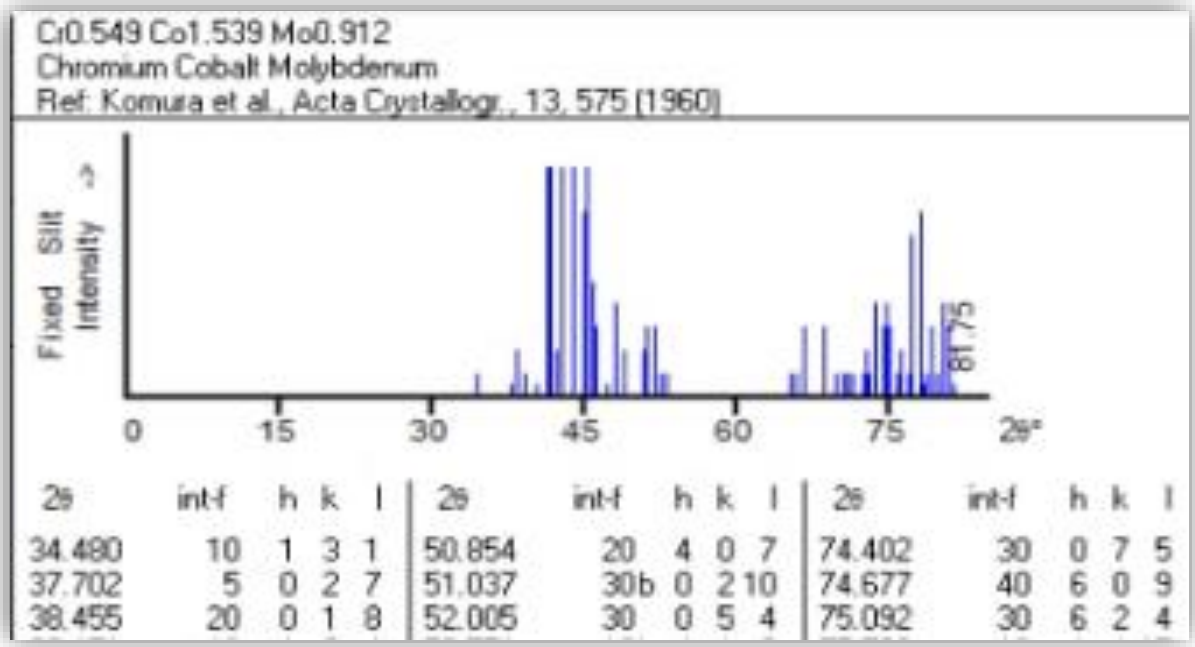

2θ	int-f	h	k	l	2θ	int-f	h	k	l	2θ	int-f	h	k	l
34.480	10	1	3	1	50.854	20	4	0	7	74.402	30	0	7	5
37.702	5	0	2	7	51.037	30b	0	2	10	74.677	40	6	0	9
38.455	20	0	1	8	52.005	30	0	5	4	75.092	30	6	2	4

Fig (4): Chart for CoCrMo Phase

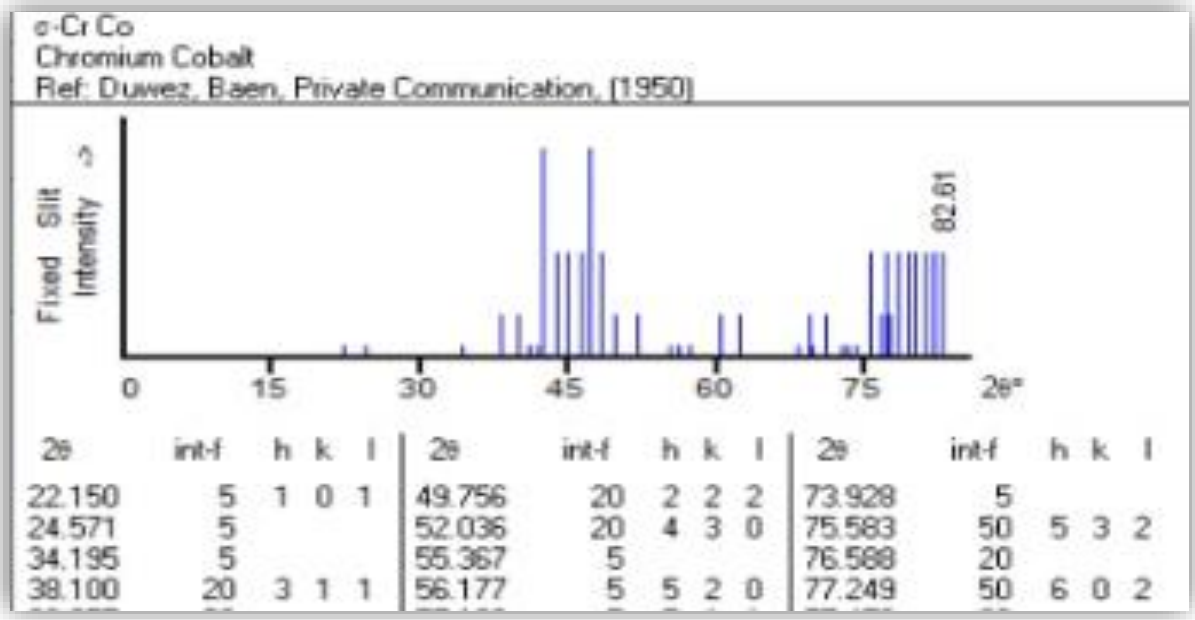

2θ	int-f	h	k	l	2θ	int-f	h	k	l	2θ	int-f	h	k	l
22.150	5	1	0	1	49.756	20	2	2	2	73.928	5			
24.571	5				52.036	20	4	3	0	75.583	50	5	3	2
34.195	5				55.367	5				76.588	20			
38.100	20	3	1	1	56.177	5	5	2	0	77.249	50	6	0	2

Fig (5): Chart for CoCr Phase

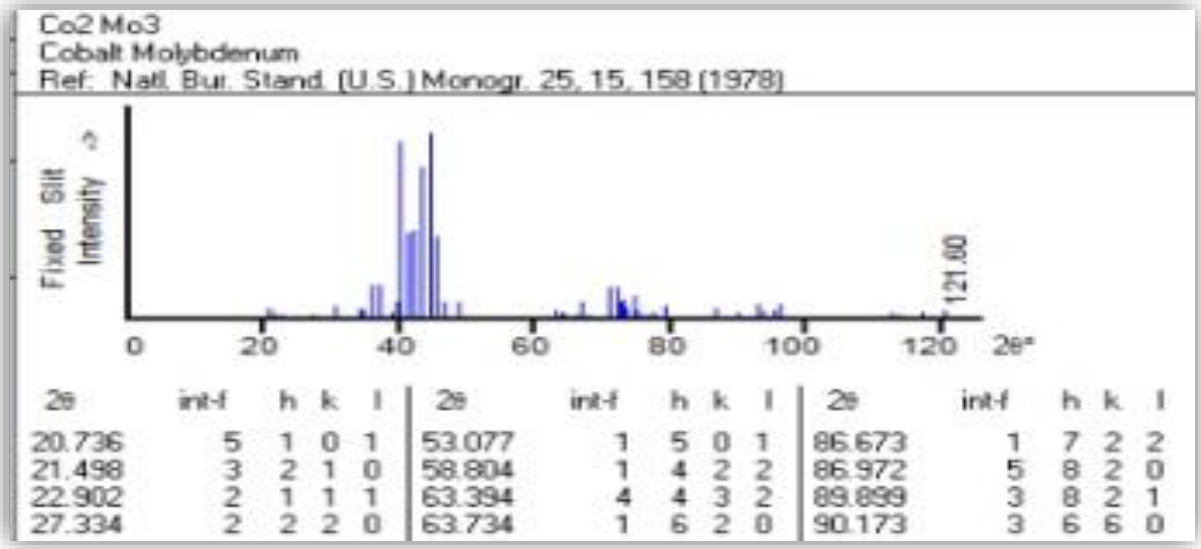

2θ	int-f	h	k	l	2θ	int-f	h	k	l	2θ	int-f	h	k	l
20.736	5	1	0	1	53.077	1	5	0	1	86.673	1	7	2	2
21.498	3	2	1	0	58.804	1	4	2	2	86.972	5	8	2	0
22.902	2	1	1	1	63.394	4	4	3	2	89.899	3	8	2	1
27.334	2	2	2	0	63.734	1	6	2	0	90.173	3	6	6	0

Fig (6): Chart for Co_2Mo_3 Phase

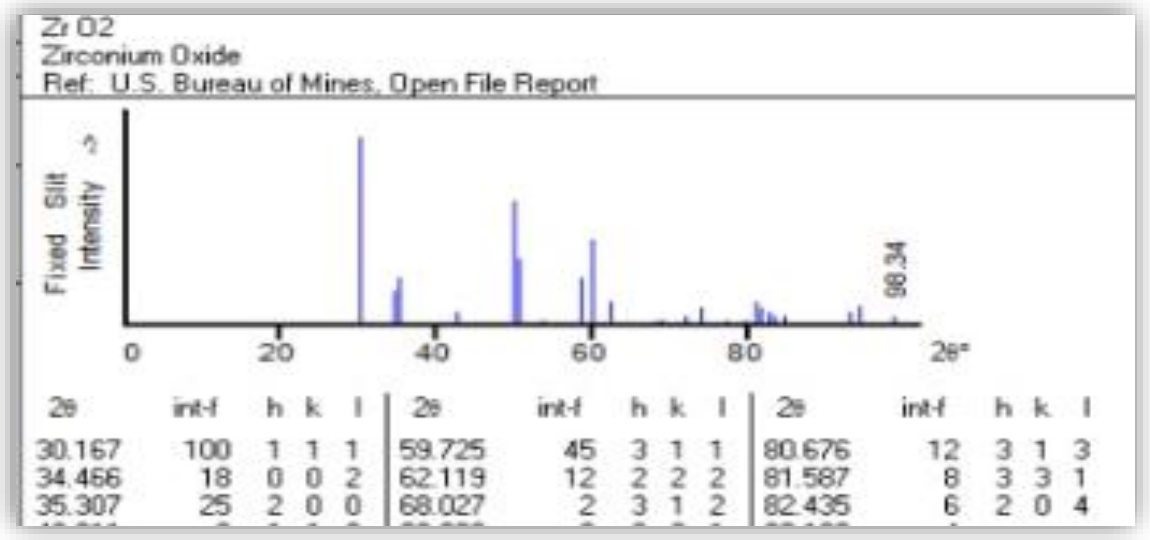

Fig (7): Chart for ZrO_2

Fig (8): Potentiodynamic Polarization Curve for B Alloy in Hank's Solution.

Fig (9): Potentiodynamic Polarization Curve for A1 Alloy in Hank's Solution.

Fig (10): Potentiodynamic Polarization Curve for A2 Alloy in Hank's Solution.

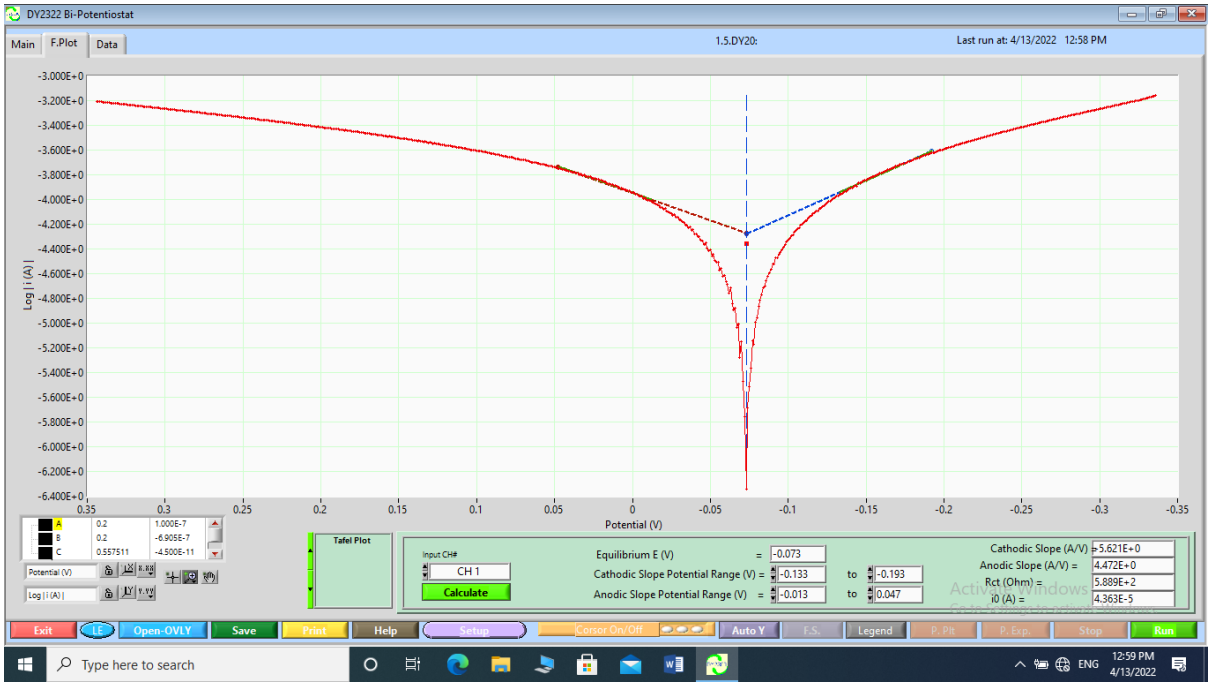

Fig (11): Potentiodynamic Polarization Curve for A3 Alloy in Hank's Solution.

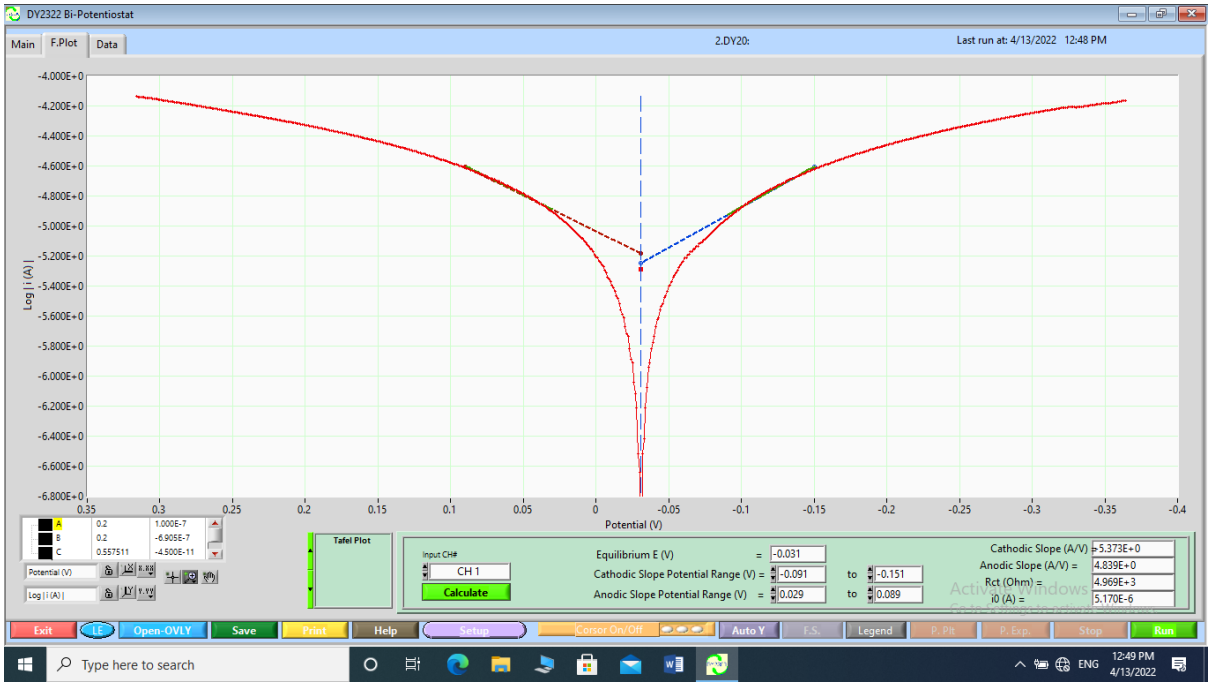

Fig (12): Potentiodynamic Polarization Curve for A4 Alloy in Hank's Solution.

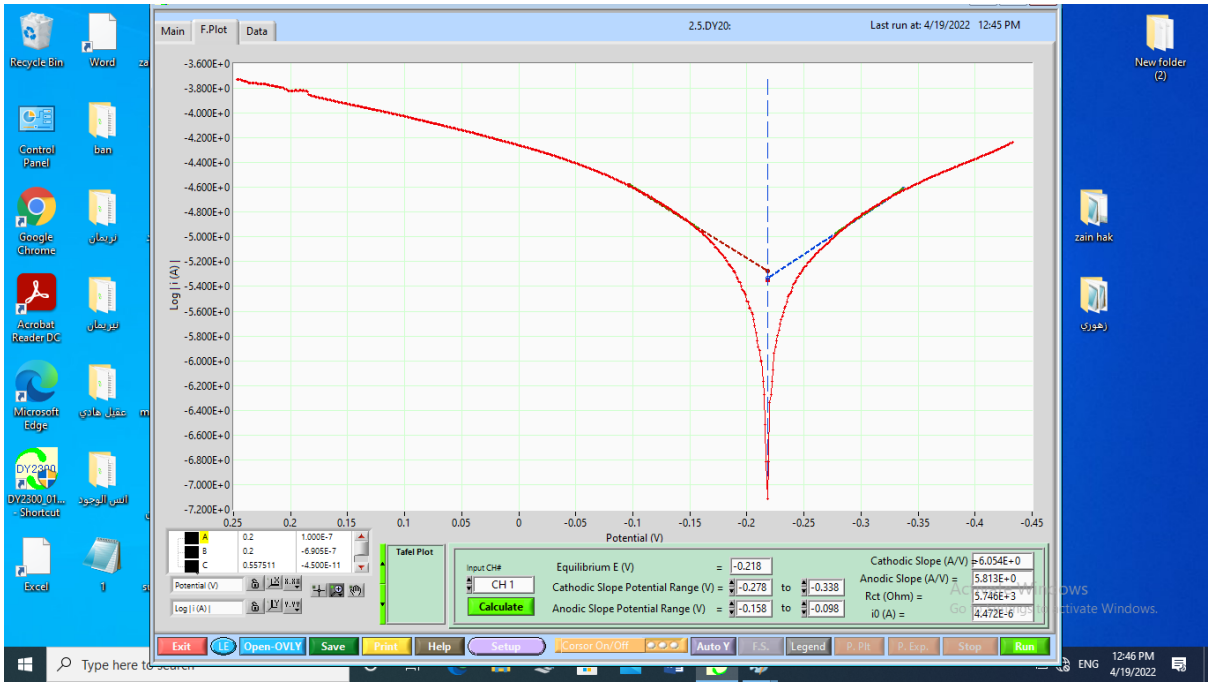

Fig (13): Potentiodynamic Polarization Curve for A5 Alloy in Hank's Solution.

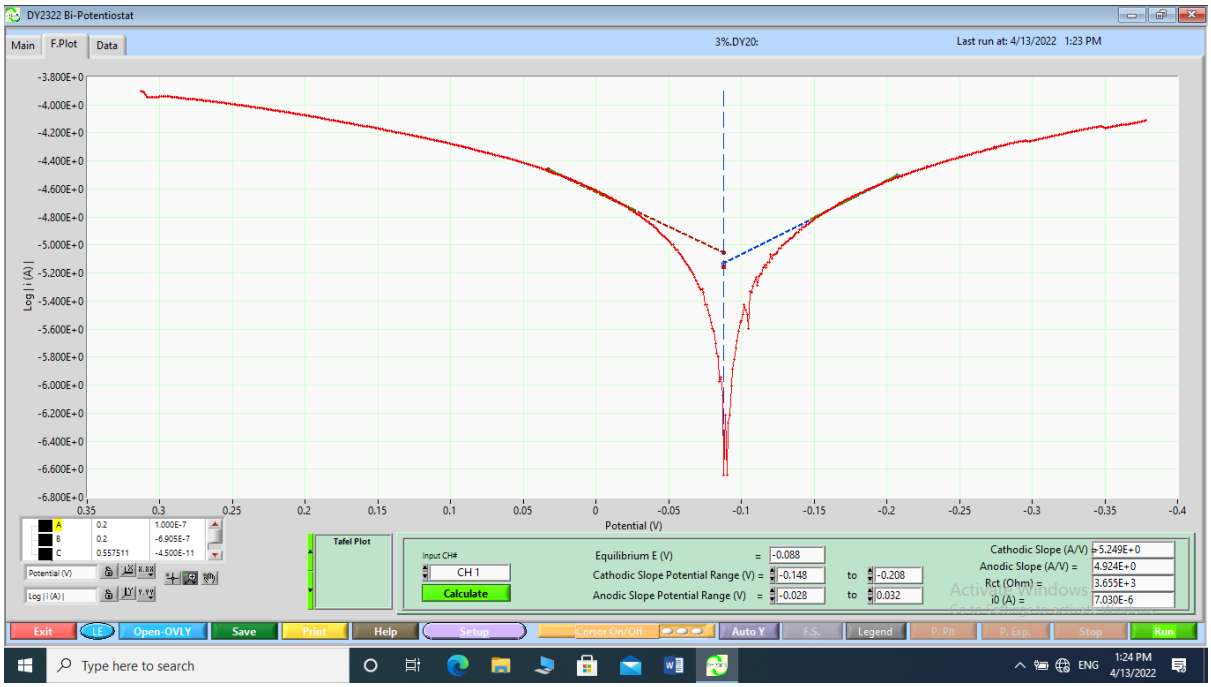

Fig (14): Potentiodynamic Polarization Curve for A6 Alloy in Hank's Solution.

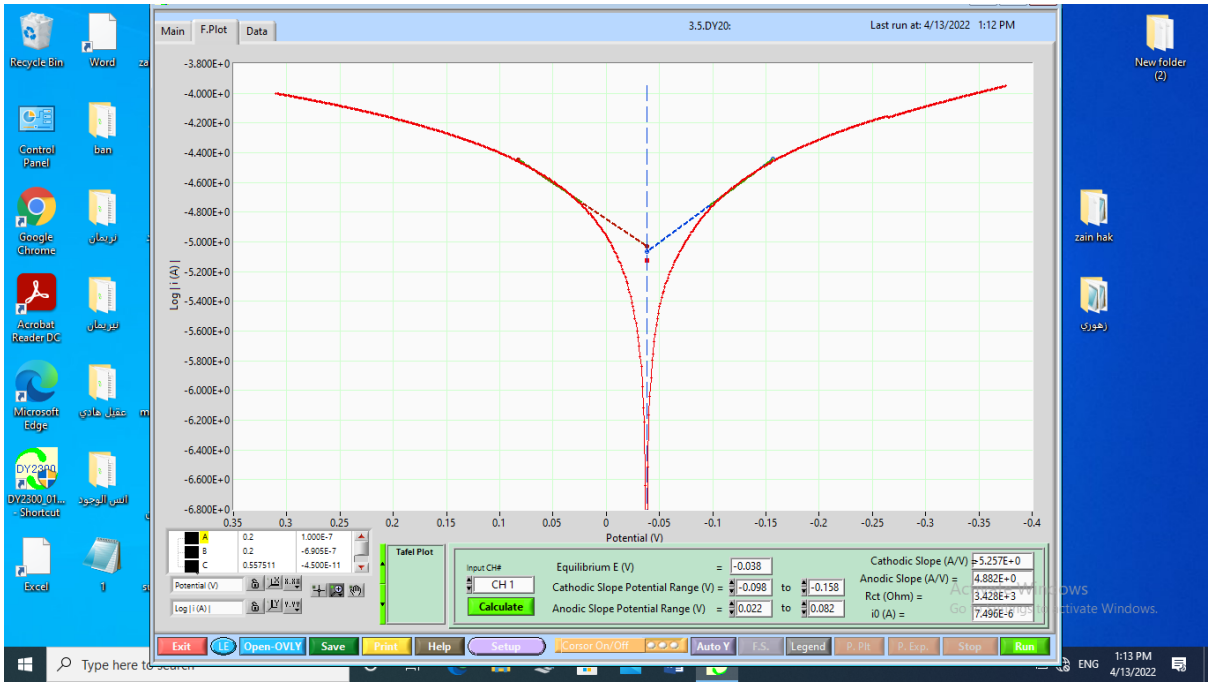

Fig (15): Potentiodynamic Polarization Curve for A7 Alloy in Hank's Solution.

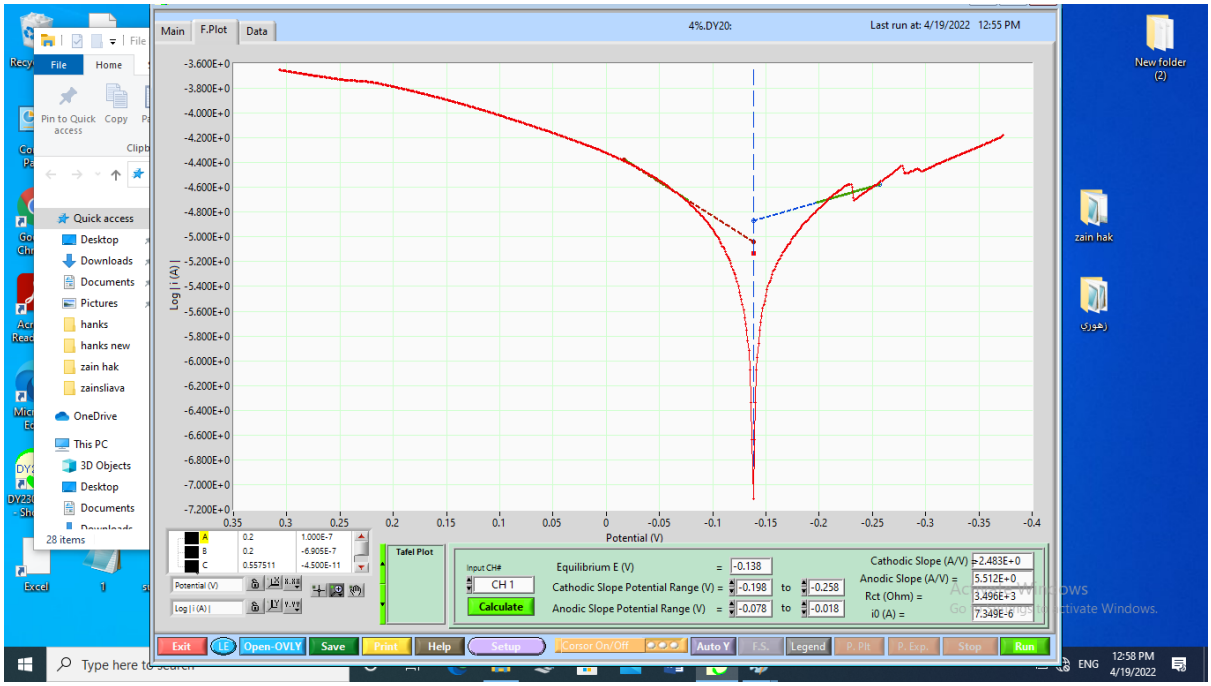

Fig (16): Potentiodynamic Polarization Curve for A8 Alloy in Hank's Solution.

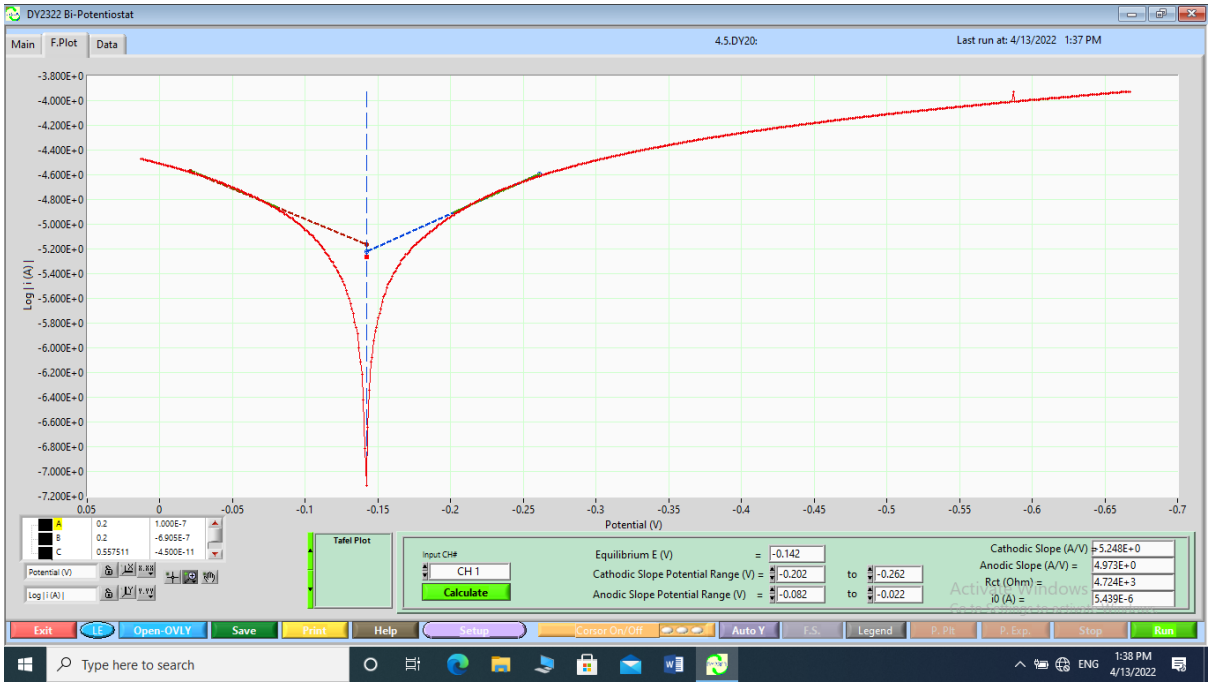

Fig (17): Potentiodynamic Polarization Curve for A9 Alloy in Hank's Solution.

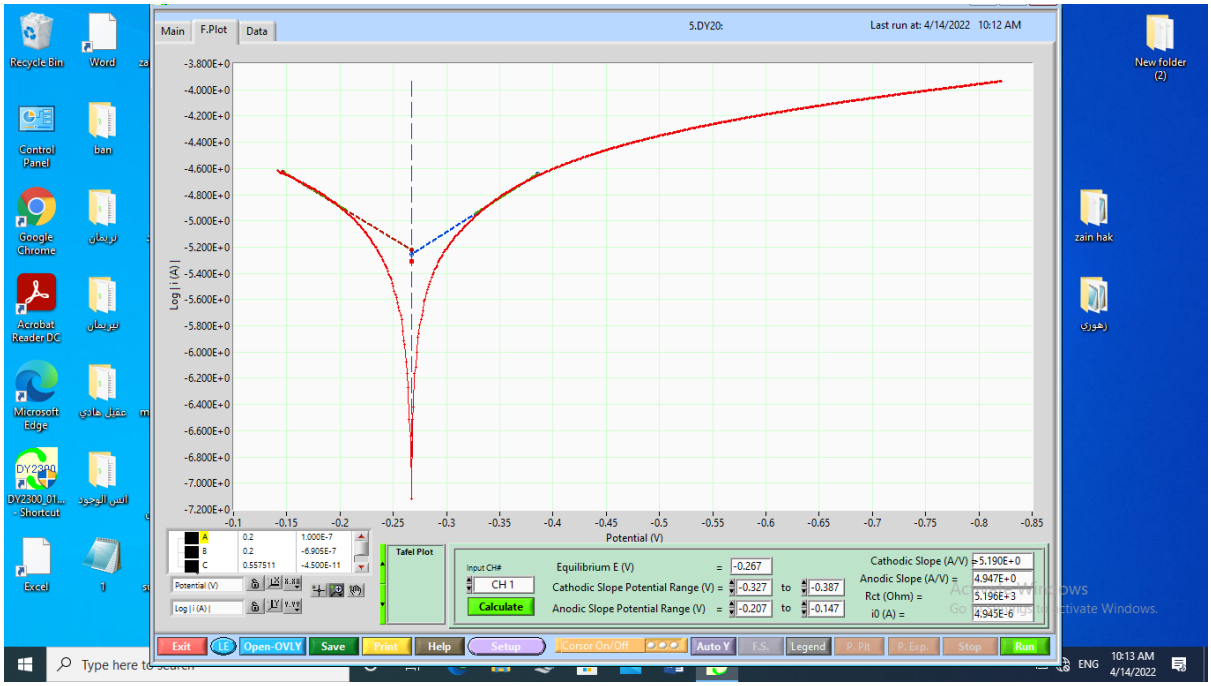

Fig (18): Potentiodynamic Polarization Curve for A10 Alloy in Hank's Solution.

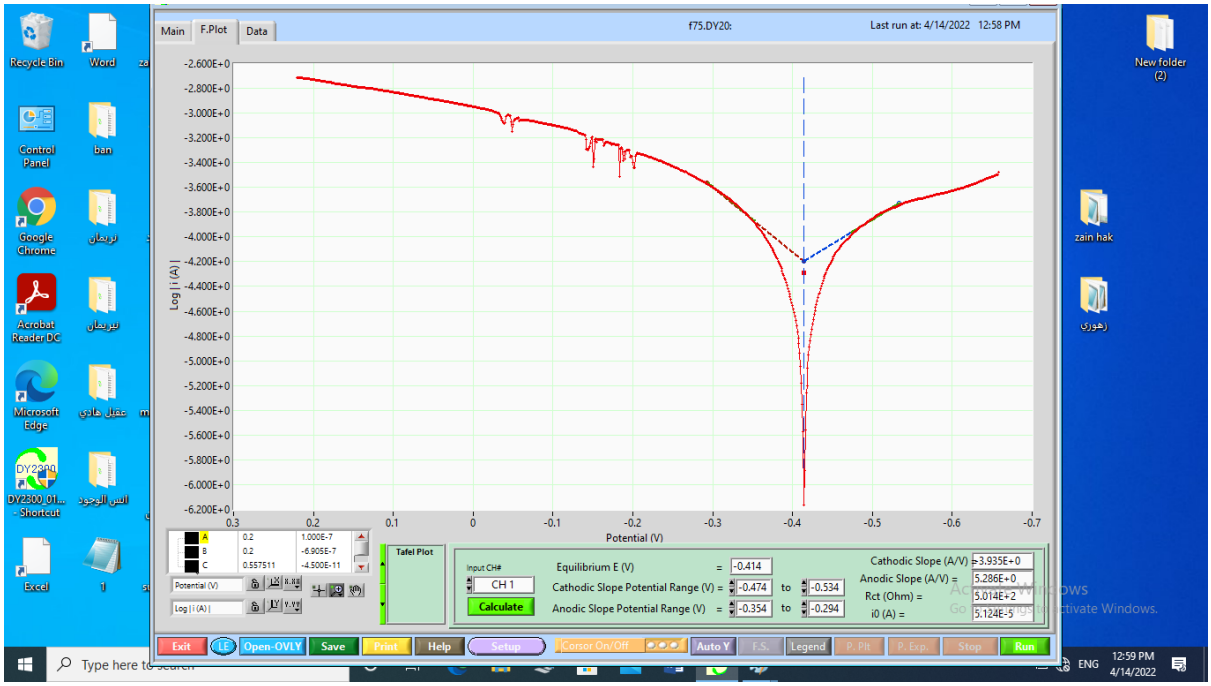

Fig (19): Potentiodynamic Polarization Curve for B Alloy in artificial saliva.

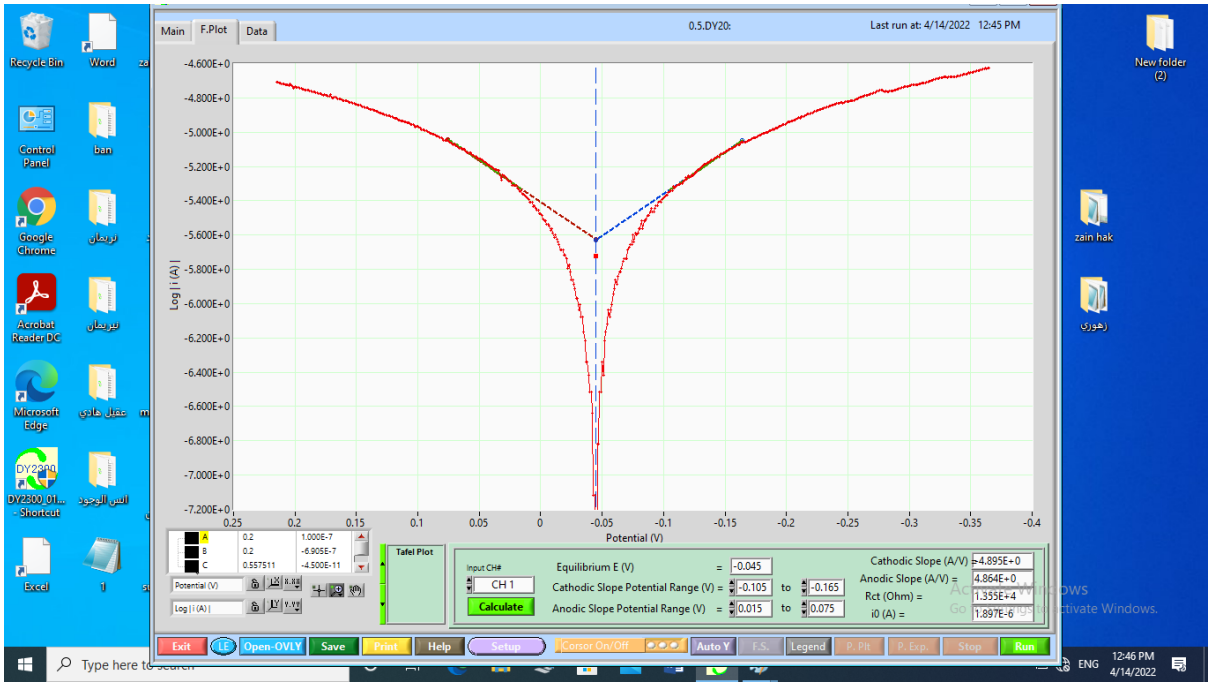

Fig (20): Potentiodynamic Polarization Curve for A1 Alloy in artificial saliva.

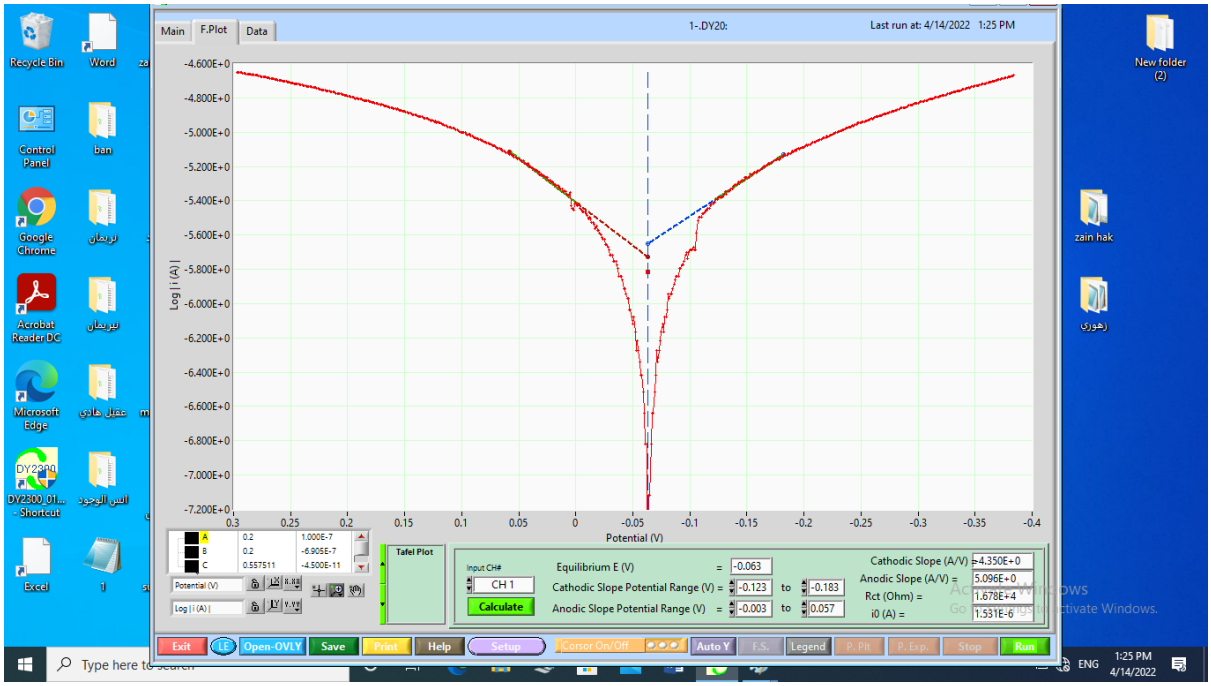

Fig (21): Potentiodynamic Polarization Curve for A2 Alloy in artificial saliva.

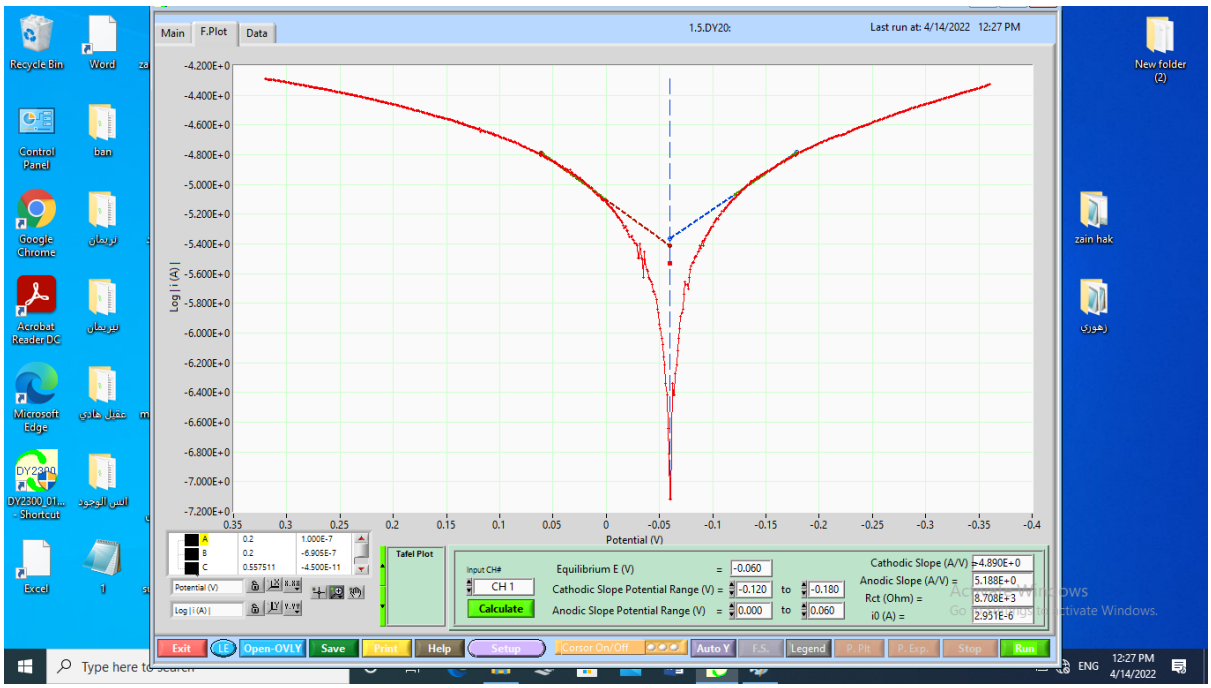

Fig (22): Potentiodynamic Polarization Curve for A3 Alloy in artificial saliva.

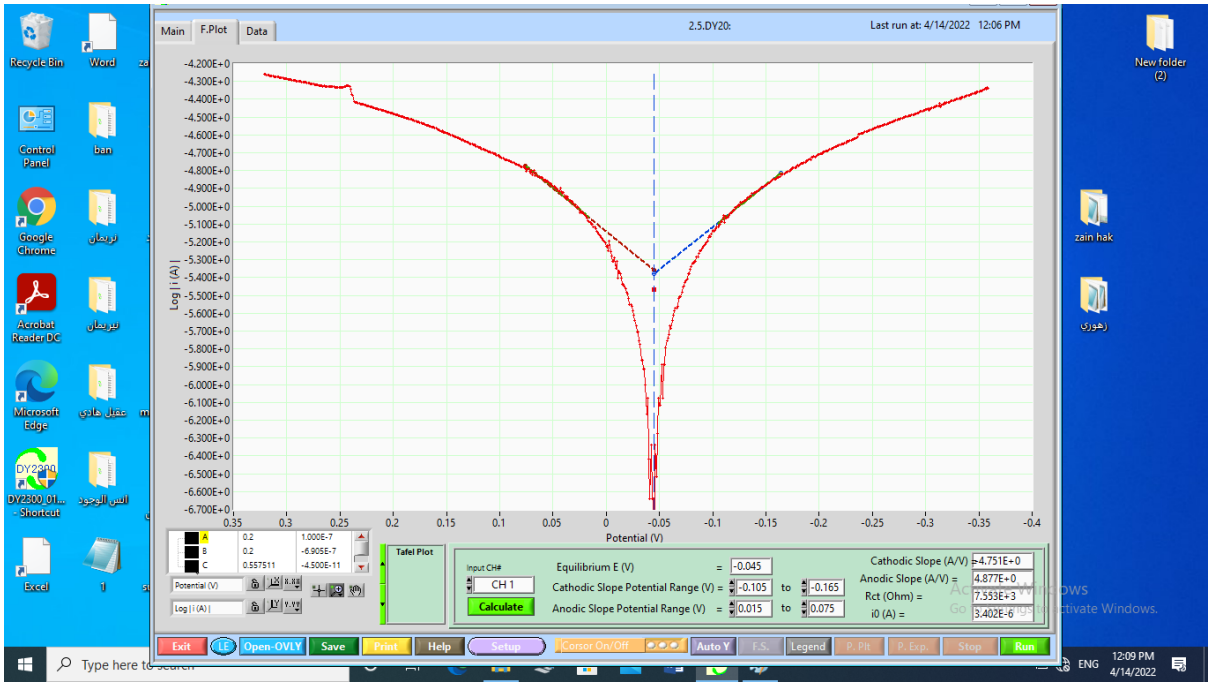

Fig (23): Potentiodynamic Polarization Curve for A4 Alloy in artificial saliva.

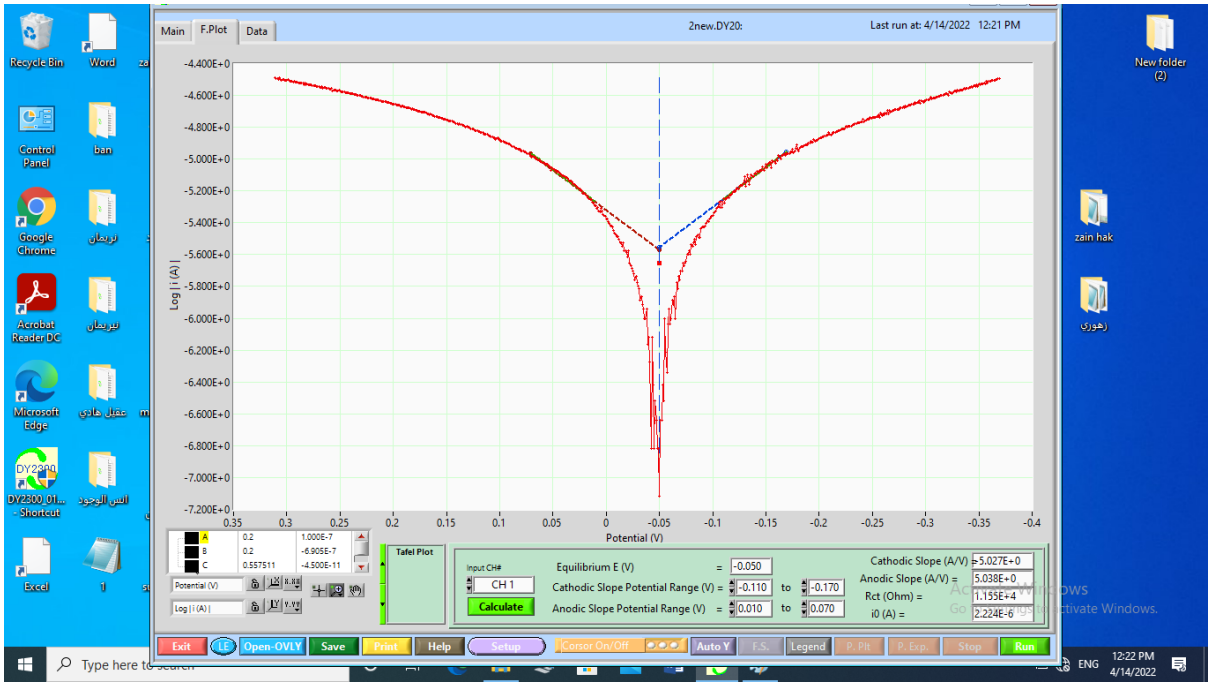

Fig (24): Potentiodynamic Polarization Curve for A5 Alloy in artificial saliva.

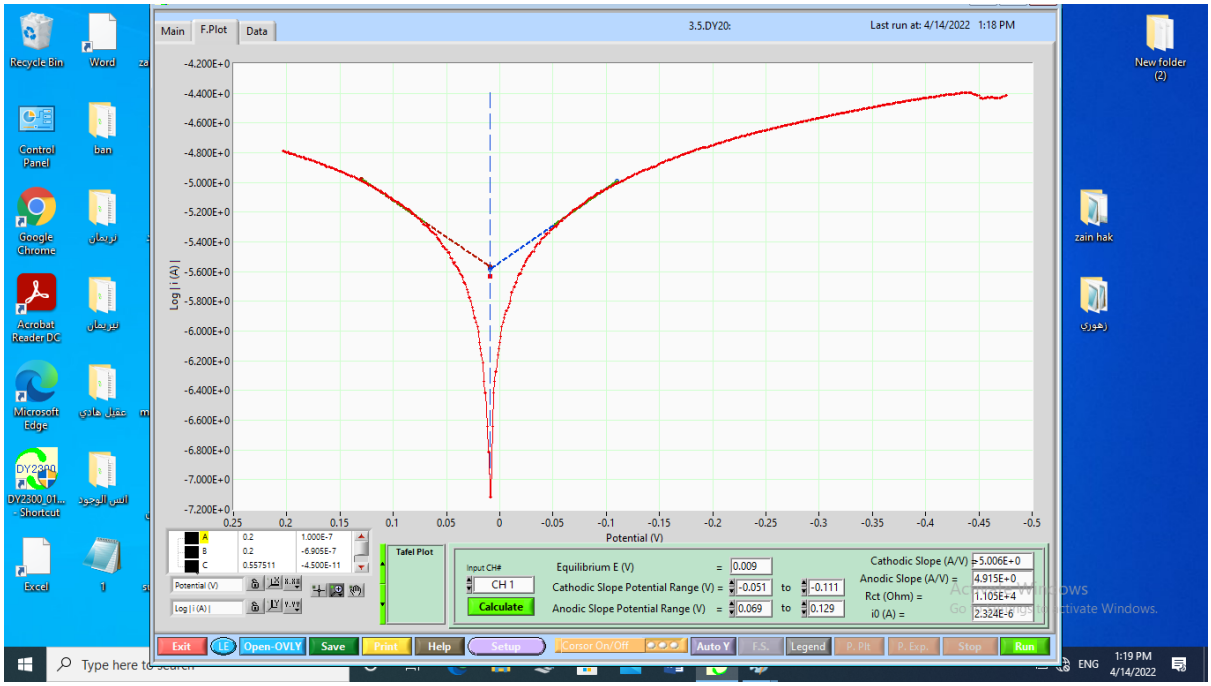

Fig (25): Potentiodynamic Polarization Curve for A6 Alloy in artificial saliva.

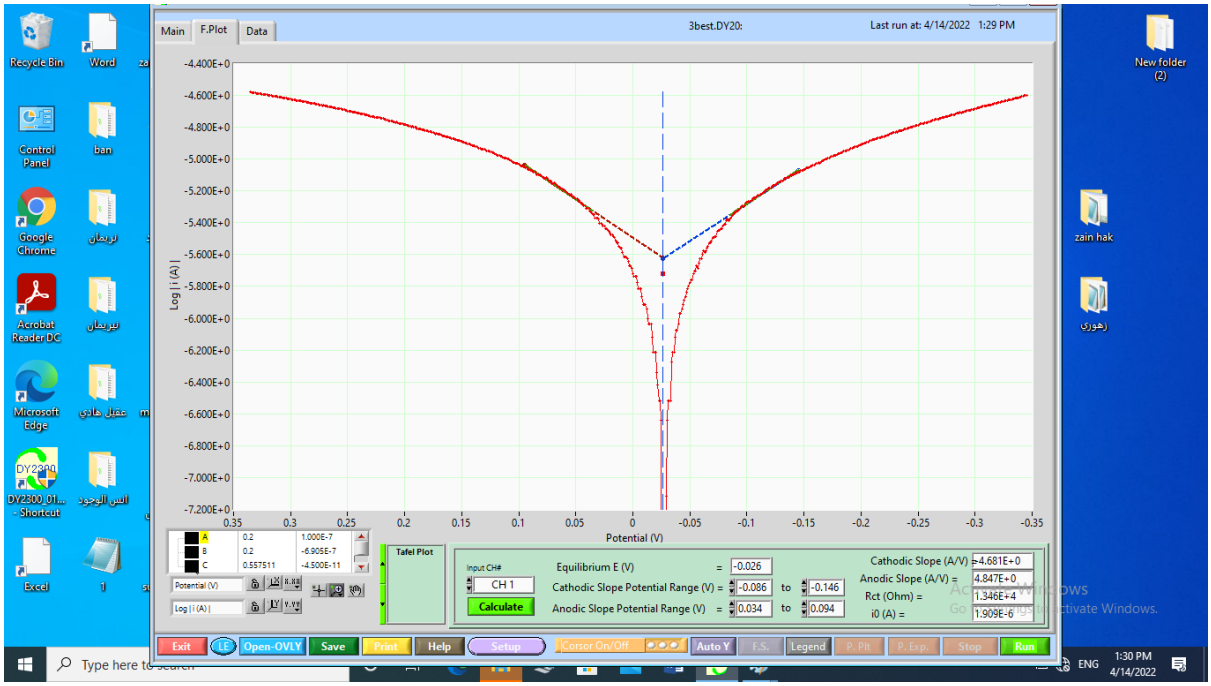

Fig (25): Potentiodynamic Polarization Curve for A7 Alloy in artificial saliva.

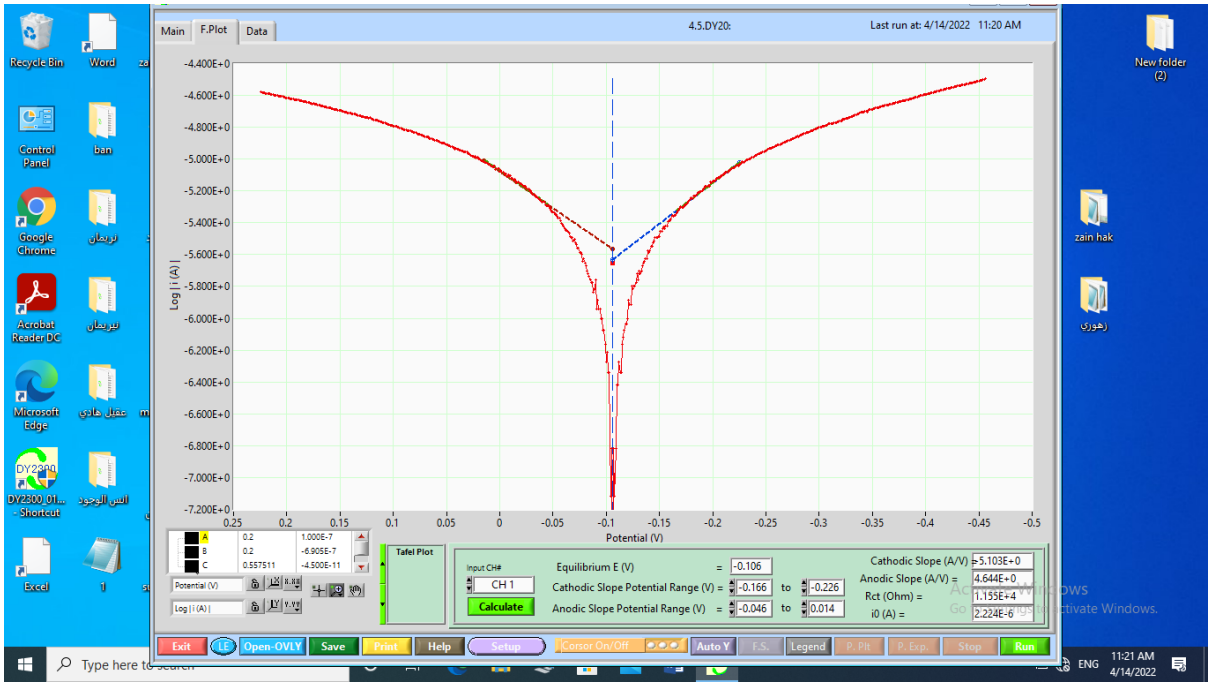

Fig (26): Potentiodynamic Polarization Curve for A8 Alloy in artificial saliva.

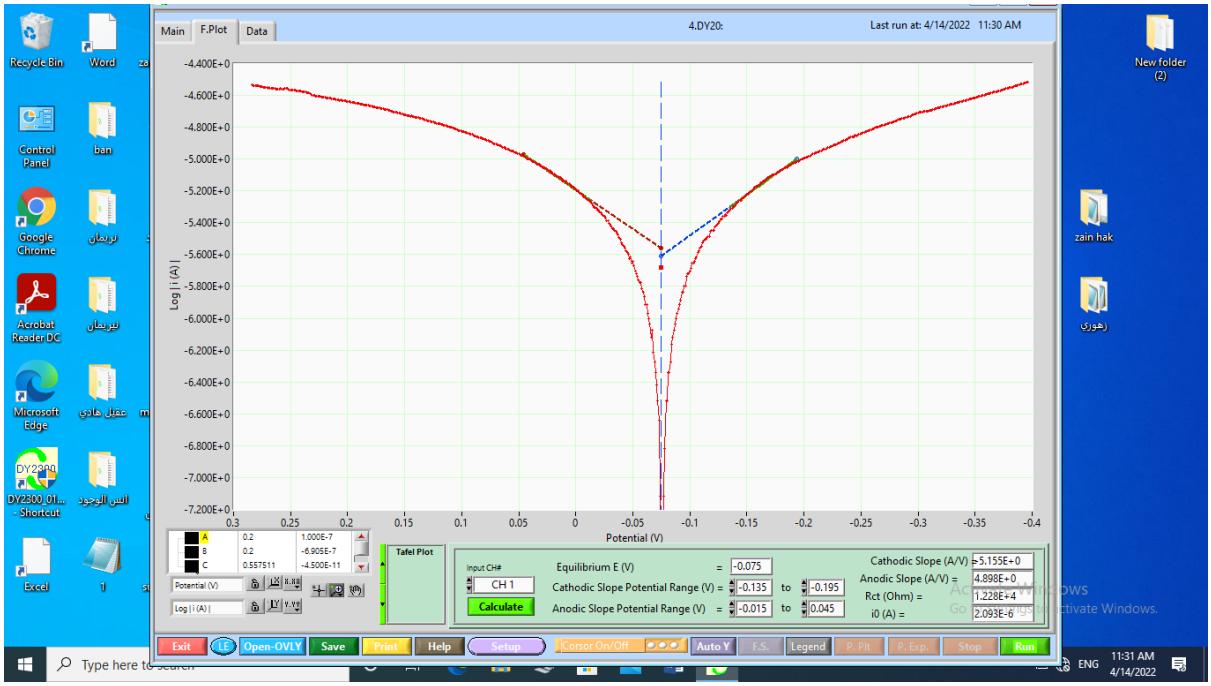

Fig (27): Potentiodynamic Polarization Curve for A9 Alloy in artificial saliva.

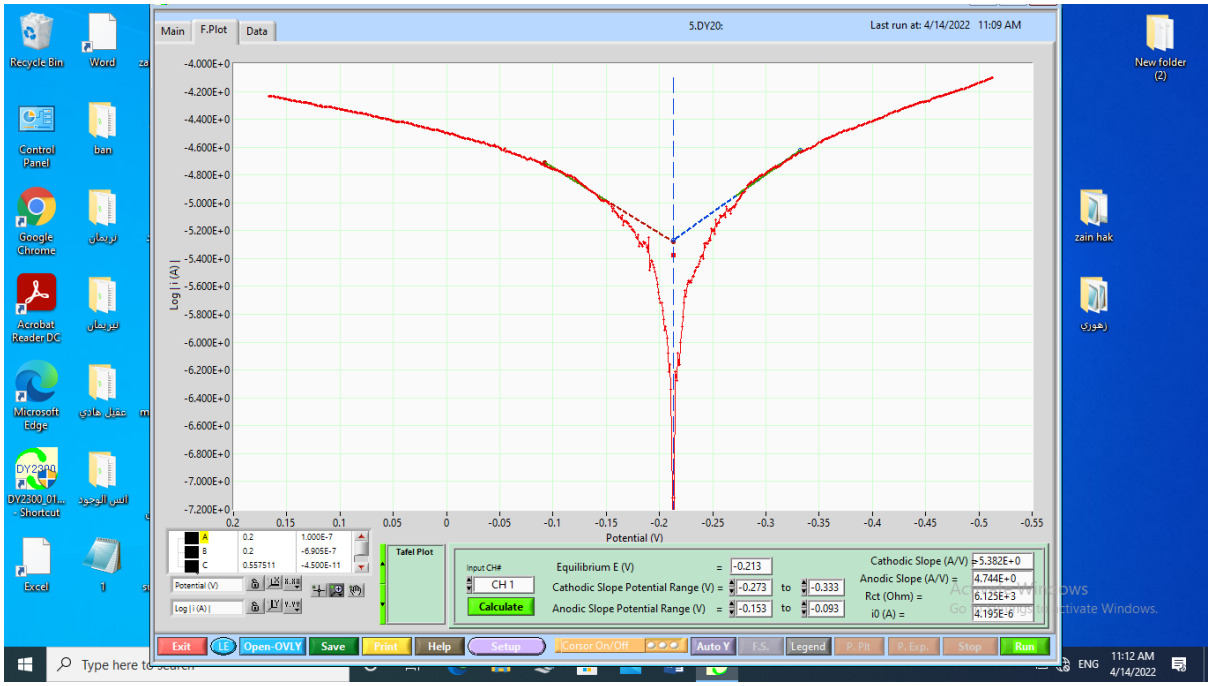

Fig (28): Potentiodynamic Polarization Curve for A10 Alloy in artificial saliva.

وزارة العلوم والتكنولوجيا

دائرة بحوث المواد

رقم الاستماره: ٢٠٥

التاريخ: ٢٠٢٢/٥/١٥

استمارة فحص

البيانات الاولية:

الجهه المستفيدة	اسم المستفيد	رقم وتاريخ الطلب	تاريخ استلام الطلب
جامعة بابل /هندسة مواد	زين العابدين علي	العدد : بلا التاريخ: 2022/5/15	2022/5/15
طبيعة النموذج	عدد النماذج	رقم النموذج	تقنية الفحص المطلوبه
سائل	6		الامتصاص الذري اللهبي

نتائج الفحص

ت	رقم النموذج	النتائج / وحدة القياس	كلفة الفحص	الملاحظات
	2.5 saliva	Co= nil	25000	
	5 saliva	Co= nil	25000	
	75 saliva	Co=0.26 ppm	25000	
	2.5 hank	Co =0.89 ppm	25000	
	5 hank	Co=1.84 ppm	25000	
	75 hank	Co= 14.22 ppm	25000	

المبلغ المطلوب بالدينار: 150.000 مئة وخمسون الف

هذه الشهادة صادرة وموثقة في :

المختبر	الشعبة	القسم	المركز
توقيع الفاحص	توقيع مسوول الشعبة	توقيع مدير القسم	توقيع مدير المركز
الاسم الثلاثي	الاسم الثلاثي:	الاسم الثلاثي:	الاسم الثلاثي:
التاريخ: ١٥/ 5 / 2022	التاريخ: ١٥/ 5 /2022	التاريخ: ١٥/ 5 /2022	التاريخ: ١٥/ 5 / 2022

نسخة منه الى :-

-قسم التخطيط والمتابعة / للعلم

-القسم المالي والتجاري /للعلم

-الجهة الفاحصة / للعلم

2022/06/30 00:55

Fig (29): Results of ion release of alloys.

الخلاصة

تعتبر سبيكة كوبلت-كروم- مولبيديوم واحدة من اهم السبائك واسعة الاستخدام في تطبيقات العظام وغرسات الاسنان. الهدف من هذه الدراسة هو التحقيق في تأثير إضافة أوكسيد الزركونيوم الى سبيكة كوبلت- كروم- مولبيديوم على الخواص الفيزيائية والميكانيكية والالكتروكيميائية.

تمت إضافة (0.5,1,1.5,2,2.5,3,3.5,4,4.5,5 %) من أوكسيد الزركونيوم الى السبيكة بواسطة الباودر ميتالورجي.

تم خلط المساحيق لمدة خمس ساعات وكبسها عند ضغط 800 Mpa. كانت ابعاد النماذج بعد عملية الكبس هي (القطر =12mm والسمك =4.5mm).

تمت عملية التلبيد عند درجة حرارة 1100درجة مئوية لمدة أربع ساعات لكل العينات وهي كانت كافية لتحويل جميع العناصر الى تركيب سبيكة.

بينت نتائج اختبار اشعة اكس ان بنية نماذج كوبلت-كروم-مولبيديوم (مع وبدون الإضافة) المكبوسة بضغط 800Mpa والملبدة بدرجة حرارة 1100 درجة مئوية لمدة 4 ساعات تتكون من ثلاث اطوار في درجة حرارة الغرفة هي ($CoCrMo$, $CoCr$ and Co_2Mo_3).

تشير النتائج الى انخفاض الكثافة بشكل طفيف وكذلك انخفاض المسامية مع زيادة إضافة أوكسيد الزركونيوم.

تزاد الصلادة للعينات المحضرة بشكل واضح مع إضافة الزركونيا من(HB109) للعينة الأساس الى (HB151) عند إضافة 5% من ZrO_2.

تزداد مقاومة البلى بشكل كبير مع إضافة الزركونيا الى السبيكة الأساس حيث ينخفض فقدان الحجم من (cm^3 0.002) للسبيكة الأساس الى ($cm^3$0.000671) عند إضافة 2.5% من أوكسيد الزركونيوم كأقل فقدان حجم والذي يعتبر أفضل نسبة تحسن لمقاومة البلى.

تزداد مقاومة الانضغاط بشكل كبير مع إضافة أوكسيد الزركونيوم والتي تزداد من (388.41 Mpa) للسبيكة الأساس الى (949.6Mpa) عند إضافة 3% من أوكسيد الزركونيوم.

أظهرت الخواص الكيميائية ونتائج التآكل للسبيكة تحسنا ملحوظا بعد إضافة دقائق أوكسيد الزركونيوم حيث انخفض معدل التاكل من (1.582mpy) الى (0.144mpy) في محلول اللعاب الصناعي ومن (0.158mpy) الى (0.169mpy) في محلول هانك عند إضافة 5% من الزركونيا.

أفضل مقاومة تاكل كانت عن إضافة (0.5%) حيث كانت نسبة التحسن في محلول اللعاب الصناعي (96.7%) بينما كانت أفضل نسبة التحسن هي (87.83%) عند نفس نسبة الإضافة.

تم الغمر الساكن للسبيكة الأساسية ومع إضافة (2.5 و5٪) من الزركونيا لمدة 21 يومًا في اللعاب الصناعي ومحلول هانك، حيث أكدت نتيجة الاختبار أن ايون عنصر Co في محلول هانك واللعاب الصناعي انخفض بشكل ملحوظ بعد إضافة اوكسيد الزركونيوم.

وزارة التعليم العالي والبحث العلمي
جامعة بابل
كلية هندسة المواد
قسم هندسة المعادن

تحسين سبيكة CoCrMo (F75) باستخدام إضافات من ZrO_2 المستخدمة في التطبيقات الطبية

رسالة

مقدمة الى قسم هندسة المعادن في كلية هندسة المواد/ جامعة بابل

كجزء من متطلبات نيل درجة الماجستير في هندسة المواد/ المعادن

بواسطة

زين العابدين علي كريم محمد

تحت اشراف

أ. د حيدر حسن جابر

2022م 1443هـ